

KU Leuven
Biomedical Sciences Group
Faculty of Medicine
Department of Imaging & Pathology



Effect of immediate and delayed implant placement on nerve fibres and bone structures: a histomorphological and radiographical evaluation

Yan HUANG

Promoters:
Prof. Dr. Reinhilde Jacobs
Prof. Dr. Ivo Lambrichts

Dissertation presented in partial fulfilment of the requirements for the degree of Doctor of Biomedical Sciences

May 2014

KU Leuven
Biomedical Sciences Group
Faculty of Medicine
Department of Imaging & Pathology



Effect of immediate and delayed implant placement on nerve fibres and bone structures: a histomorphological and radiographical evaluation

Yan HUANG

Jury:

Promoter: Prof. Reinhilde Jacobs

Co-promoter: Prof. Ivo Lambrichts

Chair: Prof. Dr. Philippe Demaerel, KU Leuven, Belgium

Secretary: Prof. Dr. Joke Duyck, KU Leuven, Belgium

Jury members: Prof. Dr. Antoon De Laat, KU Leuven, Belgium

PD. Dr. Michael Bornstein, University of Bern, Switzerland

Odont. Dr. Bruno Collaert, Heverlee, Belgium

May 2014

Acknowledgements

Table of Contents

Acknowledgements.....	I
Table of Contents.....	II
List of Abbreviation	V
Chapter 1- General Introduction	1
1.1 Osseoperception.....	2
1.1.1 General distribution of the nerve fibres of natural teeth.....	2
1.1.2 History of osseoperception.....	3
1.1.3 Psychophysical evidence	4
1.1.4 Neurophysiological evidence	5
1.1.5 Histological evidence.....	5
1.2 Bone anatomical structure	6
1.2.1 Macroscopic structure	6
1.2.1.1 Compact (cortical) bone.....	7
1.2.1.2 Trabecular (cancellous, spongy) bone.....	7
1.2.2 Microscopic structure	8
1.3 Bone quality	9
1.4 Peri-implant bone microarchitecture	10
1.4.1 Quantitative morphometry in 2D	11
1.4.2 Quantitative morphometry in 3D	12
1.4.2.1 Magnetic resonance imaging	12
1.4.2.2 Computed Tomography (CT).....	13
1.4.2.3 Micro-CT (μ CT).....	13
1.4.2.4 Cone Beam CT (CBCT).....	14
1.5 General aim and outline of the thesis	14
References.....	17
Chapter 2- A systematic review on the innervation of peri-implant tissues with special emphasis on the influence of implant placement and loading protocols	22
Abstract.....	23
2.1 Introduction.....	24
2.2 Material and methods.....	25
2.2.1 Focused question	25
2.2.2 Search strategy	25
2.2.3 Inclusion and exclusion criteria	26
2.2.4 Data collection and quality assessment	26
2.3 Results	27
2.3.1 Search results and study description	27
2.3.2 Quality assessment of studies	28
2.3.3 Description of study characteristics.....	29
2.3.4 Histological evidence on the innervation.....	29
2.3.5 Characteristics of loading parameters	30

2.4 Discussion.....	30
2.4.1 Histological evidence from peri-implant tissues.....	31
2.4.2 Histomorphological characteristics of peri-implant nerve fibres.....	39
2.4.3 Loading parameters.....	40
2.4.4 Limitations of the present study.....	41
2.4.5 Psychophysical and neurophysiological evidence from peri-implant area.....	41
2.5 Conclusions.....	42
References.....	43
Chapter 3- Sensory innervation around immediately vs. delayed loaded implants: A randomized split-mouth study.....	46
Abstract.....	47
3.1 Introduction.....	48
3.2 Materials & methods.....	49
3.2.1 Study design.....	49
3.2.2 Surgical procedure.....	50
3.2.3 Occlusion restoration.....	50
3.2.4 Animal sacrifice and histology.....	51
3.2.5 Immunohistochemistry (IHC).....	52
3.2.6 Transmission electron microscopy (TEM).....	53
3.2.7 Histomorphometric analysis.....	53
3.2.8 Statistical analysis.....	54
3.3 Results.....	54
3.4 Discussion.....	59
3.5 Conclusions.....	61
References.....	63
Chapter 4- Validating cone-beam computed tomography for peri-implant bone morphometric analysis.....	66
Abstract.....	67
4.1 Introduction.....	68
4.2 Materials & methods.....	69
4.2.1 Samples.....	69
4.2.2 CBCT image acquisition.....	69
4.2.3 Histology.....	71
4.2.4 Morphometric analysis.....	72
4.2.5 Statistical analysis.....	72
4.3 Results.....	73
4.4 Discussion.....	75
4.5 Conclusions.....	78
References.....	79
Chapter 5- A comparative evaluation of cone-beam CT and micro-CT on trabecular bone structures in the human mandible.....	82
Abstract.....	83
5.1 Introduction.....	84
5.2 Materials & methods.....	85

5.2.1 Image acquisition	85
5.2.2 Image processing and analysis	86
5.2.3 Statistical analysis	89
5.3 Results	89
5.4 Discussion	90
5.5 Conclusions	94
References	95
Chapter 6- Effects of immediate and delayed loadings on peri-implant trabecular structures: a cone-beam CT evaluation	97
Abstract	98
6.1 Introduction	99
6.2 Materials & methods	100
6.2.1 Surgical procedures	101
6.2.2 Morphometric CBCT analysis	103
6.2.3 Statistical analysis	105
6.3 Results	105
6.3.1 3D morphometric comparison of the anatomical regions	106
6.3.2 3D morphometric comparison of the implant protocols	108
6.4 Discussion	108
6.5 Conclusions	112
References	114
Chapter 7-General Discussion	118
7.1 Discussion	119
7.2 Conclusions	126
7.3 Future prospects	128
References	130
Summary	134
Samenvatting	138
Curriculum Vitae	142

List of Abbreviation

2/3-D	Two-/Three-Dimensional
BIC	Bone-To-Implant Contact
BMD	Bone Mineral Density
BS	Bone Surface
BS/TV	Bone Surface Density
BV	Bone Volume
BV/TV	Bone Volume Fraction
CBCT	Cone Beam Computed Tomography
Conn.Dn	Connectivity Density
CT	Computed Tomography
CTDI _{vol}	Volume CT dose index
CGRP	Calcitonin Gene-Related Peptide
DVT	Volumetric Tomography
DIP+DL	Delayed Implant Placement and Delayed Loading
DIP+IL	Delayed Implant Placement and Immediate Loading
FD	Fractal Dimension
fMRI	Functional Magnetic Resonance Imaging
GAP-43	Growth-Associated Protein-43
HR-MRI	High-Resolution Magnetic Resonance Imaging
HR-pQCT	High Resolution Peripheral Quantitative Computed Tomography
IHC	Immunohistochemistry
IIP+DL	Immediate Implant Placement and Delayed Loading
IIP+IL	Immediate Implant Placement and Immediate Loading
MDCT	Multi Detector Computed Tomography
MRI	Magnetic Resonance Imaging
NMR	Nuclear Magnetic Resonance
NFP	Neurofilament Protein
NK-1	Neurokinin-1
NPY	Neuropeptide Y
PDL	Periodontal Ligament
Po(tot)	Total Porosity Percentage
PRISMA	Preferred Reporting Items for Systematic Reviews and Meta-Analyses
PGP-9.5	Protein Gene Product-9.5
RCT	Randomized Clinical Trial

ROI	Regions Of Interest
SMI	Structural Model Index
SNR	Signal-To-Noise Ratio
Tb.N	Trabecular Number
Tb.Th	Trabecular Thickness
Tb.Pf	Bone Pattern Factor
Tb.Sp	Trabecular Separation
TEM	Transmission Electron Microscopy
TV	Total Volume Of Interest
μ CT	Micro Computed Tomography
VOI	Volumes Of Interest

Chapter 1

General Introduction

This chapter is partly based on a preliminary study:

*Histomorphological study of myelinated nerve fibres in the
periodontal ligament of human canine*

Yan Huang, Livia Corpas, Wendy Martens, Reinhilde Jacobs, Ivo Lambrichts

Published in *Acta Odontologica Scandinavica*

2011; 69: 279-86

This part reviews the morphometric characterization of nerve fibres in both periodontal ligament and peri-implant area, the history of osseoperception, as well as the application of various imaging techniques for bone morphometric quantification. The review and state-of-the-art allows to define the needs for further research, translated into the overall aim and outline of this thesis.

1.1 Osseoperception

1.1.1 General distribution of the nerve fibres of natural teeth

Oral function is dependent on complex sensory-motor interactions with periodontal mechanoreceptors playing a crucial role.^{1,2} By the afferent nerve in the periodontal ligament (PDL), force can be transmitted to the surrounding bone and lead to afferent nerve signals.³ Refined mechanoreceptive properties of the receptors in the PDL are related to an intimate contact between collagen fibres and Ruffini-like endings.⁴

Only a few studies concentrated on the PDL of human teeth and, if doing so, these were mainly focusing on the ultra structure of the epithelial rests of Malassez or nerve endings.^{4,5} To unravel the general distribution of the myelinated nerve fibres in the PDL of nature teeth, a preliminary study was performed focusing on the dimension, number and distribution of these nerve fibres.⁶ By serial section approaching at the light microscopy level, we found that the innervation of PDL is changing according to different root levels. The largest density of myelinated structure appeared at the apical level, while the smallest value occurred at the middle level of root. The number of grouped myelinated axons was twice as common as that of isolated ones. Both of these axons were mainly located in the alveolar-related part of the PDL (Figure 1.1). It is well in accordance with a literature review, showing that dense innervations of periodontal mechanoreceptors are distributed heterogeneously in the human PDL with increased density in the loaded (*i.e.*, the apical) areas.²

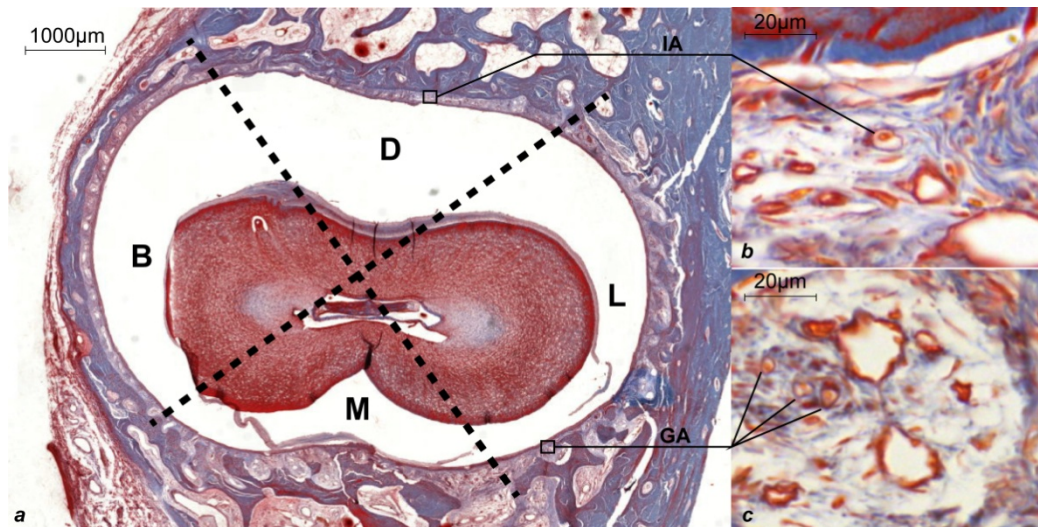


Figure 1.1: Horizontal section of the canine root with the projected line used for histomorphometrical evaluation of four quadrants of the periodontal ligament (B = buccal; D = distal; L = lingual; M = mesial; IA = isolated myelinated axons; GA = grouped myelinated axons). To investigate regional changes in the number and diameter of myelinated nerve fibres at each root level, the PDL was divided into four quadrants with a sector of 90° allocated to each region (Figure 1.1a); The “isolated” axons, which existed as individuals and were situated mainly in the area of the root cementum (Figure 1.1b) and the “grouped” axons, which were those situated predominantly in the alveolar related part of the PDL (adjacent to the bone) (Figure 1.1c).

Tooth extraction may thereby be considered as a form of amputation causing changes in oral motor behavior and impairment of natural biting function⁷ with loss of periodontal mechanoreceptors as well as intra dental nociceptors.⁸ After tooth loss, the myelinated fibre content of the inferior alveolar nerve is reduced by 20%.⁹ The remaining fibres and mechanoreceptive neurons maintain their functionality only to a certain extent.¹⁰ Either nerve degeneration¹¹ or sprouting of new nerve fibres may occur.

1.1.2 History of osseoperception

To restore impaired oral function, replacement of missing teeth is a routine clinical procedure. In 1952, Professor Brånemark revolutionized dentistry with a discovery that a titanium implant can integrate into living bone tissue.¹² With this so-called “osseointegration” now being widely accepted, endosseous (in-bone) dental implants

are placed in large and even growing numbers worldwide every year, from full arch dentures to single crowns, orthodontic anchorages and distraction osteogenesis.¹³ It has even been assumed that by anchoring prosthetic limbs directly to the bone via osseointegrated implants, a partial sensory substitution can be achieved.¹⁴ Indeed, patients with a lower limb prosthesis anchored to percutaneous osseointegrated implant reported that this allows them to feel the type of soil they walked on, while with socket prosthesis they only detected contact that was made with the floor.¹⁵

This phenomenon was denoted as “osseoperception”, suggesting that the peripheral feedback pathway can be (partly) restored by means of prostheses anchored to osseointegrated implants.¹⁶

1.1.3 Psychophysical evidence

Psychophysics includes a series of simple, non-invasive and well-defined methodologies used to determine the absolute threshold level of sensory receptors in humans. It has been reported that, if performed meticulously and under standardized conditions, this approach may disclose as precise information as neurophysiological ways.¹⁷ The psychophysical studies indicated that fixed or removable implant-supported prostheses allowed for the recovery of the inter-occlusal tactile threshold and even for the activation of the primary sensorimotor cortex at levels similar to that of natural teeth.¹⁸⁻²¹ It was further found that active tactile sensibility of implants with natural antagonistic teeth is very similar to that of teeth implying that receptors near the implant form the basis of osseoperception.²² Moreover, the magnitude of passive sensation consistently increased with an increase in loads.²³ The sensory nerve action potential of the inferior alveolar nerve stem could be recorded following stimulations to implants.^{24, 25}

1.1.4 Neurophysiological evidence

The neurophysiological approaches can be divided into direct measure of the neural activity (*i.e.*, electroencephalography, evoked related potentials, neuronal recordings, magnetoencephalography, electrocorticography and electro-cortical stimulation) and indirect measure of neural activity (*i.e.*, positron emission tomography, magnetic resonance imaging and blood-oxygen-level dependence functional MRI). By evaluating the latency period and amplitude of the sensory nerve action potential, it was shown that functional neuro receptors, though much less than that of natural tooth, exist in peri-implant bone tissue.²⁶ In a functional MRI (fMRI) study, the activation of the primary sensory motor cortex in patients with implant-supported dentures might explain the improved tactile, stereognostic ability, and mastication functions, which are more similar to the natural dentition.¹⁸ Recently, the evidence of osseoperception was again confirmed by using fMRI, showing an activation of the human sensory cortex after mechanical stimulation of incisor implants and teeth.²⁷⁻²⁹ These results are in line with those from a previous review.³⁰

1.1.5 Histological evidence

While neurophysiological and psychophysical evidence of osseoperception are accumulating, histological studies further demonstrated that this phenomenon may be attributed not only to neural endings in the bone-implant interface itself but also to neural endings located at some distance such as the periosteum, which was described as “osseoreceptors”.³¹ It is evident that oral implants offer another type of force transfer than teeth considering the intimate bone-to-implant contact. The elastic bone properties contrast with the viscoelasticity of the PDL. Thus, forces applied to osseointegrated implants are directly transferred to the surrounding bone. The resulting bone deformation may lead to receptor activation in peri-implant bone and in the neighboring periosteum which is known to be richly innervated by mechanoreceptors such as Pacini endings.³² An increased innervation in the peri-implant epithelium was confirmed after implant placement,³³ proving that

existing mechanoreceptors in the periosteum may play a role in tactile function upon implant loading. On the other hand, although surgical trauma due to implant placement may induce the degeneration of environing neural fibres, some reinnervation occurs around osseointegrated implants.³⁴⁻³⁷ With advances of immunohistochemical techniques in the 1990s, it has also been shown that nerve fibres in bone, which exhibit special staining properties (*i.e.*, substance P and neuropeptide Y), arise from dorsal root ganglia and are thus involved in sensory function.³⁸

1.2 Bone anatomical structure

The clinical success of dental implant therapy largely depends on the anchorage of the endosseous component of the implant in the bone tissue. In biological terms, bone has been described as a dynamic, mineralized connective tissue which binds structures together and is used for support within the body.³⁹ However, bone is unique among the connective tissues because it is hard. This is due to the extracellular collagenous matrix that is impregnated with a mineral phase, principally hydroxyapatite. Bones are organs made up of bone tissue as well as marrow, blood vessels, epithelium and nerves, while bone tissue refers specifically to the mineral matrix that forms the rigid sections of the organ. Generally, the structure of bone can be described at two different levels of anatomical organization: macroscopic (visible with naked eye) and microscopic (visible with various kinds of microscopes).

1.2.1 Macroscopic structure

The macroscopic structure of bone can be categorized in terms of their various proportions and structural patterns throughout the body (Figure 1.2).

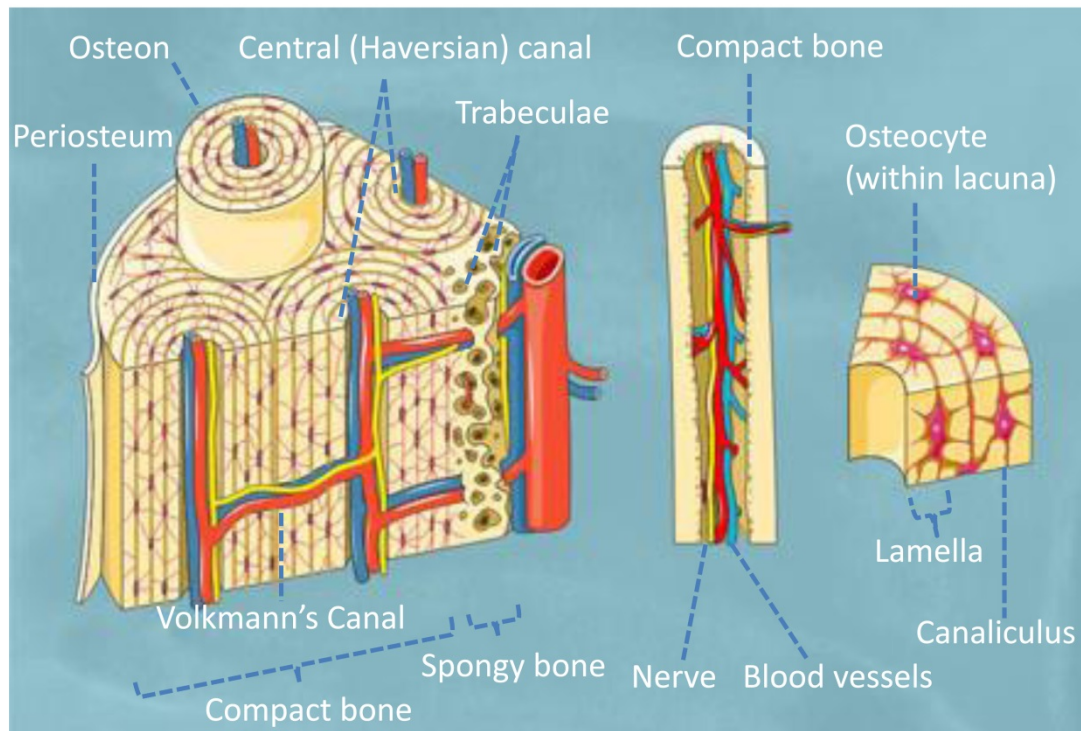


Figure 1.2: Microscopic representation of compact and trabecular bone. (Adapted from: *Qualities of Bone and the Effects of Treatment*, www.medscape.org)

1.2.1.1 Compact (cortical) bone

The hard outer layer of bone is composed of compact bone tissue because of its minimal gaps and spaces. Cortical bone porosity is 5-30% and accounts for 80% of the total bone mass of an adult skeleton. This tissue results in their smooth, white and solid appearance.

1.2.1.2 Trabecular (cancellous, spongy) bone

The trabecular bone tissue is the interior of bone. It composes of an open cell porous network, which makes the overall organ lighter and offers room for blood vessels and marrow. Trabecular bone accounts for the remaining 20% of total bone mass, but has nearly ten times the surface area of compact bone. In comparison to the other type of osseous tissue, it is softer, weaker, less dense and less stiff with a porosity range of 30-90%. From the micro perspective, the trabeculae is the primary anatomical and functional unit of cancellous bone, which is predominantly oriented depending on the

external stress or loading. The thickness of spongy bone trabeculae is normally 100-150 μm separated by spaces of 500-1000 μm .⁴⁰

1.2.2 Microscopic structure

Histologically, there are two types of bone: woven bone (primary or immature) and lamellar bone (secondary or mature). Following injury to bone, *e.g.*, the placing of dental implants, the repair process will start, including an evolution from quickly formed woven to lamellar bone.

Woven bone, with a larger number of osteocytes and minimal strength, is generally characterized by an irregular array of collagen fibers and contains a reduced mineral content. In perspective of microscope, the mature bone is an organization in concentrated layers (lamellae) round the small canals, which runs parallel to the long axis (shaft) of the bone (Figure 1.2). These canals, named Haversian canals, are interconnected with each other via Volkmann's canals and contain a bunch of blood vessels, nerves and lymph vessels. Once bone cells have completely surrounded by the hard bone matrix, they become osteocytes which are embedded in fluid-filled cavities within the concentric lamellae. These cavities, also known as lacuna, occur at regular intervals in these concentric layers of bone tissue. The lacuna are also connected to one another and to the Haversian canals by a system of interconnecting canals called canaliculi. Each Haversian canal together with its concentric lamellae, lacuna with osteocytes and canaliculi forms a long cylinder, denoted as Haversian system. Adjacent Haversian systems join to each other by means of interstitial lamellae. The microscopic difference between compact and cancellous bone is that compact bone consists of Haversian systems and osteons, while cancellous bone does not have these structures.

1.3 Bone quality

Sufficient and higher bone quality, as an important predictor of implant success, could provide good primary implant stability with only standard instruments.⁴¹ However, the concept of bone quality is elusive and there is no precise definition of bone quality.⁴² Currently, it is believed that bone quality is not only a matter of mineral content, but also of bone geometry, microarchitecture, cortical porosity, tissue-level components, degree of mineralization, and micro-damage.⁴³ As proposed by Felsenberg and Boonen, bone quality could be compared to “an umbrella term that describes the set of characteristics that influence bone strength” and interrelationships between them.⁴³ Any change of bone remodeling can affect bone quality at micro- and/ macro-structure levels, thus influencing the bone’s resistance to fracture.

Despite the lack of a generally accepted definition of bone quality, methods for measuring it are numerous. Some approaches can measure one or more aspects of bone quality and/or the mechanical strength of bone, either *in vitro* on bone specimens, or *in vivo* by imaging techniques. In this chapter, the focus was on the structural imaging rather than the functional or molecular imaging of bone.

Because of the high mineral content in bone and higher attenuation of x-rays than the surrounding soft tissue, the first noninvasive structural imaging modality for bone was given by conventional roentgenography when it was introduced in 1895. In history, the clinical bone quality classification by Lekholm & Zarb is the most widely accepted by clinicians and scientists.⁴⁴ It was based on the assessment of conventional radiographs associated with the tactile perception of the surgeon during drilling the bone and categorizes the bone quality into four groups according to the proportion and structure of compact and trabecular bone tissue: groups 1-4 or type I to IV (Bone Quality Index-BQI) (Figure 1.3). As the classification scheme is well known in clinical settings, its efficacy in diagnosis of bone types has not yet been scientifically validated.^{45, 46}

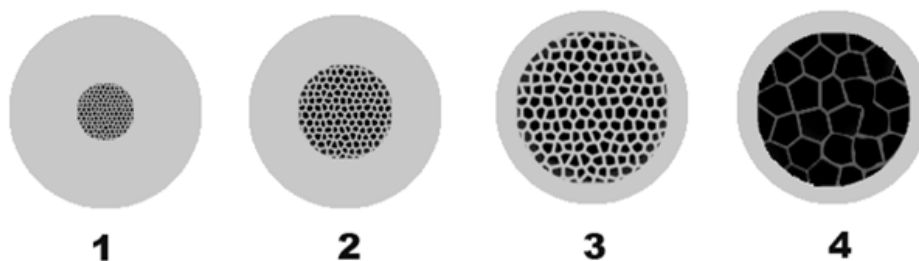


Figure 1.3: Bone Quality Index according to Lekholm and Zarb. Type I: homogeneous cortical bone; Type II: thick cortical bone with marrow cavity; Type III: thin cortical bone with dense trabecular bone of good strength; Type IV: very thin cortical bone with low density trabecular bone of poor strength. (Adapted from Lekholm and Zarb⁴⁴)

Besides this subjective criterion, other methods for the assessment of bone quality during implant treatment have also been reported, such as dual-energy X-ray absorptiometry, histomorphometry of bone biopsies and ultrasound.⁴⁷ Although most of these techniques provide a reliable quantitative measure of bone density, they are impractical for the practicing implant surgeon and may not accurately represent bone mineral density (BMD), which is an important parameter for successful implant treatments. With the advances in physics, digital geometric processing and computational power, the evolution of structural imaging are promising to process and reconstruct virtual three-dimensional (3D) images of bone and soft tissue.⁴⁸

In fact, it is still largely unknown what influences bone healing related variables on implant placement and loading. To obtain tools that can measure and quantify bone microarchitecture, both objective and *in vivo*, will enable a more complete study of bone strength, adding new information to knowledge of implant treatment outcome.

1.4 Peri-implant bone microarchitecture

Theoretically, implant failure occurs when the external force/load applied to the bone exceeds its strength. As the microarchitecture of trabecular bone has been considered as an important parameter of bone quality, appropriate assessment of the bone architecture in an objective and quantitative manner can be essential to determine the

status of successful osseointegration. Imaging techniques that can determine parameters of the trabecular bone structure may improve clinical treatment of dental implants and enhance new implant development. Quantitative bone morphometry is the standard method to assess structural properties of trabeculae by means of morphometric indices. The current mostly used imaging modalities to measure bone structures are outlined in Table 1.1.

1.4.1 Quantitative morphometry in 2D

Historically, the gold standard method used to evaluate peri-implant tissues around oral implants was available after the introduction of Parfitt's principles, by means of microscopic or histologic analysis, combined with calculation of morphometric parameters using stereologic methods.⁴⁹ This conventional approach typically comprises a substantial preparation of the specimen, including embedding in paraffin, followed by sectioning into slices. Although the method offers high spatial resolution and high image contrast, it remains, however, a time-consuming way. Moreover, it is a destructive technique that allows tissue quantification in only a limited number of 2D sections and therefore, prevents the specimen from being used for other measurements, such as analysis in different planes. The latter is highly desirable because of the anisotropic nature of cancellous bone.

Dental radiographs, *i.e.*, intra-oral and panoramic imaging, have been widely used in clinical for evaluating the amount and pattern of trabecular bone structures,^{50, 51} mainly due to their considerable advantages, such as low costs, ready availability, good patient tolerance, user friendliness and the ability to provide high-resolution images. Nevertheless, due to the limitation of the 2D image, dental radio graphs were subject to lack of information of buccal-lingual direction, magnification errors or superimposition of complex osseous structures. To overcome the limitations of the quantitative morphometry in 2D, various 3D imaging modalities of analysis techniques have been proposed.

Table 1.1: Current mostly used imaging modalities for quantitative bone morphometry

Modality	Dental Radiograph	MRI	HR-pQCT	μ CT	CBCT
Defined Variable	Trabecular amount; Trabecular pattern	Bone matrix density; Bone mineral content; Mineral-to-matrix ratio	Bone mineral density per voxel; Trabecular geometry	Trabecular geometry	Trabecular geometry
2D/3D	2D	3D	3D	3D	3D
In/Ex vivo	In vivo	In vivo	In vivo	Ex vivo	In vivo
Location assessed	Oral	Central and peripheral	Central and peripheral		Oral, Peripheral,
Image acquisition time	Seconds	Minutes to hours	Minutes	Hours	Minutes
Radiation exposure*	5-26 μ Sv	No	2- 100 μ Sv	7.4 μ Sv	43-84 μ Sv
Application	Clinical	Research	Clinical	Research	Clinical /Research

*Data source: 52-55

1.4.2 Quantitative morphometry in 3D

1.4.2.1 Magnetic resonance imaging

Magnetic resonance imaging (MRI) is a 3D imaging technique without using ionizing radiation. It is based on the phenomenon of nuclear magnetic resonance (NMR), which was first described in 1950s.^{56, 57} By employing MRI, the patient is placed in a strong magnetic field and subjected to short pulses of radio waves. In theory, trabecular bone is filled with bone marrow that contains free protons and results in a strong MR signal. Thus, MRI might represent a complementary imaging technique to visualize the maxillofacial skeleton for various purposes, *i.e.*, evaluating the bone-implant interface during osseointegration,⁵⁸ assessing the response of bone to biomaterials;⁵⁹ examining bone microstructure at different anatomic sites.⁶⁰ However, the image quality of MRI, to a greater degree, is influenced by the field strength, echo time, pulse sequence and signal to noise ratio.⁶¹ In addition, the low availability and accessibility of MRI constrain the further clinical application.

1.4.2.2 Computed Tomography (CT)

A CT machine uses a fan-shaped beam and multiple exposures around an object to reveal the internal architecture of this object, in helping the clinician to view morphologic features as well as pathology from various 3D perspectives. It was originally introduced for bone mineral analysis. With a spatial resolution ranging from 150 to 300 μm , multi detector CT (MDCT) enable a 3D assessment of the craniofacial region and give an excellent depiction of hard tissue structures.⁶² Although high-resolution peripheral quantitative CT (HR-pQCT) has an even higher spatial resolution than MDCT, scanning sites are limited to peripheral skeletal region (*e.g.* distal radius and tibia). Moreover, HR-pQCT can not avoid a relatively high radiation dose and the results of measurements are influenced by the selected threshold, image processing techniques and reconstruction software. Therefore, the application of HR-pQCT remains restricted in the oral implant studies.

1.4.2.3 Micro-CT (μCT)

In the beginning of the 1990s, Feldkamp *et al.* described for the first time the μCT technique, as the first laboratory available method to analyze bone samples in 3D.⁶³ μCT generates polychromatic radiation (photons with different energy) and diverges the beam conically. In contrast to the classical histomorphometry, bone structure parameters such as bone trabecular thickness (Tb.Th), trabecular separation (Tb.Sp) and trabecular number (Tb.N) could be directly determined from the 3D images without assuming the geometric model. Recently, the micro-CT was validated as highly reliable tool in determining trabecular bone parameters by comparing the morphometric results of conventional histomorphometry with the results of micro-CT.⁶⁴ It was generally accepted that this technique could not entirely replace the histological evaluation, but it at least could facilitate the analysis of trabecular architecture by assessing new required 3D bone parameters. Considering the importance of the microarchitecture of trabecular bone,⁴³ it might offer a further

insight into bone quality assessment by providing objective and quantitative microstructural data of the peri-implant tissues.

1.4.2.4 Cone Beam CT (CBCT)

CBCT, also known as digital volumetric tomography (DVT), was developed for imaging of the dento-maxillo-facial region in the late 1990s.⁶⁵ Basically, CBCT uses a cone- or pyramid-shaped X-ray beam and a flat-panel detector or image intensifier. Since the first commercially available CBCT equipment entered the European market in the early 2000s, there are more than 40 systems which are primarily for dental practitioners on the market now.⁶⁶ CBCT's main disadvantage compared with the CT modalities was its low spatial resolution (100-200 μ m) for a long time. With the enormous improvement of image techniques during the last decade, CBCT machines, *e.g.*, 3D Accuitomo 170 (J. Morita, Kyoto, Japan), achieve spatial resolutions as high as 80 μ m. So far, CBCT possesses plenty of benefits regarding radiation dose, cost-effectiveness, scanning time and 3D modalities in evaluating the trabecular bone structure in a clinically objective and quantitative way. Although it is a relatively new imaging technique, its accuracy and reliability to objectively assess the trabecular bone structure has not been properly studied. To validate CBCT as a method for the 3D assessment of trabecular bone structures, it is necessary to compare results obtained from this imaging modality with histomorphometry and micro-CT which remain some kind of gold standards for quantitative bone morphometry.

1.5 General aim and outline of the thesis

The primary aim of this doctoral thesis was to investigate the effect of the immediate and delayed implant placement and loading on osseoperception after tooth extraction on histomorphological levels. The parallel aim was to uncover how the peri-implant trabecular bone structure changes with immediate vs. delayed loaded implants by using a validated radiographic way.

Therefore, the detailed research objectives were:

- To systematically collect and review the evidence-based influence of dental implant placement and loading protocols on peri-implant innervation. **(Chapter 2)**

Hypothesis: There is clear evidence to confirm the effect of time between teeth extraction and implant placement or implant loading on neural fibre content in the peri-implant hard and soft tissues.

- To identify peri-implant neurosensory endings in a dog model by histological and immunohistochemical ways, and to determine the effect of the immediate and delayed implant placement and loading on peri-implant innervation after tooth extraction. **(Chapter 3)**

Hypothesis: As in the natural periodontal ligament, the presence and distribution of neural structures around implants are confirmed. Immediate implant placement and loading may allow for an optimized axonal regeneration around implants.

- To verify the accuracy of CBCT in peri-implant trabecular bone structure analyses using histomorphometry as a reference. **(Chapter 4)**

Hypothesis: peri-implant trabecular bone structures based on high-resolution CBCT measurements are representative for the underlying histologic bone morphometric characteristics.

- To determine the accuracy of CBCT for measuring the trabecular bone microstructure in comparison to μ CT. **(Chapter 5)**

Hypothesis: While compared with another 3D imaging technique μ CT, high-resolution CBCT imaging shows potential for in vivo applications of quantitative bone morphometry and bone quality assessment.

- To evaluate the 3D morphology of peri-implant trabecular bone in a dog model after immediate and delayed implant protocols by means of high-resolution CBCT. **(Chapter 6)**

Hypothesis: The implant protocols have an improved bone structural integration in comparison with normal extraction healing. Besides, there might be a different peri-implant bone healing pattern between delayed and immediate implant protocols.

References

1. Jacobs R, van Steenberghe D. Role of periodontal ligament receptors in the tactile function of teeth: a review. *J Periodontal Res* 1994; **29**: 153-167.
2. Trulsson M. Sensory-motor function of human periodontal mechanoreceptors. *J Oral Rehabil* 2006; **33**: 262-273.
3. Bonte B, Linden RW, Scott BJ, van Steenberghe D. Role of periodontal mechanoreceptors in evoking reflexes in the jaw-closing muscles of the cat. *J Physiol* 1993; **465**: 581-594.
4. Lambrechts I, Creemers J, van Steenberghe D. Morphology of neural endings in the human periodontal ligament: an electron microscopic study. *J Periodontal Res* 1992; **27**: 191-196.
5. Lambrechts I, Creemers J, Van Steenberghe D. Periodontal neural endings intimately relate to epithelial rests of Malassez in humans. A light and electron microscope study. *J Anat* 1993; **182 (Pt 2)**: 153-162.
6. Huang Y, Corpas LS, Martens W, Jacobs R, Lambrechts I. Histomorphological study of myelinated nerve fibres in the periodontal ligament of human canine. *Acta Odontol Scand* 2011; **69**: 279-286.
7. Svensson KG, Grigoriadis J, Trulsson M. Alterations in intraoral manipulation and splitting of food by subjects with tooth- or implant-supported fixed prostheses. *Clin Oral Implants Res* 2013; **24**: 549-555.
8. Mason AG, Holland GR. The reinnervation of healing extraction sockets in the ferret. *J Dent Res* 1993; **72**: 1215-1221.
9. Heasman PA. The myelinated fibre content of human inferior alveolar nerves from dentate and edentulous subjects. *J Dent* 1984; **12**: 283-286.
10. Linden RW, Scott BJ. The effect of tooth extraction on periodontal ligament mechanoreceptors represented in the mesencephalic nucleus of the cat. *Arch Oral Biol* 1989; **34**: 937-941.
11. Hansen J. Neurohistological reactions following tooth extractions. *Int J Oral Max Surg* 1980; **9**: 411-426.
12. Brånemark PI, Adell R, Breine U, Hansson BO, Lindstrom J, Ohlsson A. Intra-osseous anchorage of dental prostheses. I. Experimental studies. *Scand J Plast Reconstr Surg* 1969; **3**: 81-100.
13. Pye AD, Lockhart DE, Dawson MP, Murray CA, Smith AJ. A review of dental implants and infection. *J Hosp Infect* 2009; **72**: 104-110.
14. Jacobs R. Neurological versus psychophysical assesement of osseoperception In: Jacobs Rs, ed. *Proceedings of the Osseoperception* Catholic University Leuven, 1998: 75-88.

15. Brånemark P-I. Osseointegration: biotechnological perspective and clinical modality. In: Brånemark P-I, Rydevik B, Skalak Rs, eds. *Proceedings of the Osseointegration in skeletal reconstruction and joint replacement.*: Quintessence Publishing Co, 1997.
16. Feine J, Jacobs R, Lobbezoo F, Sessle BJ, van Steenberghe D, Trulsson M, Fejerskov O, Svensson P. A functional perspective on oral implants - state-of-the-science and future recommendations. *J Oral Rehabil* 2006; **33**: 309-312.
17. Jacobs R, Wu CH, Goossens K, Van Loven K, Van Hees J, Van Steenberghe D. Oral mucosal versus cutaneous sensory testing: a review of the literature. *J Oral Rehabil* 2002; **29**: 923-950.
18. Chen Y, Lin Y, Jin Z, Li K, Liu G. Neuroplasticity of edentulous patients with implant-supported full dentures. *Eur J Oral Sci* 2008; **116**: 387-393.
19. Batista M, Bonachela W, Soares J. Progressive recovery of osseoperception as a function of the combination of implant-supported prostheses. *Clin Oral Implants Res* 2008; **19**: 565-569.
20. Jacobs R, van Steenberghe D. Comparison between implant-supported prostheses and teeth regarding passive threshold level. *Int J Oral Maxillofac Implants* 1993; **8**: 549-554.
21. Jacobs R, van Steenberghe D. Comparative evaluation of the oral tactile function by means of teeth or implant-supported prostheses. *Clin Oral Implants Res* 1991; **2**: 75-80.
22. Enkling N, Utz KH, Bayer S, Stern RM. Osseoperception: active tactile sensibility of osseointegrated dental implants. *Int J Oral Maxillofac Implants* 2010; **25**: 1159-1167.
23. Hsieh WW, Luke A, Alster J, Weiner S. Sensory discrimination of teeth and implant-supported restorations. *Int J Oral Maxillofac Implants* 2010; **25**: 146-152.
24. Qiao SC, Lv XF, Zhuang LF, Jiang HH, Zhang ZY, Lai HC. [Animal study of sensory function of nerve fibers surrounding dental implant]. *Shanghai Kou Qiang Yi Xue* 2011; **20**: 119-124.
25. Weiner S, Sirois D, Ehrenberg D, Lehrmann N, Simon B, Zohn H. Sensory responses from loading of implants: a pilot study. *Int J Oral Maxillofac Implants* 2004; **19**: 44-51.
26. Zhu YB, Lin Y, Qiu LX, Wang Y. [An animal study of peripheral neurophysiologic mechanism in osseoperception phenomena of dental implant]. *Zhonghua Kou Qiang Yi Xue Za Zhi* 2009; **44**: 460-463.
27. Habre-Hallage P, Hermoye L, Gradkowski W, Jacobs R, Reychler H, Grandin CB. A manually controlled new device for punctuate mechanical stimulation of teeth during functional magnetic resonance imaging studies. *J Clin Periodontol* 2010; **37**:

863-872.

28. Habre-Hallage P, Dricot L, Jacobs R, van Steenberghe D, Reychler H, Grandin CB. Brain plasticity and cortical correlates of osseoperception revealed by punctate mechanical stimulation of osseointegrated oral implants during fMRI. *Eur J Oral Implantol* 2012; **5**: 175-190.

29. Habre-Hallage P, Dricot L, Hermoye L, Reychler H, van Steenberghe D, Jacobs R, Grandin CB. Cortical activation resulting from the stimulation of periodontal mechanoreceptors measured by functional magnetic resonance imaging (fMRI). *Clin Oral Investig* 2014.

30. Jacobs R, van Steenberghe D. From osseoperception to implant-mediated sensory-motor interactions and related clinical implications. *J Oral Rehabil* 2006; **33**: 282-292.

31. Rowe MJ, Tracey DJ, Mahns DA, Sahai V, Ivanusic JJ. Mechanosensory perception: Are there contributions from bone-associated receptors? *Clin Exp Pharmacol P* 2005; **32**: 100-108.

32. Sakada S. Mechanoreceptors in fascia, periosteum and periodontal ligament. *Bull Tokyo Med Dent Univ* 1974; **21 Suppl**: 11-13.

33. Suzuki Y, Matsuzaka K, Ishizaki K, Tazaki M, Sato T, Inoue T. Characterization of the peri-implant epithelium in hamster palatine mucosa: behavior of Merkel cells and nerve endings. *Biomed Res* 2005; **26**: 257-269.

34. Sawada M, Kusakari H, Sato O, Maeda T, Takano Y. Histological investigation on chronological changes in peri-implant tissues, with Special Reference to Responses of Nerve Fibers to Implantation. . *Nihon Hotetsu Shika Gakkai Zasshi(Journal of Japan Prosthodontic Society)* 1993; **37**: 144-158.

35. Buma P, Elmans L, Oestreicher AB. Changes in innervation of long bones after insertion of an implant: immunocytochemical study in goats with antibodies to calcitonin gene-related peptide and B-50/GAP-43. *J Orthop Res* 1995; **13**: 570-577.

36. Wang Y-H. Histological study of nerve distribution around different implant material in dogs. *J Kyushu Dent Soc* 1997; **51**: 521-542.

37. Lambrechts I. Histological and ultrastructural aspects of bone innervation In: Jacobs Rs, ed. *Proceedings of the Osseoperception*. Catholic University Leuven, 1998: 13-20.

38. Rydevik B, Shubayev V, Myers R. Osseoperception In: Brånemark P-Is, ed. *Proceedings of the The osseointegration book - from calvarium to calcaneus*. Quintessenz Verlags-GmbH, 2005: 149-156.

39. Cooper RR, Milgram JW, Robinson RA. Morphology of the osteon. An electron microscopic study. *J Bone Joint Surg Am* 1966; **48**: 1239-1271.

40. Cano J, Campo J, Vaquero JJ, Martinez JM, Bascones A. High resolution image

in bone biology I. Review of the literature. *Med Oral Patol Oral Cir Bucal* 2007; **12**: E454-458.

41. Lindh C, Petersson A, Rohlin M. Assessment of the trabecular pattern before endosseous implant treatment - Diagnostic outcome of periapical radiography in the mandible. *Oral Surg Oral Med Oral Pathol Oral Radiol Endod* 1996; **82**: 335-343.

42. Torres-del-Piiego E, Vilaplana L, Guerri-Fernandez R, Diez-Perez A. Measuring bone quality. *Curr Rheumatol Rep* 2013; **15**: 373.

43. Felsenberg D, Boonen S. The bone quality framework: Determinants of bone strength and their interrelationships, and implications for osteoporosis management. *Clin Ther* 2005; **27**: 1-11.

44. Lekholm U, Zarb G. Patient selection and preparation. Tissue integrated prostheses: osseointegration in clinical dentistry. Quintessence Chicago, 1985: 199-209.

45. Ribeiro-Rotta RF, Lindh C, Rohlin M. Efficacy of clinical methods to assess jawbone tissue prior to and during endosseous dental implant placement: a systematic literature review. *Int J Oral Maxillofac Implants* 2007; **22**: 289-300.

46. Ribeiro-Rotta RF, Lindh C, Pereira AC, Rohlin M. Ambiguity in bone tissue characteristics as presented in studies on dental implant planning and placement: a systematic review. *Clin Oral Implants Res* 2011; **22**: 789-801.

47. Norton MR, Gamble C. Bone classification: an objective scale of bone density using the computerized tomography scan. *Clin Oral Implants Res* 2001; **12**: 79-84.

48. Holliday RA. Inflammatory diseases of the temporal bone: evaluation with CT and MR. *Semin Ultrasound CT MR* 1989; **10**: 213-235.

49. Parfitt AM, Mathews CHE, Villanueva AR, Kleerekoper M, Frame B, Rao DS. Relationships between Surface, Volume, and Thickness of Iliac Trabecular Bone in Aging and in Osteoporosis - Implications for the Microanatomic and Cellular Mechanisms of Bone Loss. *J Clin Invest* 1983; **72**: 1396-1409.

50. Whaiters E. Essentials of dental radiography and radiology. Churchill Livingstone London, 2007.

51. Taguchi A, Sueti Y, Ohtsuka M, Otani K, Tanimoto K, Ohtaki M. Usefulness of panoramic radiography in the diagnosis of postmenopausal osteoporosis in women. Width and morphology of inferior cortex of the mandible. *Dentomaxillofac Radiol* 1996; **25**: 263-267.

52. Dhillon J, Kalra G. Cone beam computed tomography: An innovative tool in pediatric dentistry. *J Pediatr Dent* 2013; **1**: 27-31.

53. Lan SM, Wu YN, Wu PC, Sun CK, Shieh DB, Lin RM. Advances in noninvasive functional imaging of bone. *Acad Radiol* 2014; **21**: 281-301.

54. Pauwels R, Beinsberger J, Collaert B, Theodorakou C, Rogers J, Walker A, Cockmartin L, Bosmans H, Jacobs R, Bogaerts R, Horner K, Consortium SP. Effective dose range for dental cone beam computed tomography scanners. *Eur J Radiol* 2012; **81**: 267-271.
55. Arai Y, Honda K, Iwai K, Shinoda K. Practical model 3DX of limited cone-bam X-ray CT for dental use. *Int Congr Ser* 2001; **1230**: 713-718.
56. Bloch F. Nuclear induction. *Phys Rev* 1946; **70**: 460-474.
57. Purcell EM, HTorrey HC, Pound RV. Resonance absorption by nuclear magnetic moments in a solid. *Phys rev* 1946; **69**: 37-38.
58. Bernhardt R, Scharnweber D, Muller B, Thurner P, Schliephake H, Wyss P, Beckmann F, Goebbels J, Worch H. Comparison of microfocus- and synchrotron X-ray tomography for the analysis of osteointegration around Ti6Al4V implants. *Eur Cell Mater* 2004; **7**: 42-51.
59. Marechal M, Luyten F, Nijs J, Postnov A, Schepers E, van Steenberghe D. Histomorphometry and micro-computed tomography of bone augmentation under a titanium membrane. *Clin Oral Implants Res* 2005; **16**: 708-714.
60. Huh KH, Yi WJ, Jeon IS, Heo MS, Lee SS, Choi SC, Lee JI, Lee YK. Relationship between two-dimensional and three-dimensional bone architecture in predicting the mechanical strength of the pig mandible. *Oral Surg Oral Med Oral Pathol Oral Radiol Endod* 2006; **101**: 363-373.
61. Ibrahim N, Parsa A, Hassan B, van der Stelt P, Wismeijer D. Diagnostic imaging of trabecular bone microstructure for oral implants: a literature review. *Dentomaxillofac Radiol* 2013; **42**: 20120075.
62. Burghardt AJ, Link TM, Majumdar S. High-resolution computed tomography for clinical imaging of bone microarchitecture. *Clin Orthop Relat Res* 2011; **469**: 2179-2193.
63. Martin-Badosa E, Elmoutaouakkil A, Nuzzo S, Amblard D, Vico L, Peyrin F. A method for the automatic characterization of bone architecture in 3D mice microtomographic images. *Comput Med Imaging Graph* 2003; **27**: 447-458.
64. Müller R, Van Campenhout H, Van Damme B, Van Der Perre G, Dequeker J, Hildebrand T, Ruegsegger P. Morphometric analysis of human bone biopsies: a quantitative structural comparison of histological sections and micro-computed tomography. *Bone* 1998; **23**: 59-66.
65. Mozzo P, Procacci C, Tacconi A, Martini PT, Andreis IA. A new volumetric CT machine for dental imaging based on the cone-beam technique: preliminary results. *Eur Radiol* 1998; **8**: 1558-1564.
66. Horner K, Jacobs R, Schulze R. Dental CBCT equipment and performance issues. *Radiat Prot Dosimetry* 2013; **153**: 212-218.

Chapter 2

A systematic review on the innervation of peri-implant tissues with special emphasis on the influence of implant placement and loading protocols

This chapter is based on following manuscript:

A systematic review on the innervation of peri-implant tissues with special emphasis on the influence of implant placement and loading protocols

Yan Huang, Reinhilde Jacobs, Jeroen Van Dessel, Michael M. Bornstein,

Ivo Lambrichts, Constantinus Politis

Published in *Clinical Oral Implants Research*

[Epub ahead of print]

Abstract

Objectives: To systematically review the available literature on the influence of dental implant placement and loading protocols on peri-implant innervation. **Material and methods:** The database MEDLINE, Cochrane, EMBASE, Web of Science, LILACS, OpenGrey and hand searching were used to identify the studies published up to July 2013, with a PICO search strategy using MeSH keywords, focusing on time-dependent effects of implant loading on peri-implant innervation in hard and soft tissues. **Results:** Of 683 titles retrieved based on the standardized search strategy, only 10 articles fulfilled the inclusion criteria, five evaluating the innervation of peri-implant mucosa, five elucidating the sensory function in the peri-implant bone area. All those papers reported a sensory innervation around osseointegrated implants, either in the bone-implant interface or peri-implant mucosa, which expressed particular innervation pattern. Compared to unloaded implants or extraction sites without implantation, a significant higher density of nerve fibres or better nerve recovery around loaded dental implants was confirmed. **Conclusions:** To date, the published literature describes peri-implant innervation with a distinct pattern in hard and soft tissues. Implant loading seems to increase the density of nerve fibres in peri-implant tissues, with insufficient evidence to distinguish between the innervation patterns following immediate and delayed implant placement and loading protocols. Variability in study design and loading protocols across the literature and a high risk of bias in the studies included may contribute to this inconsistency, revealing the need for more uniformity reporting, randomized controlled trials, longer observation periods and standardization of protocols.

2.1 Introduction

The neurophysiologic integration of osseointegrated implants in the jaw bone has hardly received attention, though it may be as important as osseointegration to allow global integration in the human body, acceptance of the artificial limb and a more nature functioning in clinical practice.

After tooth extraction, damages to a large number of sensory nerve fibres may occur. The latter could thus be compared to an amputation, where the target organ and peripheral nervous structures have been destroyed.¹ Nevertheless, clinical observations on patients with oral implants, have confirmed a special sensory perception skill.² The underlying mechanism of this so-called “osseoperception” phenomenon was first proposed by P-I Brånemark in a personal communication. This perception could be derived from other compensatory mechanisms by activation of mechanoreceptors in the temporomandibular joint, muscle, skin, mucosal, and/or periosteal mechanoreceptors.³ It was not until 2005 that a consensus statement on osseoperception was published: the conscious perception of the external stimuli transmitted via bone-anchored prosthesis by activation of neural receptors in the peri-implant environment such as bone and more likely the periosteum, together with a change in central neural processing.⁴

Histological evidence further indicated that there may be some re-innervation around osseointegrated implants.⁵ A subsequent study found an increased innervation in the peri-implant epithelium after implant placement.⁶ While animal studies and clinical evidence of osseoperception are accumulating, still little is known about the potential use of this phenomenon to optimize the physical integration of implants in patients. How mechanoreceptors and nerve fibres around implants could potentially be reactivated or regenerated remains a matter of debate.

The abovementioned findings have triggered our interest on whether variation in the intervals between tooth extraction and implant placement and subsequent loading protocols could have an influence on the neural fibre content in peri-implant tissues.

The overall aim of this systematic review is therefore related to exploring the innervation of peri-implant hard and soft tissues, focusing on the influence of various implant placement and loading protocols. Information on the latter may be of particular interest for optimizing of the physiological integration of implant-supported prostheses and its clinical meaning.

2.2 Material and methods

This systematic review was conducted in accordance to the Preferred Reporting Items for Systematic Reviews and Meta-Analyses (PRISMA).^{7, 8} The search strategy, inclusion criteria, data collection and assessment methodology were determined by the authors before the review process according to the protocol described below.

2.2.1 Focused question

The focused question used to guide the literature search was as follows: Is there histological evidence and data on histomorphological characteristics of peri-implant innervation in hard and soft tissues in humans and mammals, and is this peri-implant innervation influenced by time-dependent variations in implant placement and implant loading protocols?

2.2.2 Search strategy

One formulated PICO search strategy was performed on each selected electronic database from the earliest record to July 2013 (Table 2.1). Final hand searching based on the references of the selected articles and books on the topic of osseoperception⁹⁻¹¹ was also used to identify the potential matching literature. No language limits were imposed and respective papers were translated, if needed.

2.2.3 Inclusion and exclusion criteria

Inclusion criteria were: (1) clinical as well as animal studies, both randomized clinical trials (RCTs) and non-randomized trials, anticipating that RCTs on this topic are scarce; (2) at least one outcome relating to either peri-implant bone or peri-implant mucosa; (3) subjects were humans or mammals; (4) groups comparing loaded (physiological occlusal load or external simulated stimuli) vs. non-loaded, or immediate/early vs. delayed loading (immediate means loading within 1 week after surgery; early means loading launched between 1 week and 2 months from surgery onwards; delayed means loading starts 2 months or more post-surgery);¹² (5) results relating to histological evaluations on innervation; and (6) articles were published and full length.

Exclusion criteria were: (1) studies not including measured or defined parameters that could be associated with innervation or osseoperception around dental implants; (2) studies in the absence of a control group or loading group; (3) narrative or systematic reviews; and (4) abstracts and publications not printed or retrievable online.

2.2.4 Data collection and quality assessment

The potentially relevant titles identified were examined independently and in duplicate by two reviewers (YH and RJ). When there was any doubt from the title, the abstract was retrieved and reviewed. The relevant full papers selected on the basis of the abstract were subsequently reviewed. Information was extracted from included studies by one of reviewers (YH) and confirmed by another (RJ) using a predefined data extraction form on assessment of risk of bias, study characteristics and related loading parameters (Tables 2.1-2.4). Disagreements or uncertainties were discussed with the other reviewers (MB, IL and SP) until an agreement was reached. Authors of the included papers were also contacted for missing or unpublished data (JVD).

2.2.5 Data synthesis

Given the heterogeneity of the populations under investigation, intervention methods, and reported outcome measures across the included studies, no meta-analyses could be carried out. Instead, results of this review were assessed qualitatively.

2.3 Results

2.3.1 Search results and study description

From a total of 683 titles of potentially relevant papers retrieved after following the PICO search strategy, only 10 full text papers met the inclusion criteria of this review including 1 RCT, 2 prospective controlled clinical trials and 7 animal trials (Figure 2.1). These articles were composed of 3 clinical and 7 animal studies respectively. Five measured peri-implant mucosa outcomes, and the others (n=5) addressed sensory function in the peri-implant bone area.

Table 2.1: Systematic search strategy (via PubMed)

Search strategy	Search items
P: Population	#1. ((dental OR dent\$ OR oral) AND implant\$)
E: Exposure	#2. (dental implant\$ OR dental implantation) #3. (load\$ OR force\$ OR occlusal load OR dental occlusion) #4. (immediate implant placement OR immediate placement OR delayed implant placement OR immediate loading OR immediate restoration OR immediate installation)
O: outcome	#5. (osseoperception OR innervation OR nerve fibre\$ OR neuro\$ OR neural OR sensory OR receptor\$ OR mechanoreceptor\$)
Search combination	(#1 OR #2) AND (#3 OR #4) AND #5
Electronic database	MEDLINE (PubMed), Cochrane Central Register of Controlled Trials (CENTRAL), Excerpta Medica Database (EMBASE), Web of Science (ISI Web of knowledge), Latin American and Caribbean Health Sciences (LILACS) database, and grey literature in OpenGrey (System for Information on Grey Literature in Europe)
Hand searching	Related reference lists of selected articles and books: 'Osseoperception (Jacobs 1998)', 'Osseointegration in skeletal reconstruction and joint replacement (Brånemark, <i>et al.</i> 1997)' and 'The osseointegration book-from calvarium to calcaneus (Brånemark, <i>et al.</i> 2006)'

Free text-terms, key words, and other controlled terms from the Medical Subject Headings (MeSH) were used for searching, and Boolean operators (OR, AND, \$) were performed to combine searches.

2.3.2 Quality assessment of studies

The methodological quality assessments of the included studies and possible bias are summarized in Table 2.2. Only one of these studies reported generation of a randomization sequence.¹³ None of the studies reported how the sample size of the experiment was planned except one that was based on a previous study design.¹⁴ None of them reported allocation concealment, that is to say the observer might be aware of the next treatment allocation before the experiments. The blinding of observers was reported in two studies.^{13, 15} None of selected papers described withdrawals and drop-outs from the study. In total, only one RCT was considered to be at low risk of bias,¹³ and the remaining studies (n=9) were classified at a high and unclear risk of bias.

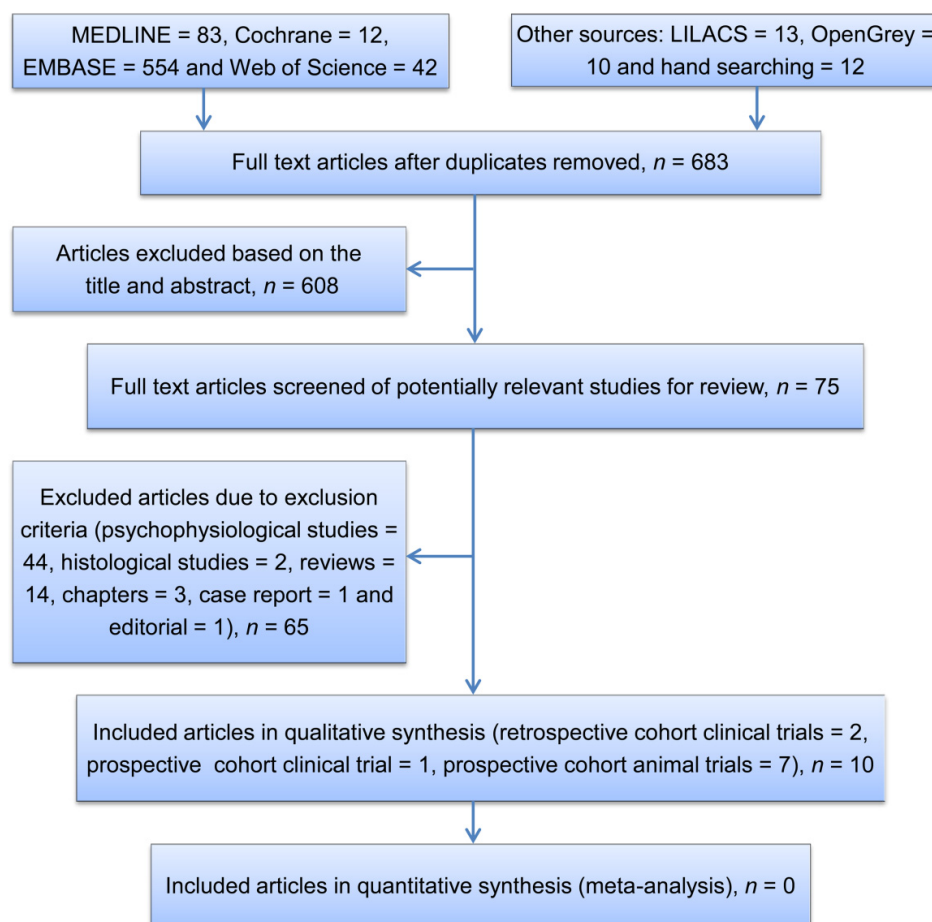


Figure 2.1: Flow chart of screened, withdrawn and included articles through the review process.

2.3.3 Description of study characteristics

Table 2.3 presents details regarding study design. The participants varied from humans to mongrel dogs and rats. In the 10 studies included, four main loading protocols could be differentiated: delayed implant placement with delayed loading (DIP+DL), delayed implant placement with immediate loading (DIP+IL); immediate implant placement with immediate loading (IIP+IL); immediate implant placement with delayed loading (IIP+DL). The control groups included healthy gingiva from extracted natural teeth, non-loaded implants, epithelium/bone from extraction sites without implantation and DIP with non-loaded implants. Two of the 3 human studies mentioned specific loading protocols (*i.e.*, DIP+DL)¹⁵ or the type of restoration (*i.e.*, implant-supported over dentures),¹³ while the remaining one did not report either on loading protocols nor type of restoration.¹⁶ Some animal studies compared implants with different coatings¹⁷⁻¹⁹ and found that investigated coatings had no influence on the nerve density. Regarding the animal studies, four publications reported the diet during the experiment and one mentioned plaque control. Almost all studies employed immunohistochemical staining with either Neuro filament Protein (NFP),^{17, 19-21} Protein Gene Product-9.5 (PGP-9.5),^{13, 16, 22, 23} Calcitonin Gene-Related Peptide (CGRP),²² Substance P,¹⁴ Growth-Associated Protein-43 (GAP-43),¹³ S-100¹⁶ or Neurokinin-1(NK-1)¹⁴ receptor as a marker to identify axons. Three studies used conventional H&E or urea-silver nitrate stain technique.^{18, 19, 21}

2.3.4 Histological evidence on the innervation

The main outcomes revealed the regeneration process of the nerve fibres both in peri-implant mucosa and bone tissue following placement of dental implants (Table 2.3). In the five papers assessing innervation in peri-implant mucosa, only one¹⁵ recognized significant changes while the rest four failed to do so.^{14, 16, 22, 24} For those patients who received DIP+DL, the analyzed implants had a nerve density similar to that of healthy gingiva, and more than that of mucosa in edentulous patients.²³

Regarding nerve fibres in peri-implant bone, one paper revealed higher innervation density in the group with loaded implants compared to non-loaded implants.¹⁹ No significant changes were reported in the other four papers included regarding the density of the fibre population in bone area.^{17, 18, 20, 21} Yet, the regeneration of nerve fibres around implants appeared to be improved in the DIP group compared to the IIP group, with few nerve fibres observed in the group with non-loaded implants.²⁰

In all 10 studies selected, there were two papers reporting a significant difference in the DIP+DL group. One clinical human experiment showed a minor increase of innervation in the peri-implant mucosa compared to healthy gingiva from natural teeth over the course of 18 months following implant-supported rehabilitation.²³ Another animal research reported higher innervation density in the peri-implant bone area in comparison to non-loaded implants after a 3-month observation period.¹⁹

2.3.5 Characteristics of loading parameters

Loading protocol varied between the included studies (Table 2.4). They all performed physiological occlusal loads. The loading amplitude or frequency was not reported due to the application of physiological dynamic loads. The type of loading was all dynamic and intermittent, categorizing as a combination of vertical and horizontal loads. Loading duration ranged from 1 day²² to 3 years.¹³ The regeneration of nerve fibres after implant placement occurred between 7-14 days in the peri-implant bone¹⁸ and after 15 days in the peri-implant epithelium.²² The lower 2nd to 4th premolars and 1st molars in dogs were the most investigated sites in the studies selected.

2.4 Discussion

To the best of our knowledge, this is the first systematic review to assess the effect of immediate and delayed loading protocols on innervation of peri-implant tissues in comparison to non-loaded dental implants or control groups such as natural teeth. From initially 683 titles, a total of 10 studies were included and evaluated in detail.

2.4.1 Histological evidence from peri-implant tissues

Timing of loading. Regarding the peri-implant mucosa, there was a reduction of all neural elements in edentulous patients, whereas those patients who received delayed loaded implants had a nerve density similar to that of healthy gingiva surrounding natural teeth.²³ The same longitudinal morphometric analysis further revealed a decrease in the amount of sensory receptors in the mucosa of edentulous patients and a significant increase in the number of nerve fibres in the mucosa covering the distal edentulous mandibular ridges supporting the prostheses after implant-retained rehabilitation. However, there were only minor increases in the number of nerves in the peri-implant mucosa one year after implant-based rehabilitation. The semi-quantitative analysis of biopsies detected a large number of intraepithelial nerves around teeth and delayed loaded implants, but not in edentulous mucosa.¹³ Furthermore, the other three papers^{16, 21, 22} also discovered a regeneration process of peri-implant nerve fibres in the epithelium but failed to uncover any differences between loaded and non-load bearing dental implants.

With regard to the peri-implant bone, the nerve density around delayed loaded implants was found to be considerably higher than that of non-loaded implants, no matter which dental implant surface was utilized.¹⁹ While compared to the bone from extraction sites without implantation, nerve fibres around non-loaded implants were found abundantly present around the bone-to-implant interface, which might originate from what innervated the PDL before the extraction.¹⁸

Table 2.2: Characteristics of the study settings

Study and design(language)	Study subject, gender, mean age / weight	Test implants (surface)	Test Groups (sample size)	Control group (sample size)	Diet during the study	Plaque control	Staining activity of nerve fibres	Region of interest	Funding
Clinical									
Ramieri <i>et al.</i> 2004; retrospective, cohort(in English)	Humans, M and F, 64.5 year	Unclear	ISO occluding with CD (n=11); Edentulous group with CD (n=11); Mucosa specimens from the area of the mandible 1 st molar	Dentate group (n=7): mucosa from the mesial side of the flap created to extract the 3 rd molars, mean age 28yrs. old	Unclear	Unclear	PGP-9.5 and GAP-43	PIE, about 2 mm ² in size, full-thickness, prevalently adherent mucosa	No
Marchetti <i>et al.</i> 2002; retrospective, cohort(in English)	Humans, gender unclear, 30-56 year	Unclear	PIE from loaded implants (n=10)	Healthy gingiva from an extracted tooth (n=1)	Unclear	Unclear	PGP-9.5 and S-100	PIE	Yes, research grant from the Ministry of University Scientific Research and Technology, Italy(MURST)
Garzino <i>et al.</i> 1996; prospective, cohort (in English)	Humans, gender unclear, 40.5-60.1 year	Nobel pharma	DIP+DL: distal ridge mucosa (n=18); DIP+DL: PIE (n=18)	Healthy gingiva from routine oral surgical procedures (n=18)	Unclear	Unclear	PGP-9.5	PIE	No
Animal									
Zhu & Lin. 2012; prospective, cohort (in Chinese)	Beagle dogs, gender unclear, 2 yrs.	Noble Biocare Replace	IIP+DL (n=6); IIP+IL (n=6); DIP+IL (n=6); DIP+DL (n=6)	DIP+non-loaded (n=3)	Unclear	Unclear	NFP	PIB, region of implant threads	Yes, research funding for doctoral study

Table 2.2: (Continued)

Study and design(language)	Study subject, gender, mean age / weight	Test implants (surface)	Test Groups (sample size)	Control group (sample size)	Diet during the study	Plaque control	Staining activity of nerve fibres	Region of interest	Funding
Yamaza <i>et al.</i> 2009; prospective, cohort (in English)	Wista rats, M, 150-180g, 6-wk-old rats for IIP; 4-wk-old rats for DIP	Screw-type, pure Ti, Kondo [®]	IIP+IL (n=8); DIP+IL (n=8)	Healthy gingiva from extracted opposite natural teeth (n=8)	Unclear	Unclear	Substance P and NK-1 receptor	PIE	No
Fujii <i>et al.</i> 2003; prospective, cohort (in English)	Wista rats, M and F, 4wks old	Custom-made titanium cylindrical implants	DIP+IL: 1 d (n=8); 3 d (n=8); 5 d (n=8); 10 d (n=8); 15 d (n=8); 20 d (n=8); 30 d (n=8)	Epithelium from extraction sites without implantation (n=4)	Powder diet	No	PGP-9.5 and CGRP	PIE	Yes, research grant from the Ministry of Education, Culture, Sports, Science and Technology in Japan
Wada <i>et al.</i> 2001; prospective, cohort (in English)	Mongrel dogs, M, adult, 12-20kg	Screw-type, Finafix [®] (Anode Oxidized Titanium or Hydroxyapatite-coating)	DIP+DL (n=6)	DIP+non-loaded implants (n=6)	Soft diet	Yes (5x/wk.)	NFP, H&E and urea-silver nitrate	PIB, within a region of 200µm away from implants	No
Wang. 1997; prospective, cohort (in English)	Mongrel dogs, M and F, adult	Custom-made cylindrical implants, (BIO, FFX or HAC)	DIP+non-loaded: 3 d (n=6); 1 wk. (n=6); 1 month (n=6); 3 months (n=6)	Bone from extraction sites without implantation (n=12)	Unclear	Unclear	Urea-silver nitrate stain	PIB, within a region of 200 µm away from implants	Yes, Kyocera company supplied implant materials and Buzen Rotary Club provided financial support for the study

Table 2.2: (Continued)

Study and design(language)	Study subject, gender, mean age / weight	Test implants (surface)	Test Groups (sample size)	Control group (sample size)	Diet during the study	Plaque control	Staining activity of nerve fibres	Region of interest	Funding
Weiner <i>et al.</i> 1995; prospective, cohort (in English)	Mongrel dogs, gender unclear, 15-20 kg	HA-coated, press-fit titanium implants	DIP+DL: 2 months (n=4); 4 months (n=2); 6 months (n=2)	DIP+non-loaded (n=4)	Soft diet	Unclear	NFP and H&E	PIB, within a region of 250-300µm away from implants	Yes, Orthomatrix, the Alpha Omega Foundation, the American Society of Osseointegration, and the New Jersey Dental School BSRG fund
Sawada <i>et al.</i> 1993; prospective, cohort (in Japanese)	Mongrel dogs, gender unclear, 8-10 kg	Kobe Seiko (pure titanium bio-inactivity type); Hoya (crystallized glass bioactivity type)	DIP+non-loaded: 3 d (n=15), 1 wk. (n=15), 2 wks. (n=15), 4 wks. (n=15) and 8 wks. (n=15)	Bone from extraction sites without implantation (n=6)	Soft diet for 3 d	Unclear	NFP	PIB, within a region of implant threads	No

Abbreviations: M, male; F, female; d, day; wk., week; yr., year; DIP+DL, delayed implant placement with delayed loading; DIP+IL, delayed implant placement with immediate loading; IP+IL, immediate implant placement with immediate loading; IIP+DL, immediate implant placement with delayed loading; PDL, periodontal ligament; CD, complete denture; ISO, implant-supported overdenture; H&E, Hematoxylin-Eosin stain; NFP, neurofilament protein; PGP-9.5, protein gene product-9.5; CGRP, calcitonin gene-related peptide; GAP-43, growth-associated protein-43; NK-1, Neurokinin-1; BIO, single crystal sapphire implant; FFX, anode-oxidized implant; HAC, hydroxyapatite; PIB, peri-implant bone; PIE, peri-implant epithelium.

Table 2.3: Characteristics of exposure and outcome measures

Study (language)	Loading stimulus	Amplitude and frequency	Type of loading (static/ dynamic)	Loading duration	Loading site	Outcome measures
Clinical						
Ramieri <i>et al.</i> 2004 (in English)	Physiologic al occlusal load	Unclear	Dynamic, vertical and horizontal loads	ISO and CD groups loading at least 3 yrs	Lower ISO with implant sites unclear	Semi-quantitative results without accurate <i>P</i> -values; Edentulous patients had reduced innervation; Number of intraepithelial nerves increased in implanted patients and dentate group
Marchetti <i>et al.</i> 2002 (in English)	Physiologic al occlusal load	Unclear	Dynamic, vertical and horizontal loads	16-18 months	Unclear	Qualitative results without accurate <i>P</i> -values; The reconstructed tissue had a good support of regularly distributed nerve fibres; All the epithelial and connective components of the mucosa played a part in the substantial regrowth of the peri-implant tissues
Garzino <i>et al.</i> 1996 (in English)	Physiologic al occlusal load	Unclear	Dynamic, vertical and horizontal loads	DIP+DL: 18 months	Lower ISO with implants in the canine region	The density of nerve fibres and endings were significant higher ($P < 0.01$) in the dentate ($2.44 \pm 0.75\%$) than the DIP+DL ($0.93 \pm 0.72\%$) group; One year after rehabilitation, nerve number increased in the distal ridge mucosa of DIP+DL (1.85 ± 0.43 vs. 0.91 ± 0.76) group ($P < 0.01$), but only a minor increase (NS) in PIE (1.15 ± 0.39 vs. 0.91 ± 0.76)
Animal						
Zhu & Lin. 2012 (in Chinese)	physiologic al occlusal load	Unclear	Dynamic, vertical and horizontal loads	IIP+DL: 3 months; DIP+DL: 3 months; IIP+IL: 6 months; DIP+IL: 6 months	Lower 2 nd - 4 th premolars and 1 st molars	Qualitative results without accurate <i>P</i> -values; Nerve fibre regeneration seems to be improved as the loading time increased; IIP group, thick lamellar bone but less nerve fibres; DIP group, thinner lamellar bone but more nerve fibres; Non-loaded implants group, few nerve fibres

Table 2.3: (Continued)

Study (language)	Loading stimulus	Amplitude and frequency	Type of loading (static/dynamic)	Loading duration	Loading site	Outcome measures
Yamaza <i>et al.</i> 2009 (in English)	Physiologic al occlusal load	Unclear	Dynamic, vertical and horizontal loads	4 wks	Upper 1 st molars	Qualitative results without accurate <i>P</i> -values; Regenerated substance P immune-positive nerves expressed in PIE, and less in the coronal portion of PIE; Substance P/NK1 receptors system may modulate several cellular functions (<i>i.e.</i> , neurogenic inflammation) as in healthy gingiva
Fujii <i>et al.</i> 2003 (in English)	Physiologic al occlusal load	Unclear	Dynamic, vertical and horizontal loads	DIP+IL: 1 d, 3 d, 5 d, 10 d, 15 d, 20 d and 30 d	Upper 1 st molars	Qualitative results without accurate <i>P</i> -values; The distribution pattern of CGRP-positive nerves in PIE were identical to those of PGP 9.5-reactive nerves; Nerve density was lower than that seen in the nature control epithelium, but no difference in nerve density was recognized in PIE between post 20 and 30d; Intraepithelial nerves were recognized in PIE after 15 d, and never from 1-10 d post-implantation
Wada <i>et al.</i> 2001 (in English)	Physiologic al occlusal load	Unclear but kept the same	Dynamic, vertical and horizontal loads	DIP+DL: 3 months	Lower 2 nd - 4 th premolars and 1 st molars	Nerve density of DIP+DL group (HAC, 0.07±0.04%; AOT, 0.07±0.02%) was considerably higher (<i>P</i> < 0.05) than that of DIP+ non-loaded group (HAC, 0.03±0.03%; AOT, 0.04±0.03%); For HAC implants, BIC of loaded implants (66.5±9.4%) was considerably lower (<i>P</i> < 0.01) than that of unloaded implants (75.2±4.3%); For AOT implants, <i>NS</i> in BIC of loaded implants (73.9±4.9%) and that of unloaded implants (66.5±13.3%)

Table 2.3:(Continued)

Study (language)	Loading stimulus	Amplitude and frequency	Type of loading (static/dynamic)	Loading duration	Loading site	Outcome measures
Wang, 1997 (in English)	Physiologic al occlusal load	Unclear	Dynamic, vertical and horizontal loads	DIP+non-loaded: 3 d, 1 wk., 1 month and 3 months	Lower 2 nd - 4 th premolars and 1 st molars	In the control group (natural bone healing), nerve trunks extended from the inferior alveolar nerve to the gingival mucosa and less nerve fibres existed in alveolar sockets; NS in nerve density between three kinds of implants (HAC, 0.83±0.35 µm/mm ² ; FFX, 1.46±0.81 µm/mm ² ; BIO, 1.87±0.82 µm/mm ²); Significant differences (P < 0.01) in BIC between three kind of implants (HAC, 78.09%; FFX, 44.41%; BIO, 8.40%); A negative correlation between nerve density and loaded and non-loaded implants BIC (R=-0.63, P < 0.05); These fibres might originate from what innervated the PDL before the extraction
Weiner <i>et al.</i> 1995 (in English)	Physiologic al occlusal load	Unclear	Dynamic, vertical and horizontal loads	DIP+DL: 2 months, 4 months and 6 months	Lower premolars	Qualitative results without accurate P-values; While labeled axons existed more often in connective tissue, some were present in bone as well; No particular distribution to the labeled fibres; No conclusions regarding nerve density
Sawada <i>et al.</i> 1993 (in Japanese)	Physiologic al occlusal load	Unclear	Dynamic, vertical and horizontal loads	DIP+non-loaded: 3 d, 1 wk., 2 wks., 4 wks. and 8 wks.	Lower 2 nd - 4 th premolars and 1 st molars	Qualitative results without accurate P-values; Nerve number gradually decreased; The distribution and number of nerve fibres were almost identical to those in the bone marrow of the edentulous area; NS in nerve density between two kinds of implants (Kobe Seiko and Hoya)

Abbreviations: CD, complete denture; ISO, implant-supported overdenture; PIE, peri-implant epithelium; PGP-9.5, protein gene product-9.5; CGRP, calcitonin gene-related peptide; NK1, neurokinin-1; BIO, single crystal sapphire coating implant; FFX, anode-oxidized coating implant; HAC, hydroxyapatite coating implant; AOT, anode oxidized coating implant; Kobe Seiko, pure titanium bio-inactivity type; Hoya, crystallized glass bioactivity type.

Table 2.4: Methodological quality of included observational studies

Study (language)	Sample size calculation	Representative population with exposures	Defined methods assessing histology	Data collection and clear inclusion / exclusion	Comparability in study designs / analysis	Blinding of participants or observers	Repeatability of methods	Adequacy of follow-up	Validity of statistical analysis	Unit of analysis	Overall quality
Clinical											
Ramieri <i>et al.</i> 2004 (in English)	No	Yes	Yes	No	No	Yes, observers	Adequate	Unclear	No	Yes	Low
Marchetti <i>et al.</i> 2002 (in English)	No	Yes	Yes	No	No	Unclear	Adequate	Unclear	No	Yes	Low
Garzino <i>et al.</i> 1996 (in English)	No	Yes	Yes	Unclear	No	Yes, observers	Adequate	Yes	Yes	Yes	Medium
Animal											
Zhu & Lin. 2012 (in Chinese)	No	Yes	Yes	No	Yes	Unclear	Inadequate	Unclear	No	Yes	Low
Yamaza <i>et al.</i> 2009 (in English)	Yes	Yes	Yes	No	Yes	Unclear	Inadequate	Unclear	No	Yes	Low
Fujii <i>et al.</i> 2003 (in English)	No	Yes	Yes	No	Yes	Unclear	Inadequate	Unclear	No	Yes	Low
Wada <i>et al.</i> 2001 (in English)	No	Yes	Yes	No	Yes	Unclear	Adequate	Yes	Yes	Yes	Medium
Wang. 1997 (in English)	No	Yes	Yes	No	Yes	Unclear	Adequate	Unclear	Yes	Yes	Medium
Weiner <i>et al.</i> 1995 (in English)	No	Yes	Yes	No	Yes	Unclear	Inadequate	Unclear	No	Yes	Low
Sawada <i>et al.</i> 1993 (in Japanese)	No	Yes	Yes	No	Yes	Unclear	Inadequate	Unclear	No	Yes	Low

The inconsistency between the outcomes of these studies may be caused by testing non-loaded implants in the experimental group of the latter study, and by having density changes occurring outside the observation period.

Timing of implant placement. The included studies do not permit to report obvious differences on the innervation of peri-implant tissues between immediate and delayed groups. One study compared between the IIP, DIP and healthy gingiva from extracted opposite natural teeth, but few data exist on the comparison in the amount of nerve fibres.¹⁴ A recent study observed thick lamellar bone with less nerve in the IIP group while thinner lamellar bone with more nerve fibers was found in the DIP group,²⁰ suggesting that DIP group may promote the regeneration of nerve fibres. Yet, this inference concerning the timing of implant placement was based on a qualitative analysis only because a large number of nerve structures were damaged during the preparation process of decalcified sections.

2.4.2 Histomorphological characteristics of peri-implant nerve fibres

By using immunohistochemistry, all the included studies in this review have confirmed that nerve fibres are present around osseointegrated implants, either in bone or mucosa. Regarding the innervation pattern around implants, there might be some differences between hard and soft tissues. One study pointed out that the nerve density of gingiva from the implant-supported over denture is similar to that of the healthy gingiva from natural teeth.²³ In contrast, free nerve endings in a region of 200 μm away from the bone-implant surface were found at a higher nerve density in the DIP+DL group than in the non-loaded implants group,¹⁹ while the nerve density of non-loaded implants were almost identical to those seen in the extraction sites of natural teeth.^{17, 18} It is still not very clear whether those nerves are distributed in a regular or heterogeneous pattern around implants, though they were reported preferentially existing either under the implant thread area or localized in the bone marrow space around implants.¹⁹ According to the included studies, the number and density of free nerve endings were

mostly reported and compared as an estimate for reinnervation. Some other important parameters of those free or specialized nerve endings have not yet been well documented by histomorphometric assessments (*i.e.*, myelinated/unmyelinated fibre diameter, axon diameter and myelin thickness, conduction velocity). It was suggested that the regenerated nerve around implants might have a higher tactile threshold²⁵ and a lower conduction speed,¹⁸ which remains to be verified in future neurophysiological studies.

2.4.3 Loading parameters

In order to simulate natural loading as much as possible *in vivo*, most of the included papers employed physiological dynamic occlusal loads (chewing) rather than mechanical loads or static stimuli on various mammals, which has been demonstrated to have superior osteogenic potential than static loads.²⁶ On the other hand, this has led to some loading parameters that are difficult to standardize and compare. Only one of the studies applying physiological dynamic occlusal loads kept the loading amplitude the same during the whole experiment by using articulating paper.¹⁹ Thus, the odds of overloading were minimized. However, whether loading forces vary in direction due to various types and consistencies of food still remains doubtful. For those studies which applied electronic or mechanical loads, they may have more possibilities to control and standardize these parameters. Despite indefinite information about loading frequency and amplitude in the papers selected, animal experiments suggested that the mechanical stimuli, with a frequency 2-3 Hz and amplitude 2-20 N, increase peri-implant bone response.^{27,28} Although a decreasing number of neuroreceptors from anterior teeth towards molars were reported in human PDL,²⁹ the two studies which revealed significant higher innervation density in peri-implant tissues were performed respectively in posterior area and anterior area.^{19,23} Whether the spatial relationship of the anatomic position of the nerve trunk and the site of implantation would affect the distribution of nerve fibres in peri-implant area needs further investigation. Neurophysiological and psychophysical measures such as vibratory loads with visual

analog scale,³⁰ active/passive tactile threshold assessment³¹ and punctate stimuli with functional MRI test,³² which are better able to control biological (implant angulation, occlusal type, loading sites, peri-implant bone thickness, application of bone grafts, *etc.*), psychological (attention, distraction , motivation, anxiety, alertness, *etc.*), and methodological factors (interstimulus interval, instructions to test subjects, training before tests, *etc.*) could be helpful to further investigate the effects of these load-modulating factors on peri-implant innervation in humans.

2.4.4 Limitations of the present study

Due to the high level of bias in the selected studies, there are several potential limitations to consider. First, as a consequence of using immunohistochemical antibodies, which only identify specific nerve fibres, a substantial difference between groups may still be present.²¹ Besides, researchers reported that a longer decalcification time at high concentration could lower the capability of detecting nerve fibres.³³ The immunostaining may also be affected by structural characteristics of nerve fibres such as thin or absent Schwann cell covering.³⁴ Second, due to the lack of clinical trials, the data were extracted mainly from animal investigations (*i.e.*, 3 human studies *vs.* 7 animal studies) and not even all animal studies were from dogs, leading to difficulties while comparing results from those animal studies selected. It is thus desirable to stress that the results may systematically bias the effects of implant placement and loading protocols on innervation. Third, RCTs were rarely seen in the selected literature (*i.e.*, 1 RCT out of 10 studies) and the blinding of observers was only reported in two of human studies.^{24, 35} The final limitation is that controls in some studies were not sufficiently described.^{14, 18, 20, 24, 35}

2.4.5 Psychophysical and neurophysiological evidence from peri-implant area

Although this review is focusing on histological proves on the innervation around dental implants, it is worth reminding that most psychophysical and neurophysiological assessments evaluated occlusal tactile thresholds not only in peri-implant bone, but

also in the neighboring mucosa, which means that they did not exclude sensory information originating from soft tissues. It has been reported that the responses to vibrational loading of implants was less strong than that to the loading of the natural tooth.^{30, 36} A recent human study using functional MRI indicated that punctate mechanical stimulation of oral implants is able to activate both primary and secondary cortical somatosensory areas representing an underlying hot field in cortex level for osseoperception.³² Yet, there is still little information about the effects of different loading protocols and time-dependent changes in osseoperception.

2.5 Conclusions

The present systematic review focusing on the current histological evidence from humans and mammals confirms the presence of nerve fibres in peri-implant mucosa and bone tissue. Additionally, the regenerated nerve fibres in the peri-implant area appear to have distinct and different innervation patterns in hard and soft tissues. Furthermore, it suggests that occlusal loading may improve innervation in the peri-implant tissues when compared to the sites without implantation or with non-loaded implants. Nevertheless, the chronological changes of nerve density in peri-implant bone are still not clear and under debate. To help clarify the origins and functions of identified nerve fibres, basic histomorphological observation along with immunohistochemical tests over a long follow-up period should be considered for an accurate and specific quantitative assessment on the innervation of peri-implant tissues. Well-designed RCTs and animal experiments, including additional neurophysiological testing to standardize the frequency and direction of loading, are needed to predict the impact of timing of implant placement and loading protocols on the recovery of sensory perception in peri-implant tissues.

References

1. Mason AG, Holland GR. The reinnervation of healing extraction sockets in the ferret. *J Dent Res* 1993; **72**: 1215-1221.
2. Van Steenberghe D, Jacobs R. Jaw motor inputs originating from osseointegrated oral implants. *J Oral Rehabil* 2006; **33**: 274-281.
3. Klineberg I, Murray G. Osseoperception: sensory function and proprioception. *Adv Dent Res* 1999; **13**: 120-129.
4. Klineberg I, Calford MB, Dreher B, Henry P, Macefield V, Miles T, Rowe M, Sessle B, Trulsson M. A consensus statement on osseoperception. *Clin Exp Pharmacol Physiol* 2005; **32**: 145-146.
5. Lambrechts I. Histological and ultrastructural aspects of bone innervation In: Jacobs Rs, ed. *Proceedings of the Osseoperception*. Catholic University Leuven, 1998: 13-20.
6. Suzuki Y, Matsuzaka K, Ishizaki K, Tazaki M, Sato T, Inoue T. Characterization of the peri-implant epithelium in hamster palatine mucosa: behavior of Merkel cells and nerve endings. *Biomed Res* 2005; **26**: 257-269.
7. Moher D, Liberati A, Tetzlaff J, Altman DG, PRISMA-Group. Preferred Reporting Items for Systematic Reviews and Meta-Analyses: the PRISMA Statement. *Ann Intern Med* 2009; **151**: 264-269.
8. Liberati A, Altman DG, Tetzlaff J, Mulrow C, Gotzsche PC, Ioannidis JP, Clarke M, Devereaux PJ, Kleijnen J, Moher D. The PRISMA statement for reporting systematic reviews and meta-analyses of studies that evaluate health care interventions: explanation and elaboration. *Ann Intern Med* 2009; **151**: W65-94.
9. Brånemark PI, Rydevik B, Skalak R. Osseointegration in skeletal reconstruction and joint replacement. Quintessence Publishing Co Chicago, 1997.
10. Jacobs R. Neurological versus psychophysical assessment of osseoperception In: Jacobs Rs, ed. *Proceedings of the Osseoperception*. Catholic University Leuven, 1998: 75-88.
11. Brånemark PI, Chien S, Grondahl HG, Robinson K. The osseointegration book-from calvarium to calcaneus. Quintessence Pub Co, 2006.
12. Esposito M, Grusovin MG, Maghaireh H, Worthington HV. Interventions for replacing missing teeth: different times for loading dental implants. *Cochrane Database Syst Rev* 2013; **3**: CD003878.
13. Ramieri GA, Schierano G, Spada MC, Giovando ML, Verze L, Preti G. Growth-associated protein-43 immunoreactivity in human oral mucosa in dentate subjects, in edentulous patients and after implant-anchored rehabilitation. *Clin Oral Implants Res* 2004; **15**: 66-72.

14. Yamaza T, Kido MA, Wang B, Danjo A, Shimohira D, Murata N, Yoshinari M, Tanaka T. Distribution of substance P and neurokinin-1 receptors in the peri-implant epithelium around titanium dental implants in rats. *Cell Tissue Res* 2009; **335**: 407-415.
15. Garzino M, Ramieri G, Panzica G, Preti G. Changes in the density of PGR 9.5-immunoreactive nerve fibres in human oral mucosa under implant-retained overdentures. *Arch Oral Bio* 1996; **41**: 1073-1079.
16. Marchetti C, Farina A, Cornaglia AI. Microscopic, immunocytochemical, and ultrastructural properties of peri-implant mucosa in humans. *J Periodontol* 2002; **73**: 555-563.
17. Sawada M, Kusakari H, Sato O, Maeda T, Takano Y. Histological investigation on chronological changes in peri-implant tissues, with Special Reference to Responses of Nerve Fibers to Implantation. . *Nihon Hotetsu Shika Gakkai Zasshi(Journal of Japan Prosthodontic Society)* 1993; **37**: 144-158.
18. Wang Y-H. Histological study of nerve distribution around different implant material in dogs. *J Kyushu Dent Soc* 1997; **51**: 521-542.
19. Wada S, Kojo T, Wang YH, Ando H, Nakanishi E, Zhang M, Fukuyama H, Uchida Y. Effect of loading on the development of nerve fibers around oral implants in the dog mandible. *Clin Oral Implants Res* 2001; **12**: 219-224.
20. Zhu YB, Lin Y (2012) Electrophysiological study of peripheral neurophysiologic mechanism in osseoperception phenomena[OL].<http://www.paper.edu.cn/releasepaper/content/201212-746>
21. Weiner S, Klein M, Doyle JL, Brunner M. Identification of axons in the peri-implant region by immunohistochemistry. *Int J Oral Maxillofac Implants* 1995; **10**: 689-695.
22. Fujii N, Ohnishi H, Shirakura M, Nomura S, Ohshima H, Maeda T. Regeneration of nerve fibres in the peri-implant epithelium incident to implantation in the rat maxilla as demonstrated by immunocytochemistry for protein gene product 9.5 (PGP9.5) and calcitonin gene-related peptide (CGRP). *Clin Oral Implants Res* 2003; **14**: 240-247.
23. Garzino M, G. R, G. P, G. P. Changes in the density of PGR 9.5-immunoreactive nerve fibres in human oral mucosa under implant-retained overdentures. *Arch Oral Bio* 1996; **41**: 1073-1079.
24. Ramieri GA, Schierano G, Spada MC, Giovando ML, Verze L, Preti G. Growth-associated protein-43 immunoreactivity in human oral mucosa in dentate subjects, in edentulous patients and after implant-anchored rehabilitation. *Clin Oral Implants Res* 2004; **15**: 66-72.
25. Hämmerle CH, Wagner D, Bragger U, Lussi A, Karayiannis A, Joss A, Lang NP. Threshold of tactile sensitivity perceived with dental endosseous implants and natural teeth. *Clin Oral Implants Res* 1995; **6**: 83-90.

26. Hert J, Lisková M, Landa J. Reaction of bone to mechanical stimuli. Continuous and intermittent loading of tibia in rabbit. *Folia Morphologica*. *Folia Morphologica* 1971; **19**: 290-300.
27. De Smet E, Jaecques SVN, Jansen JJ, Walboomers F, Sloten JV, Naert IE. Effect of constant strain rate, composed of varying amplitude and frequency, of early loading on peri-implant bone (re)modelling. *J Clin Periodontol* 2007; **34**: 618-624.
28. Zhang X, Vandamme K, Torcasio A, Ogawa T, van Lenthe GH, Naert I, Duyck J. In vivo assessment of the effect of controlled high- and low-frequency mechanical loading on peri-implant bone healing. *J R Soc Interface* 2012; **9**: 1697-1704.
29. Trulsson M, Johansson RS, Olsson KA. Directional sensitivity of human periodontal mechanoreceptive afferents to forces applied to the teeth. *J Physiol* 1992; **447**: 373-389.
30. Hsieh WW, Luke A, Alster J, Weiner S. Sensory discrimination of teeth and implant-supported restorations. *Int J Oral Maxillofac Implants* 2010; **25**: 146-152.
31. Luraschi J, Schimmel M, Bernard JP, Gallucci GO, Belser U, Muller F. Mechanosensation and maximum bite force in edentulous patients rehabilitated with bimaxillary implant-supported fixed dental prostheses. *Clin Oral Implants Res* 2012; **23**: 577-583.
32. Habre-Hallage P, Dricot L, Jacobs R, van Steenberghe D, Reyckler H, Grandin CB. Brain plasticity and cortical correlates of osseoperception revealed by punctate mechanical stimulation of osseointegrated oral implants during fMRI. *Eur J Oral Implantol* 2012; **5**: 175-190.
33. Ikeda H, Yamaza T, Yoshinari M, Ohsaki Y, Ayukawa Y, Kido MA, Inoue T, Shimono M, Koyano K, Tanaka T. Ultrastructural and immunoelectron microscopic studies of the peri-implant epithelium-implant (Ti-6Al-4V) interface of rat maxilla. *J Periodontol* 2000; **71**: 961-973.
34. Mapp PI, Kidd BL, Gibson SJ, Terry JM, Revell PA, Ibrahim NB, Blake DR, Polak JM. Substance P-, calcitonin gene-related peptide- and C-flanking peptide of neuropeptide Y-immunoreactive fibres are present in normal synovium but depleted in patients with rheumatoid arthritis. *Neuroscience* 1990; **37**: 143-153.
35. Garzino M, Ramieri G, Panzica G, Preti G. Changes in the density of protein gene product 9.5-immunoreactive nerve fibres in human oral mucosa under implant-retained overdentures. *Arch Oral Biol* 1996; **41**: 1073-1079.
36. Weiner S, Sirois D, Ehrenberg D, Lehrmann N, Simon B, Zohn H. Sensory responses from loading of implants: a pilot study. *Int J Oral Maxillofac Implants* 2004; **19**: 44-51.

Chapter 3

Sensory innervation around immediately vs. delayed loaded implants: A randomized split-mouth study

This chapter is based on following manuscript:

Sensory innervation around immediately vs. delayed loaded implants: A randomized split-mouth study

Yan Huang, Jeroen Van Dessel, Wendy Martens, Ivo Lambrichts, Weijian Zhong, Guowu Ma, Dan Lin, Xin Liang, Reinhilde Jacobs

Submitted to *International Journal of Oral Science*

[Conditional Acceptance]

Abstract

While neurophysiological and psychophysical proofs on osseoperception are accumulating, histomorphometric evidence for neural mechanisms of functional compensation following immediate and delayed implant loading is still lacking. For this randomized split-mouth study, six mongrel dogs randomly received one out of four treatment protocols at 36 implant-recipient sites during 16 weeks (3rd maxillary incisor, 3rd and 4th mandibular premolar): immediate implant placement and immediate loading (IIP+IL); delayed implant placement and delayed loading (DIP+DL); delayed implant placement and immediate loading (DIP+IL) and natural extraction socket healing (control). Histomorphometry was performed in the peri-implant bone and soft tissues within 300 µm around implants. Immunocytochemistry and transmission electron microscopy were used to confirm the presence of neural structures and to reveal their ultrastructural characteristics, respectively. Myelinated nerve fibres densely populated peri-implant crestal gingival and apical regions, though they were also identified in the woven bone as well as the osteons near the implant threads. Compared to the control group, higher innervation, smaller fibre diameter and g-ratio were shown in all implant groups. More specifically, IIP+IL had a higher nerve density, greater fibre diameter and axon diameter, and lower g-ratio in both jaws than in DIP+DL and DIP+IL, albeit with a tendency towards significance. It might be assumed that the treatment protocol with IIP+IL is preferred to allow optimized peri-implant reinnervation, but further functional measures are still required.

3.1 Introduction

Periodontal mechanoreceptors play a crucial role during oral function.^{1,2} Tooth extraction, as a kind of amputation, may consequently change oral motor behavior and impair natural biting function³ with excessive damage to periodontal mechanoreceptors and intradental nociceptors.⁴

Inspired by the report of lower limb amputees with a bone-anchored prosthesis,⁵ who are able to differentiate between the kind of soil walking on, the concept of ‘osseoperception’ emerged.^{6,7,8} Psychophysical and neurophysiological studies indicated (partial) recovery of tactile function^{9,10,11} and even activation of the primary sensorimotor cortex upon dental implant stimulation,^{12,13} hypothesizing a restoration of the sensory feedback pathway in humans.

Meanwhile, histological evidence revealed the presence of specialized Ruffini mechanoreceptive terminals in the immediate vicinity of implants¹⁴ as well as in the peri-implant epithelium,^{15,16} which were predominantly derived from myelinated fibres. Moreover, researchers identified abundant unmyelinated nerve fibres under the implant thread area, with implant loading increasing the number of free nerve endings.¹⁷ Although myelinated nerve fibres are known to be involved in numerous neurophysiological functions, the quantitative observation of these peri-implant fibres is hardly addressed or characterized histomorphologically. Furthermore, there is hardly any data available on the influence of extraction implant loading protocols, on nerve regeneration and activation.

Therefore, the aim of this study is to histomorphometrically assess the effect of immediate and delayed implant loading on peri-implant innervation in a randomized split-mouth trial.

3.2 Materials & methods

3.2.1 Study design

The protocol of animal experiment was approved by the bioethics committees of Dalian Medical University, Hasselt University and KU Leuven (P059-2012-TK) and complied with ARRIVE guidelines for preclinical studies. To reduce the number of animals used in the experiment and avoid individual differences, or even inter-subject regional heterogeneity, a split-mouth randomized design using four treatment protocols in 6 tooth positions of 6 male mongrel dogs was applied (Table 3.1). The investigators ensured the maximum degree of unpredictability of the allocation sequence by coin toss before surgeries. Sample size calculation was based on our previous study on dogs.¹⁸ Briefly, 6 healthy male mongrel dogs (weight 14.8-18.1 kg, age 20-24 months old) without any oral health or systemic diseases were included and housed individually in indoor cages. The diet during the course of the experiment (including whole grain flour, corn meal, soybean cake, fishbone meal and eggs) abided by the general feeding program at the Experimental Animal Center of Dalian Medical University, China.

Table 3.1: Random distribution of split-mouth design in six experimental dogs

Teeth	1 # dog	2 # dog	3 # dog	4 # dog	5 # dog	6 # dog
I (R)	Control	DIP+DL	DIP+IL	IIP+IL	Control	DIP+DL
I (L)	DIP+DL	DIP+IL	IIP+IL	Control	DIP+DL	DIP+IL
P3 (R)	DIP+DL	DIP+IL	IIP+IL	Control	DIP+DL	DIP+IL
P3 (L)	DIP+IL	IIP+IL	Control	DIP+DL	DIP+IL	IIP+IL
P4 (R)	Control	DIP+DL	DIP+IL	IIP+IL	Control	DIP+DL
P4 (L)	IIP+IL	Control	DIP+DL	DIP+IL	IIP+IL	Control

I = 3rd maxillary incisors; P3 = 3rd mandibular premolars; P4 = 4th mandibular premolars; R = right side; L = left side; DIP: Delayed implant placement; IIP: Immediate implant placement; DL: Delayed loading; IL: Immediate loading. In total, 36 samples were used in the study (Control = 9; IIP+IL = 8; DIP+DL = 10; DIP+IL = 9).

3.2.2 Surgical procedure

Before the surgery, all animals received 1 week of antibiotics prophylaxis (Gentamicin Sulfate, 1600000 U/day, Lingrui Pharmaceutical Co. Ltd., Zhengzhou, China). Custom-made threaded titanium implants (Grade V, machined surface, 3.1 mm Ø for the 3rd maxillary incisors, and 4.1 mm Ø for the 3rd and 4th mandibular premolars, L = 11 mm long) were manufactured and sterilized for surgery. The surgical procedures were performed under general anesthesia with Sumianxin (0.1 ml/kg Xylazine Hydrochloride, Changchun Military Academy of Medical Sciences, China), while local anesthesia (2-4 ml lidocaine 2% with epinephrine 1:100000, Tianjin Pharmaceutical Co. Ltd., Tianjin, China) was only used at the surgical sites. Each implant recipient site was randomly assigned to one of four treatment protocols that are frequently used in the clinic (Figure 3.1), and a general two-stage implant placement was applied accordingly: (1) immediate implant placement and immediate loading (IIP+IL); (2) delayed implant placement (eight weeks after tooth extraction) and delayed loading (four weeks after implant placement) (DIP+DL); (3) delayed implant placement (eight weeks after tooth extraction) and immediate loading (DIP+IL); (4) control group, normal extraction socket healing. The intervals between the implant placement surgery and the animal sacrifice for IIP+IL, DIP+DL and DIP+IL groups were kept all the same as 8 weeks. The same surgeon (WZ) with a decade of clinical experience on implant dentistry performed the whole surgical procedure, who was kept blinded to the allocation process until tooth extraction had been carried out, as he could no longer be blinded to the further allocated implant placement.

3.2.3 Occlusion restoration

The shoulder of implant was placed at the level of the marginal bone, under the same surgical conditions as the tooth extractions in terms of sterility, operation room and anesthesia. Primary stability of implants was confirmed by percussion testing. Customized posts with a Ni-Ti crown (College of Stomatology, Dalian Medical University) were then set using resin cement (RelyX, Unicem, RX, 3M ESPE, St. Paul,

USA). After the post-crown restoration, the edge to edge occlusion contacts during chewing between the implant-recipient sites and antagonist teeth were assured at the most extent. The loading pressure on the implants was kept similar using 20-mm articulating papers during the experimental period (Accufilm II, RX, 3M ESPE, St. Paul, USA). Plaque control was ensured at least one time per week using a 0.2% chlorhexidine gel with a soft toothbrush.

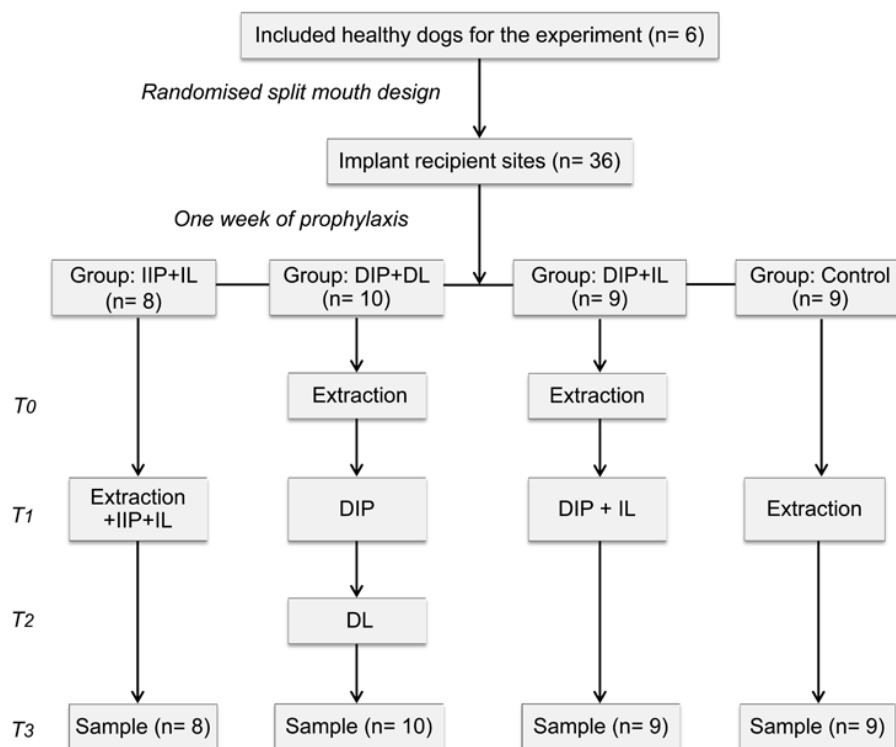


Figure 3.1: Flow chart of study design and time table. IIP+IL (immediate implant placement and immediate loading); DIP+DL (delayed implant placement and delayed loading); DIP+IL (delayed implant placement and immediate loading); Control (normal extraction socket healing); T₀, baseline; T₁, 8 weeks; T₂, 12 weeks; T₃, 16 weeks.

3.2.4 Animal sacrifice and histology

At the 16th week, all animals were sacrificed with an overdose of xylazine hydrochloride (intravenous injection) and immediately perfused with 4% paraformaldehyde and 0.0125% glutaraldehyde in 0.1 M phosphate buffer (pH 7.4). Specimen blocks with a 3- to 5-mm piece of peri-implant bone and gingiva tissue were

retrieved and immersed in 0.5 M EDTA phosphate buffered saline (pH 7.4) at 4°C for 10 months, allowing the implants to be easily removed from the specimens using surgical forceps. Followed by the dehydration and embedding in paraffin, thin serial sections (~6 µm) were prepared along the mesial-distal direction in the middle of the implant or extraction area, considering the vertical loading at implant-recipient sites and abundant trabecular bone structures at mesial-distal direction (more trabecular bone means more space for the development of neuro-receptors). All sections were stained with the Masson trichrome stain.

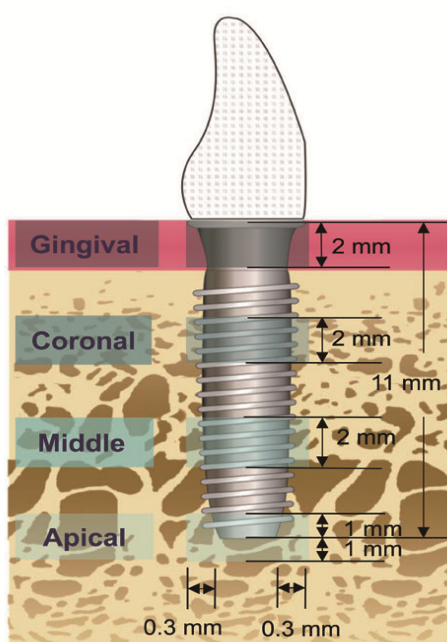


Figure 3.2: The schematic diagram of the regions of interest (ROIs) for histomorphometric analysis of peri-implant innervation. Four different ROIs were displayed in gingival, coronal, middle, and apical regions along the axis of the implant at a mesial-distal view (width = 0.3 mm; height = 2 mm for each region).

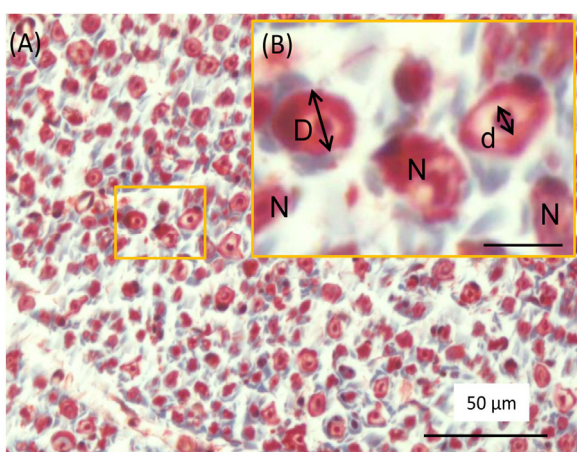


Figure 3.3: Morphometric analyses on the histologic sections with Masson trichrome stain. (A) Myelinated nerve fibres in the light microscopy with well defined structures. The axons were surrounded by myelin sheaths formed by the Schwann cells; (B) A magnification of selected box region in (A) showed the basic morphometric parameters of myelinated nerve fibres (scale bar, 10 µm). N, nerve fibres; D, nerve fibre diameter; d, axon diameter.

3.2.5 Immunohistochemistry (IHC)

IHC was performed on the same serial sections in each group to confirm the presence

of myelinated nerve structures by using the labelled avidin-biotin method as previously described.¹⁹ After fixation, embedded sections were deparaffinized. Subsequently, sections were micro waved in 10 mM citrate buffer pH 6.0 and endogenous peroxidase activity was quenched with 0.5% H₂O₂. Non-specific binding sites were blocked with 10% normal goat serum. Then, sections were stained with primary antibody mouse monoclonal anti-neurofilament (NF, Abcam, Cambridge, UK, 1: 1000) or goat monoclonal anti-neuropeptide Y (NPY, Santa Cruz Biotechnology, CA, USA, 1:1000) followed by incubation with peroxidase-conjugated anti-mouse/goat IgG (DakoCytomation, Glostrup, Denmark) for 30 min. Sections were counterstained with Mayer's hematoxylin, coverslipped with an aqueous mounting medium and examined using a photomicroscope equipped with an automated camera (Nikon Eclipse 80i, Nikon Co.). Controls from adjacent sections were subjected to the same staining, with omission of the primary antibody.

3.2.6 Transmission electron microscopy (TEM)

To analyze the ultra structural characteristics of nerve fibres, one decalcified sample from each group was randomly selected after isolation of the implants. Following fixation with 2% glutaraldehyde in 0.05 M cacodylate buffer (pH 7.3), samples were post-fixed in 2% osmium tetroxide for 1 h, and stained with 2% uranyl acetate in 10% acetone for 20 min. Subsequently, samples were put through dehydrating series of graded concentrations of acetone, and embedded in araldite. Serial ultrathin sections (~0.06 μ m) were mounted on 0.7% formvar coated copper grids, contrasted with 0.5% uranyl acetate and a stabilized solution of lead citrate, and examined in a TEM (Philips EM 208, Eindhoven, The Netherlands) operated at 80 kV. The microscope was provided with a Morada Soft Imaging System (SIS: Olympus, Tokyo Japan) camera to acquire high resolution images of the evaluated samples. Images were processed digitally with iTEM-FEI software (Olympus SIS).

3.2.7 Histomorphometric analysis

Three serial sections from each sample were digitized using MiraxScan (Carl Zeiss, Göttingen, Germany) and evaluated to get an overall mean value. The density of nerve fibres (N/mm^2 , number of myelinated nerve fibres per area), were evaluated by one experienced observer (Y.H.) who was blinded to implant groups, at a magnification of $100\times$ with a 17-inch LCD monitor (Dell, CA, USA.) using an image software package (Panoramic Viewer, Hungary). Four regions of interest (ROIs) at a distance of $300\ \mu m$ from the implant were selected (Figure 3.2) as an approximate width of the periodontal ligament (PDL) because this is the region mostly affected by loading transmission through implants.²⁰ The following morphological predictors of regeneration were further estimated in four ROIs (Figure 3.3) in the peri-implant bone and crestal gingiva tissues above placed implants: fibre diameter (D , μm , the outer diameter of the myelinated fibre), axon diameter (d , μm , the diameter of the axon proper) and g-ratio (d/D , a functional and structural index of optimal axonal myelination).²¹ To acquire a maximum precision, the D and d were measured using the “lesser fibre diameter” method, defined as the maximum diameter across the lesser aspect of the nerve fibre and axon, to prevent any kind of potential distortion.¹⁹ Partial fibres at the borderline of ROI were excluded.

3.2.8 Statistical analysis

In order to fully consider the potential fixed and random effects in the split-mouth design, the linear mixed model was used after appropriate transformation of the raw data, including the fixed effects of implant groups, jaws (upper vs. lower), regions (from the gingiva to apex), their two-way and three-way interaction terms, the random effects of dogs and error terms, with the number of measurements in each region and dog as weights. The region comparisons and the implant group comparisons were respectively performed due to the significance of the three-way interaction effect (group*jaw*region). All the hypotheses testing were implemented in SAS 9.2 at a significance level of 0.05.

3.3 Results

All animals recovered well and without any clinical signs of inflammation during the experimental period, and all implants were clinically stable until euthanasia. The peri-implant bone and soft tissue were overall healthy.

The histological observation illustrated myelinated nerve fibres in the peri-implant crestal gingiva, the woven bone around the implants as well as the osteons near implant threads (Figure 3.4A-D). Nerve fibres were mainly distributed perivascularly with frequent branching, and orientated along the axis of the blood vessels. These myelinated fibres were also located at natural extraction healing socket and in the Haversian canal of an osteon (Figure 3.4E-F). NF and NPY immunoreactivity (Figure 3.4G-H) further confirmed the existence of myelinated nerve fibres in the peri-implant bone and gingiva. Ultrastructurally (Figure 3.4I-J), myelinated nerve fibres were without obvious defects and occasionally accompanied by unmyelinated nerve fibres and the peripherally oriented mitochondria were identified, characteristic for type A-delta nerve endings. Gingiva regions demonstrated a significantly greater ($p < 0.05$) amount of innervation than any peri-implant bone region (Figure 3.5), though this difference was not fully significant in the maxilla. In the peri-implant bone regions, the nerve density increased in apical direction with statistical significance, except in the DIP+IL group in the maxilla. There was another trend that nerve density around mandible implants was higher compared to those around maxilla implants, especially in the peri-implant gingiva of the three implant groups. Nerve density in implant groups was higher compared to the control bone sites, especially in the mandible. The IIP+IL group had the highest density in both jaws, though the statistical differences of nerve density between three implant groups were mostly seen in the gingival and apical region. No difference in nerve density between the DIP+DL and DIP+IL groups was observed ($P > 0.05$).

Further morphological analyses on predictors of regeneration of myelinated nerve fibres showed that all implant groups had slightly smaller fibre diameter when compared to the natural extraction and healing group (Table 2), especially in the

mandible. The fibre diameter and axon diameter in the IIP+IL group was greater than in the DIP+DL and DIP+IL group, or with a tendency towards significance. Whereas for g-ratio, smaller values were observed in the IIP+IL group than those obtained in the DIP+DL and DIP+IL group in both gingiva and bone regions around implants, which could be related to an increased degree of the myelination. No significant differences in measured fibre diameter, axon diameter and g-ratio were however observed when comparing the delayed implant placement, whether or not with immediate implant loading (DIP+DL vs. DIP+IL, $P > 0.05$).

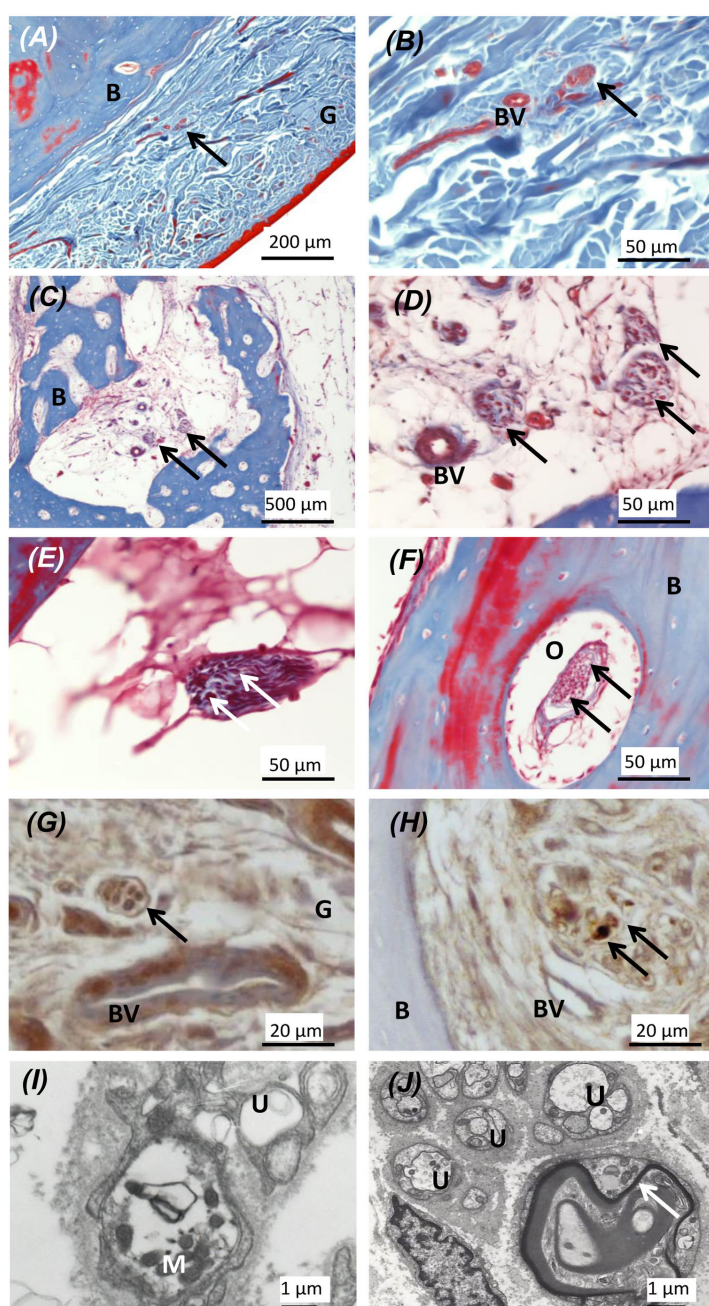


Figure 3.4: Decalcified sections stained with Masson trichrome stain (A-F), neurofilament protein (G), neuropeptide Y (H) positive expression and observation of transmission electron microscopy (I-J). (A) Myelinated nerve fibres existed in the peri-implant crestal gingiva (DIP+IL group). (B) A magnification of (A) showing a bundle of nerve fibres and blood vessel; (C) Myelinated nerve fibres presented in the woven bone area at apical region (IIP+IL group); (D) A magnification of (C) showing several bundles of myelinated nerve fibres accompanied by a blood vessel; (E) A bundle of myelinated nerve fibres was observed at the middle region of natural extraction healing socket (Control group); (F) Myelinated nerve fibres were located in the Haversian canal of an osteon at apical region (DIP+DL group). (G) Myelinated nerve fibres were identified in the crestal gingiva around implants (Control group); (H) Cross-sectioned myelinated

nerve fibres were shown in peri-implant bone tissue (Control group); (I) Unmyelinated afferent nerve ending, which normally could not be distinguished under the light microscopy, was enveloped by a thin lamina of Schwann cell sheets, characterized by the peripheral localization of mitochondria (IIP+IL group); (J) A bundle of unmyelinated and one myelinated nerve fibre in the peri-implant bone tissue (DIP+IL group). Arrows indicates myelinated nerve fibres; B, bone; G, gingiva; BV, blood vessel; O, osteon; M, mitochondria; U, unmyelinated nerve fibres.

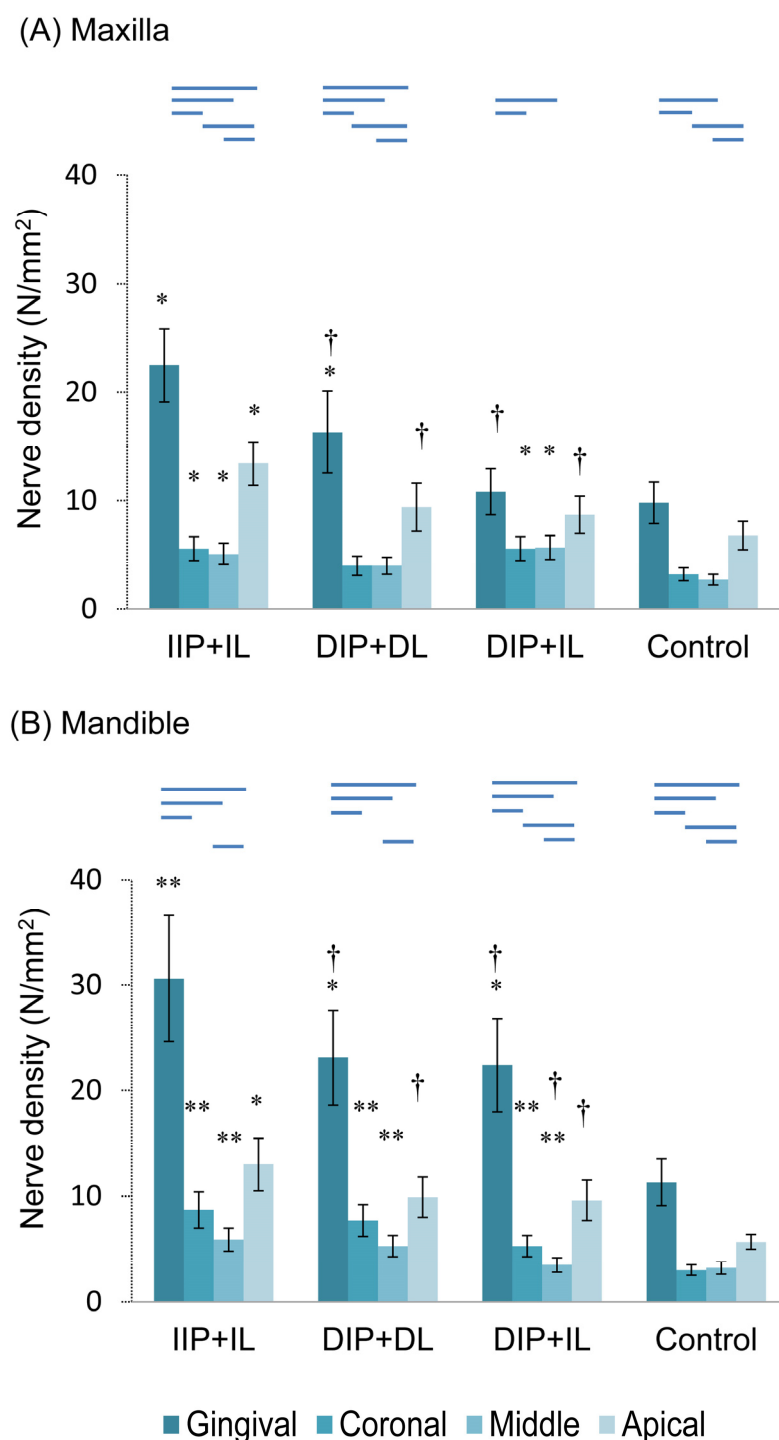


Figure 3.5: The distribution of mean nerve density of myelinated axons (N/mm^2) in each region for different groups. (A) Maxilla ($n = 12$); (B) Mandible ($n = 20$). The bar and the end of the whisker represent the mean of nerve density and standard error respectively. Statistical differences within regions in the same implant group are indicated by horizontal bars above and extending to the mid points of histogram ($p < 0.05$). Statistical differences of implant groups compared to the control group in the same region (*, $p < 0.05$; **, $p < 0.001$). Statistical differences of other groups compared to the IIP+IL group in the same region (†, $p < 0.05$).

Table 3.2: Comparison of histomorphometric parameters of regenerated nerve fibres for different groups

Histomorphometric parameters	Maxilla (n=12)				Mandible (n=20)			
	Gingiva	Coronal	Middle	Apical	Gingiva	Coronal	Middle	Apical
Fibre diameter (μm)								
IIP+IL	1.23 (0.02)	1.42 (0.08)*	1.18 (0.08)	1.35 (0.03)	1.10 (0.02)*	1.38 (0.05)*	1.37 (0.05)*	1.32 (0.02)
DIP+DL	1.20 (0.05)*†	1.40 (0.20)*	1.07 (0.18)*†	1.34 (0.05)	1.09 (0.02)*	1.34 (0.06)*†	1.36 (0.09)*	1.29 (0.02)
DIP+IL	1.21 (0.03)*	1.29 (0.09)*†	1.14 (0.09)*	1.23 (0.04)*††	1.04 (0.03)*	1.14 (0.07)*†	1.22 (0.13)*†	1.20 (0.04)*†
Control	1.29 (0.03)	1.48 (0.18)	1.23 (0.19)	1.37 (0.07)	1.13 (0.02)	1.66 (0.20)	1.64 (0.13)	1.34 (0.05)
Axon diameter (μm)								
IIP+IL	0.87 (0.02)*	1.05 (0.04)*	0.87 (0.05)	0.98 (0.02)*	0.83 (0.02)*	0.94 (0.03)*	0.89 (0.05)*	0.92 (0.01)*
DIP+DL	0.86 (0.03)*	1.01 (0.11)*	0.80 (0.05)*†	0.97 (0.03)*	0.82 (0.02)*	0.93 (0.05)*	0.88 (0.06)*	0.91 (0.02)*
DIP+IL	0.86 (0.03)*	0.92 (0.05)*†	0.86 (0.05)*	0.91 (0.02)*††	0.79 (0.02)*†	0.79 (0.06)*†	0.83 (0.09)*†	0.89 (0.03)*†
Control	0.97 (0.02)	1.18 (0.12)	0.93 (0.13)	1.08 (0.05)	0.88 (0.02)	1.17 (0.15)	1.24 (0.10)	1.03 (0.03)
G-ratio								
IIP+IL	0.68 (0.01)*	0.70 (0.03)*	0.74 (0.03)	0.72 (0.01)*	0.75 (0.01)*	0.68 (0.02)*	0.64 (0.04)**	0.69 (0.01)**
DIP+DL	0.73 (0.02)†	0.75 (0.08)†	0.75 (0.07)	0.73 (0.02)*	0.75 (0.01)*	0.69 (0.03)	0.67 (0.03)*†	0.72 (0.01)* *†
DIP+IL	0.71 (0.01)*†	0.71 (0.04)*	0.75 (0.04)	0.74 (0.01)	0.76 (0.01)	0.69 (0.03)	0.68 (0.05)*†	0.74 (0.01)* †
Control	0.75 (0.01)	0.80 (0.07)	0.76 (0.07)	0.79 (0.03)	0.78 (0.01)	0.71 (0.08)	0.76 (0.05)	0.77 (0.02)

Values are shown as estimate mean (SE). Significant difference (*, $p < 0.05$; **, $p < 0.001$) of implant groups and the control group in the same region. Significant differences (†, $p < 0.05$; ††, $p < 0.001$) of other groups and the IIP+IL group in the same region.

3.4 Discussion

As far as we know, this is the first time that a histomorphological change of myelinated nerve fibres following different loading protocols in the peri-implant hard and soft tissues has been described in a randomized controlled animal experiment, focusing on the clinical hypothesis of osseoperception of dental implants could be potentially improved by applying immediate implant placement and loading protocol. The present findings may be of particular importance for understanding the underlying mechanisms of osseoperception and optimizing of the physiological integration of implant-supported prostheses and its clinical significance.

To minimize the potential bias and variations (*e.g.*, dynamic loading forces in the mouth) between experimental animals, a split-mouth design was used in this study to assist the comparison under standardized healing and test conditions. Based on this unique design with randomized implant recipient site selection and isolated loading conditions of individual implants, the potential carry-over effects could be excluded.²²

After a 10-month complete decalcification process, we were able to confirm the presence of myelinated nerve fibres adjacent to implants and quantified their distribution features by maintaining fine structure of nerve fibres. As the cytoskeletal elements in axon and as the sympathetic neurotransmitter,²³ NF and NPY were found in the same nerve fibres, suggesting that these regenerated nerves next to the bone trabeculae could have a sensory and/or sympathetic origin. TEM observation was in line with an ultrastructure study supporting the possibility of sympathetic modulation of peri-implant mechanoreceptors.²⁴

In the present study, myelinated nerve fibres reached the highest density in the gingival region and in the apical region for all groups, which was probably contributed by the numerous local blood supply and innervation originally present in the PDL. Similarly, it was reported that the apical region of natural teeth is highly innervated where the PDL received most loading.^{2,19} The differences of nerve density between left and right

sites of jaws were not significant, which was consistent with another morphological study.²⁵ Due to the small sample size in the maxilla, there was only a tendency that nerve density around mandible implants is higher than around maxilla implants. Nevertheless, it presented histological evidence to the clinical observation that mandibular teeth and implants might be more sensitive to tactile tests.²⁶

Previous morphometric studies which reported the existence of free nerve endings in the peri-implant tissues were mostly qualitatively or semi-quantitatively,²⁷ not to mention a comprehensive comparing between various implant protocols. The main results found in our study were an higher nerve density, greater fibre diameter and axon diameter for implants immediately placed and loaded. It should be mentioned that not all comparisons reached statistical significance, yet the limits related to animal research, sample size and animal variability which may have prevented reaching significance. The fact that fibre diameter and axon diameter increased when immediately placed implants were also immediately loaded might indicate a better peri-implant innervation recovery.^{28,29} While the mechanism is still unclear, it can be assumed that immediate implant placement after extraction leaves the nerves in place with activation preventing degeneration. Upon implant loading, sufficient stimulation of dedifferentiated Schwann cells and/or activation of peri-implant nerve signals might occur to promote peri-implant nerve regeneration. Furthermore, these immediately placed and loaded implants also show thicker myelin sheaths, in accordance to previous research.³⁰

On the other hand, higher innervation density together with smaller fibre diameter and g-ratio presented in the implant groups than in the natural extraction healing group. It can be hypothesized that myelinated nerve fibres become more sprouted and smaller as they receive mechanical loading transmitted via implant surface, thus the fibre diameter was smaller than those observed in the natural healing sites. Moreover, the g-ratio could significantly decreased when regeneration became stabilized in a long-term study.²¹ Despite a shorter loading duration in DIP+DL, it was believed to be

sufficient after implant placement since the regeneration of vascular and neural elements in the PDL was almost completed by 4 weeks after replantation.³¹ Whether these regenerated nerves around implants could continue to mature and develop to larger fibre diameter remains to be elucidated in further studies using longer follow-ups.

However, it is worth noting some limitations of this study. First, as we are aiming to compare clinically relevant immediate vs. delayed implant loading protocols, an unloaded implant control was therefore not included for comparison. Nevertheless, this concern might be addressed by the fact that more free nerve endings have already been found around delayed loaded implants than non-loaded control implants after a 3 month observation period.¹⁷ Second, despite the neurophysiological and psychophysical evidence, it is not yet fully clear whether those differences in morphometric parameters resulted in the actual sensory activation with clinical significance. There is evidence that neural receptors around implants could evoke sensory nerve action potential of the inferior alveolar nerve stem following electrical stimulus,³² or possess a higher tactile threshold after implant rehabilitation.¹¹ Besides, the morphological findings in this study would, in turn, prompt related mechanism studies and hypotheses, such as local graft of Schwann cell or calcitonin gene-related peptide-alpha to improve peripheral nerve fibers regeneration after dental implant surgery.^{33,34} Finally, this study provided a general animal model for the assessment of reinnervation around implants, yet precise-defined loading frequency, implant surface designs, implant-supported restorations and masticatory behaviors were not included which might favor the generalization of our findings.

3.5 Conclusions

Based on the histomorphometric exploratory of the origin and distribution of peri-implant innervation, the current study helped to uncover the tendency that the immediately placed and loaded implant group may have an improved peri-implant innervation pattern, including higher nerve density, larger fibre diameter and axon

diameter, and more axonal myelination. The effective intervention for producing appropriate functional neurons may broaden osseoperception to more challenging levels and evolve with osseointegration in the oral environment as well as in ENT and orthopedics. Further research is required examining the functional role of the identified nerve fibres and establishing the potential morpho-physiological relationship.

References

1. Jacobs R, van Steenberghe D. Role of periodontal ligament receptors in the tactile function of teeth: a review. *J Periodontal Res* 1994; **29**: 153-167.
2. Trulsson M. Sensory-motor function of human periodontal mechanoreceptors. *J Oral Rehabil* 2006; **33**: 262-273.
3. Svensson KG, Grigoriadis J, Trulsson M. Alterations in intraoral manipulation and splitting of food by subjects with tooth- or implant-supported fixed prostheses. *Clin Oral Implants Res* 2013; **24**: 549-555.
4. Mason AG, Holland GR. The reinnervation of healing extraction sockets in the ferret. *J Dent Res* 1993; **72**: 1215-1221.
5. Brånemark P-I. Osseointegration: biotechnological perspective and clinical modality. In: Brånemark P-I, Rydevik B, Skalak Rs, (ed.) Proceedings of the Osseointegration in skeletal reconstruction and joint replacement. Quintessence Publishing Co, 1997: 1-24.
6. van Steenberghe D. From osseointegration to osseoperception. *J Dent Res* 2000; **79**: 1833-1837.
7. Jacobs R, van Steenberghe D. From osseoperception to implant-mediated sensory-motor interactions and related clinical implications. *J Oral Rehabil* 2006; **33**: 282-292.
8. Jacobs R. Neurological versus psychophysical assessment of osseoperception In: Jacobs R(ed.) Proceedings of the Osseoperception. Catholic University Leuven, 1998: 75-88.
9. Jacobs R, van Steenberghe D. Comparative evaluation of the oral tactile function by means of teeth or implant-supported prostheses. *Clin Oral Implants Res* 1991; **2**: 75-80.
10. Enkling N, Heussner S, Nicolay C *et al.* Tactile sensibility of single-tooth implants and natural teeth under local anesthesia of the natural antagonistic teeth. *Clin Implant Dent Relat Res* 2012; **14**: 273-280.
11. Kazemi M, Geramipanah F, Negahdari R *et al.* Active Tactile Sensibility of Single-Tooth Implants versus Natural Dentition: A Split-Mouth Double-Blind Randomized Clinical Trial. *Clin Implant Dent Relat Res* 2013.
12. Habre-Hallage P, Dricot L, Jacobs R *et al.* Brain plasticity and cortical correlates of osseoperception revealed by punctate mechanical stimulation of osseointegrated oral implants during fMRI. *Eur J Oral Implantol* 2012; **5**: 175-190.
13. Habre-Hallage P, Dricot L, Hermoye L *et al.* Cortical activation resulting from the stimulation of periodontal mechanoreceptors measured by functional magnetic resonance imaging (fMRI). *Clin Oral Investig* 2014.

14. Lambrechts I. Histological and ultrastructural aspects of bone innervation In: Jacobs R(ed.) Proceedings of the Osseoperception. Catholic University Leuven, 1998: 13-20.
15. Suzuki Y, Matsuzaka K, Ishizaki K *et al.* Characterization of the peri-implant epithelium in hamster palatine mucosa: behavior of Merkel cells and nerve endings. *Biomed Res* 2005; **26**: 257-269.
16. Yamaza T, Kido MA, Wang B *et al.* Distribution of substance P and neurokinin-1 receptors in the peri-implant epithelium around titanium dental implants in rats. *Cell Tissue Res* 2009; **335**: 407-415.
17. Wada S, Kojo T, Wang YH *et al.* Effect of loading on the development of nerve fibers around oral implants in the dog mandible. *Clin Oral Implants Res* 2001; **12**: 219-224.
18. Huang Y, Van Dessel J, Liang X *et al.* Effects of Immediate and Delayed Loading on Peri-Implant Trabecular Structures: A Cone Beam CT Evaluation. *Clin Implant Dent Relat Res* 2013.
19. Huang Y, Corpas LS, Martens W *et al.* Histomorphological study of myelinated nerve fibres in the periodontal ligament of human canine. *Acta Odontol Scand* 2011; **69**: 279-286.
20. Weiner S, Klein M, Doyle JL *et al.* Identification of axons in the peri-implant region by immunohistochemistry. *Int J Oral Maxillofac Implants* 1995; **10**: 689-695.
21. Muratori L, Ronchi G, Raimondo S *et al.* Can regenerated nerve fibers return to normal size? A long-term post-traumatic study of the rat median nerve crush injury model. *Microsurgery* 2012; **32**: 383-387.
22. Lesaffre E, Philstrom B, Needleman I *et al.* The design and analysis of split-mouth studies: what statisticians and clinicians should know. *Stat Med* 2009; **28**: 3470-3482.
23. Georgiou M, Bunting SC, Davies HA *et al.* Engineered neural tissue for peripheral nerve repair. *Biomaterials* 2013; **34**: 7335-7343.
24. Lambrechts I, Creemers J, vandenabeele F *et al.* Possible sympathetic modulation of periodontal ligament mechanoreceptors. An ultrastructural study. *Biology of the Cell* 1995; **84**: 230-230(231).
25. Long A, Loescher AR, Robinson PP. A Quantitative Study on the Myelinated Fiber Innervation of the Periodontal-Ligament of Cat Canine Teeth. *J Dent Res* 1995; **74**: 1310-1317.
26. Yoshida K. Tactile threshold for static and dynamic loads in tissue surrounding osseointegrated implants In: Jacobs Rs, ed. Proceedings of the Osseoperception. Catholic University Leuven, 1998: 143-156.
27. Huang Y, Jacobs R, Van Dessel J *et al.* A systematic review on the innervation of peri-implant tissues with special emphasis on the influence of implant placement and

loading protocols. *Clin Oral Implants Res* 2014.

28. de Medinaceli L. Interpreting nerve morphometry data after experimental traumatic lesions. *J Neurosci Methods* 1995; **58**: 29-37.

29. Wolthers M, Moldovan M, Binderup T *et al.* Comparative electrophysiological, functional, and histological studies of nerve lesions in rats. *Microsurgery* 2005; **25**: 508-519.

30. Ikeda M, Oka Y. The relationship between nerve conduction velocity and fiber morphology during peripheral nerve regeneration. *Brain Behav* 2012; **2**: 382-390.

31. Yamada H, Maeda T, Hanada K *et al.* Re-innervation in the canine periodontal ligament of replanted teeth using an antibody to protein gene product 9.5: an immunohistochemical study. *Endodont Dent Traumatol* 1999; **15**: 221-234.

32. Qiao SC, Lv XF, Zhuang LF *et al.* [Animal study of sensory function of nerve fibers surrounding dental implant]. *Shanghai Kou Qiang Yi Xue* 2011; **20**: 119-124.

33. Ma L, Xiang L, Yao Y *et al.* CGRP-alpha application: a potential treatment to improve osseoperception of endosseous dental implants. *Med Hypotheses* 2013; **81**: 297-299.

34. Yuan Q, Gong P, Tan Z. Schwann cell graft: a method to promote sensory responses of osseointegrated implants. *Med Hypotheses* 2007; **69**: 800-803.

Chapter 4

Validating cone-beam computed tomography for peri-implant bone morphometric analysis

This chapter is based on following manuscript:

Validating cone-beam computed tomography for peri-implant bone morphometric analysis

Yan Huang, Jeroen Van Dessel, Maarten Depypere, Mostafa EzEldeen, Alexandru Andrei Iliescu, Emanuela Dos Santos, Ivo Lambrichts, Xin

Liang, Reinhilde Jacobs

Submitted to ***Bone Research***

[Conditional Acceptance]

Abstract

Cone-beam computed tomography (CBCT) has been recently used to analyse trabecular bone structure around dental implants. To validate the use of CBCT for three-dimensional (3D) peri-implant trabecular bone morphometry by comparing it to two-dimensional (2D) histology, thirty-six alveolar bone samples (with implants n=27 vs. without implants n=9) from 6 mongrel dogs, were scanned *ex vivo* using a high resolution (80 μm) CBCT. After scanning, all samples were decalcified and then sectioned into thin histologic sections ($\sim 6 \mu\text{m}$) to obtain high contrast 2D images. By using CTAn imaging software, bone morphometric parameters including trabecular number (Tb.N), thickness (Tb.Th), separation (Tb.Sp) and bone volume fraction (BV/TV) were examined on both CBCT and corresponding histologic images. Higher Tb.Th and Tb.Sp, lower BV/TV and Tb.N were found on CBCT images ($P < 0.001$). Both measurements on the peri-implant trabecular bone structure showed moderate to high correlation ($r=0.65-0.85$). The Bland-Altman plots showed strongest agreement for Tb.Th followed by Tb.Sp, Tb.N and BV/TV, regardless of the presence of implants. The current findings support the assumption that peri-implant trabecular bone structures based on high-resolution CBCT measurements are representative for the underlying histologic bone characteristics, indicating a potential clinical diagnostic use of CBCT-based peri-implant bone morphometric characterization.

4.1 Introduction

Bone quality, which is a significant determinant of the survival rate of an implant,^{1,2} depends on the bone mineral density as well as the spatial structure of trabecular bone.³ ⁴ To determine the internal structural properties of peri-implant trabeculae, a proper quantitative morphometry with the imaging resolution superior to trabecular dimensions is desirable.⁵

Conventionally, bone structure could be assessed *in vitro* by histomorphometry. This approach remains the gold standard due to its high spatial resolution and image contrast, though it is time-consuming and destructive for secondary measurements.⁶ Another alternate technique to quantify bone structure *in vitro* is micro-computed tomography (micro-CT), which has been mainly applied in small animal bones and bone biopsies. *In vivo* imaging of trabecular bone structure is feasible using high resolution magnetic resonance imaging and multi-slice CT,^{7,8} but these are limited by metal artefacts (MRI/CT) or abundant radiation exposure (CT). In contrast, cone-beam computed tomography (CBCT), as an easily available clinical imaging modality developed since the late 1990s,^{9,10} offers an efficient non-invasive scanning in combination with higher spatial resolution, reduced radiation dose and scan costs.^{11,12}

The value of CBCT in clinical practice has been largely demonstrated in oral and maxillofacial pathology, surgery and implantology.¹³ Nevertheless, only a few studies described the use of CBCT for trabecular bone structure assessment.^{12,14,15} Recently, this imaging modality was utilized in a pilot study for analyzing peri-implant trabecular bone morphology.¹⁶ To date, although CBCT for bone morphometric evaluation has been validated with other imaging acquisition modalities such as micro-CT¹⁷ or conventional CT¹⁸ in human cadavers, less is known about the effectiveness and accuracy of CBCT in comparison to histomorphometry, especially in the peri-implant bone area, which will actually add to understanding of previous 3D findings, and help to explain the mechanical behavior of bone tissues.

Therefore, the aim of this study was to verify the accuracy of high-resolution CBCT in peri-implant trabecular bone structure analyses using histology as a reference.

4.2 Materials & methods

4.2.1 Samples

The current samples consisted of 27 alveolar bone biopsies with custom-made implants and 9 alveolar bone biopsies without the implants (natural healing after teeth extraction, Table 4.1) retrieved from six mongrel dogs (male, weight 14.8-18.1 kg, age 20-24 months old). The detail of biopsies were outlined in a previous study.¹⁶ Briefly, all dogs were sacrificed by means of an intravenous injection of an overdose 0.1 ml/kg Xylazine Hydrochloride (Changchun Military Academy of Medical Sciences, China). The jawbones were dissected and defleshed. Then, each implant was removed with a careful preservation of 3- to 5 mm peri-implant bone as one piece of sample. The experiment protocol was in accordance with the ethical guidelines of KU Leuven (P059-2012-TK).

Table 4.1: *Distribution of alveolar bone samples in six experimental dogs*

Group	I (R)	I (L)	P3 (R)	P3 (L)	P4 (R)	P4 (L)	Total
Bone with implants	4	5	5	5	4	4	27
Bone without implants	2	1	1	1	2	2	9

I = 3rd maxillary incisors; P3 = 3rd mandibular premolars; P4 = 4th mandibular premolars; R = right side; L = left side; implants, custom-made threaded, grade five pure titanium, machined surface, $\varnothing = 3.1$ mm for I and 4.1 mm for P3 and P4, L = 11 mm.

4.2.2 CBCT image acquisition

All the bone samples were scanned using a high resolution CBCT (Accuitomo 170, Morita, Japan). The exposition and reconstruction parameters for the scan were as following: 0.08 mm voxel size, 360° rotation, ~950 projections, 90 kV tube voltage,

2.0 mA tube current, 30.8 s scanning time, 40×40 mm field of view (FOV), CsI-aSi flat panel detector and 43 (lower jaw)-54 (upper jaw) μSv effective dose.¹⁹ To prevent any movement during the scanning process, each sample was mounted vertically into a sponge block, with the long axis of the implant perpendicular to the scanning beam. The calibration of CBCT imager was performed by the manufacturer before the radiographic study.

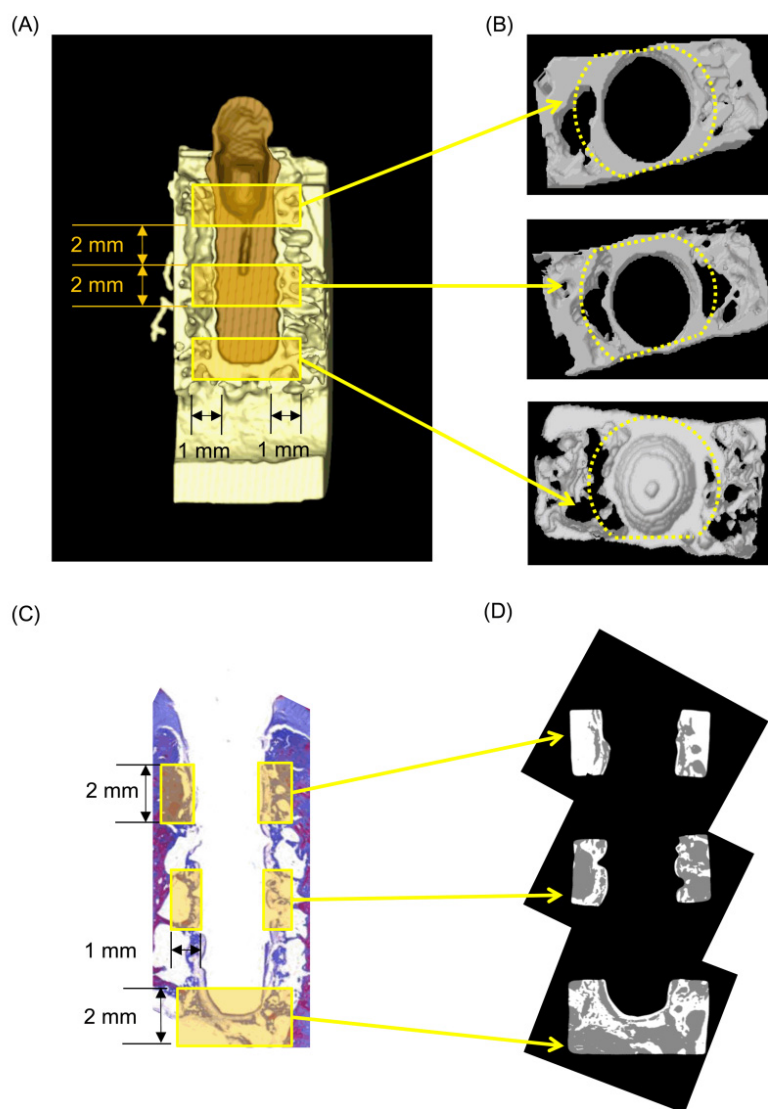


Figure 4.1: (A) Three-dimensional models reconstructed from CBCT images in the coronal plane (mesial-distal view); (B) Three volumes of interest (VOIs, coronal, middle & apical levels) were automatically selected from (A) along the surface of implant by a custom processing algorithm based on thresholding segmentation; (C) Histologic slice of bone specimens (trichrome Masson stain; magnification $\times 5$) showed the trabecular bone (blue) and bone marrow (pink); (D) Trabecular bone in the binarized histologic image at three manually selected regions of interest (ROIs).

The original CBCT data were reconstructed as 3D images by CTAn V1.11 software (CTAnalyser, Skyscan, Antwerp, Belgium). Three ring-shaped volumes of interest (VOIs) were automatically selected in a distance of 1 mm away from the surface of the implant, at coronal, middle and apical sections along the axis of the implant as

indicated in Figure 4.1A. The VOIs was selected through intermediate cross sections by using a custom processing by an experienced observer (JVD).

4.2.3 Histology

After CBCT analysis, the samples were decalcified in 0.5 M EDTA phosphate buffered saline (pH 7.4) at 4°C for 10 months. The implants were then removed from the specimens using surgical forceps. Followed by the dehydration and embedding in paraffin, thin serial sections (~6 µm) were sectioned along the mesial-distal direction in the middle of the implant or extraction area, where more trabecular bone could be observed. The most central cut sections, corresponding to the greatest dimensions of the samples in length and diameter, were selected and stained with the trichrome Masson stain.

Digital microscopic images of 2D histologic sections were captured by an automated and calibrated camera (Nikon Eclipse 80i, Nikon Co.) and then transferred to gray-level images. The gray-level images were transformed to binary images, enabling a clear separation of trabecular bone and bone marrow (image J, NIH). Similar regions of interest (ROIs) in the mesial-distal plane, as previously defined in the CBCT measurements, were manually selected by one trained observer (EDS) independently. Those selected ROIs were then exported as BMP images and imported into trabecular bone analysis software CTAn for a semi-automatic 2D histomorphometry. Three sections per sample were averaged. All observations were guaranteed to use a standard PC (Intel Pentium Dual-Core, CPU at 3.20GHz, 4GB of RAM, and a 64-bit operating system) with a 17-inch LCD monitor (Dell, CA, USA.).

4.2.4 Morphometric analysis

CBCT provided measurements obtained directly from reconstructed images based on consecutive 2D images. Only those 3D morphometric parameters that could be compared with 2D histomorphometric measurements were selected for this study. Therefore, 2D and 3D parameters of trabecular bone architecture, which are most commonly used and directly measured,²⁰ were quantified from CBCT images (VOIs) and histologic images (ROIs) using 3D and 2D imaging processing in CTAn respectively, following the recommendations of the American Society of Bone and Mineral Metabolism²¹ and Parfitt's system.²² The formulas and correspondence between these 2D and 3D measurement were described in Table 4.2. All parameters assumed a plate model for the trabecular bone in the derivation of the equations used for calculation, as a previous study observed for the bone samples used in this study.¹⁶

Table 4.2: Trabecular morphologic parameters quantified from CBCT and histologic images in selected regions of interest and volumes of interest, based on the parallel plate model

Morphologic parameter	Abbreviation	Unit	2D measurements	3D measurements
Bone volume fraction	BV/TV	%	$(A_B/A_T)100$	BV/TV
Trabecular thickness	Tb.Th	mm	$(2/1.199)(A_B/P_B)$	2BV/BS
Trabecular separation	Tb.Sp	mm	$(2/1.199)(A_T - A_B)/P_B$	1/Tb.N – Tb.Th
Trabecular number	Tb.N	mm ⁻¹	$(1.199/2)(P_B/A_T)$	$(BV/TV)/Tb.Th$

A_B = bone area; A_T = total area; P_B = bone perimeter; BV = bone volume; TV = tissue volume; BS = bone surface.

4.2.5 Statistical analysis

Results were summarized by descriptive statistics as mean values with standard deviations and coefficient of variation. Wilcoxon signed-rank test and Spearman correlation test were adopted among all variables analyzed in the study, after the normality test for the distribution of data by means of Shapiro-Wilks test. All the hypotheses testing were implemented in STATISTICA 8.0 (StatSoft, Inc., Tulsa, USA)

at a significance level of 0.05. The degree of agreement between the measured parameters from CBCT and histologic data was compared using the method of Bland and Altman. In this method, the difference between the measurements was plotted against their mean, which was considered to be the best estimate of the true values.

4.3 Results

In total, 36 alveolar bone samples (27 with implants and 9 without implants) were analyzed. Normal distribution was checked first for all continuous variables according to Shapiro-Wilk test ($p < 0.05$). Descriptive statistics of all variables were presented in Table 4.3. Wilcoxon signed-rank test showed significant differences between the CBCT and histology for all morphometric parameters ($p < 0.001$). Although Tb.Th and Tb.Sp were higher on CBCT images than on histologic images, lower BV/TV and Tb.N were also found on CBCT images. The Spearman correlation between CBCT and histology for all analyzed parameters showed significant correlation at $P < 0.04$.

Bland-Altman plots (Figure 4.2) indicated systematic bias, including constant bias for BV/TV, Tb.Sp and Tb.N, and proportional bias for Tb.Th. For the samples with implant, the smallest bias of measurements in Tb.Th (-0.12 mm) followed by Tb.Sp (-0.28 mm), Tb.N (+0.84 mm⁻¹) and BV/TV (+23%). For the samples without implant, the smallest bias of measurements in Tb.Th (-0.13 mm) followed by Tb.Sp (-0.23 mm), Tb.N (+0.67 mm⁻¹) and BV/TV (+14.02 %). The lines of mean under the zero showed a slight overestimation of Tb.Sp and Tb.Th (Figure 4.2 C-F), and the lines of mean above the zero demonstrated a slight underestimation of Tb.N by CBCT as compared with the histology (Figure 4.2 G-H).

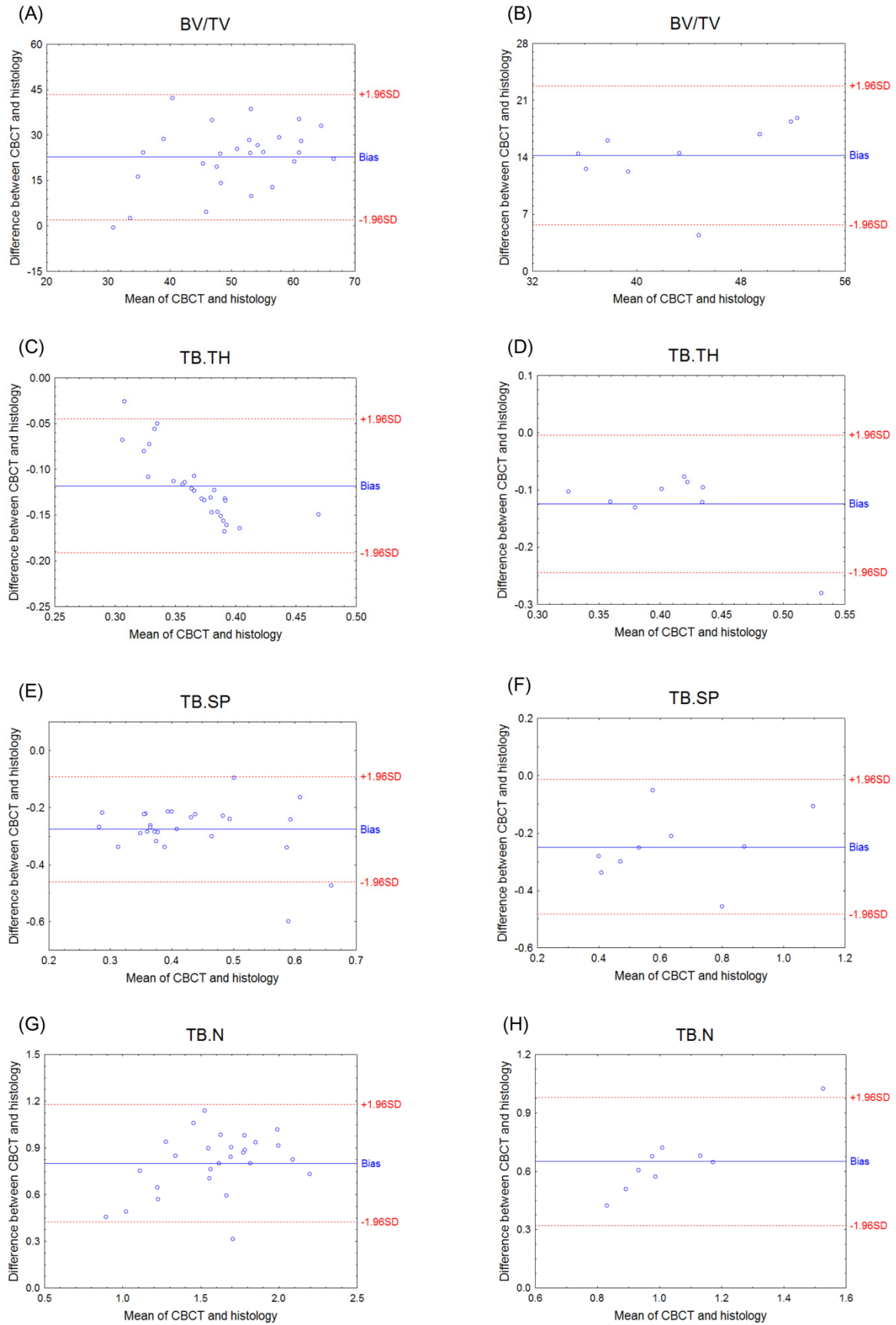


Figure 4.2: Bland–Altman plot comparing the agreement between cone-beam CT (CBCT) and

histology in the bone samples with implant (A, C, E, G) and without implant (B, D, F, H) for the following bone structural parameters measurements: bone volume fraction (BV/TV), bone thickness (Tb.TH), bone separation (Tb.Sp) and trabecular number (Tb.N). Positive values represented larger BV/TV and Tb.N obtained from histologic data compared with CBCT (A, B,G, H), while negative values showed smaller Tb.TH and Tb.Sp calculated from histology when comparing CBCT (C - F). The dotted lines on the Bland-Altman plot indicated the mean difference \pm 1.96SD (standard deviation).

Table 4.3: Comparison of morphometric parameters obtained by CBCT and histology

Morphometric parameters	CBCT		Histology		Wilcoxon	Spearman's
	Mean (SD)	CV	Mean (SD)	CV	P	r (P)
Bone with Implant (N=27)						
BV/TV (%)	39.21 \pm 9.21	0.23	62.7 \pm 11.9	0.19	<.001	0.65 (<.001)
Tb.Th (mm)	0.43 \pm 0.05	0.11	0.31 \pm 0.02	0.07	<.001	0.75 (<.001)
Tb.Sp (mm)	0.57 \pm 0.13	0.22	0.29 \pm 0.10	0.35	<.001	0.67 (<.001)
Tb.N (mm ⁻¹)	1.19 \pm 0.21	0.25	1.99 \pm 0.37	0.19	<.001	0.85 (<.001)
Bone without Implant (N=9)						
BV/TV (%)	36.26 \pm 6.15	0.33	50.50 \pm 7.72	0.16	<.001	0.82 (<.006)
Tb.Th (mm)	0.47 \pm 0.08	0.17	0.35 \pm 0.04	0.02	<.001	0.68 (<.04)
Tb.Sp (mm)	0.77 \pm 0.23	0.30	0.52 \pm 0.26	0.51	<.001	0.88 (<.002)
Tb.N (mm ⁻¹)	0.73 \pm 0.13	0.19	1.38 \pm 0.29	0.21	<.001	0.94 (<.001)

CBCT, cone-beam computed tomography; BV/TV, bone volume fraction; Tb.Th, trabecular thickness; Tb.Sp, trabecular separation; Tb.N, trabecular number; SD, standard deviation; CV, coefficient of variation.

4.4 Discussion

The present study showed that CBCT imager, with a spatial resolution as high as 80 μ m, had significant correlations with histomorphometry on decalcified bone specimens for *ex vivo* quantification of peri-implant trabecular microstructure. In the evaluation of the agreement between CBCT and histology techniques, a combination of the Pearson's correlation coefficient and Bland-Altman analyses was applied, which would help to avoid the potential affects by the observed outliers or extreme values.^{17, 23} The reasons for choosing decalcified histologic sectioning as the "gold standard" were: (1) better

resolution (to $\sim 6 \mu\text{m}$) when compared with the CBCT imaging modality; (2) the feasibility in color detection for the bone segmentation and (3) no evidence at present that decalcification and embedding technique would significantly influence histomorphometric results.

In this study, comparisons between Tb.Th, Tb.Sp and Tb.N analyses showed highly significant correlation and good agreement between CBCT and histologic images. This was well in accordance with a recent study which compared CBCT with micro-CT data on human jawbones.¹⁷ Interestingly, CBCT had a tendency to underestimate BV/TV in our study. The latter might be explained by differences between the voxel size ($80 \mu\text{m}$ for CBCT vs. $6 \mu\text{m}$ for histology), resulting in smaller trabecular boundaries less well defined by CBCT than the histologic images. This is consistent with studies which reported decreasing BV/TV and Tb.N with increasing pixel size (lower resolution).^{20,24} On the other hand, CBCT tended to overestimate Tb.Th and Tb.Sp, but the bias remained relatively low (-0.12 mm and -0.28 mm , respectively). This overestimation could be attributed to the sphere algorithm used for 3D measurement is influenced by the number of nodes (for Tb.Th) or shape and opening of the narrow cavities (for Tb.Sp), as observed in other comparisons of histomorphometry and micro-CT measurements.^{6,23}

However, caution should be taken when applying those trabecular parameters because systematic bias was also observed. There might be several reasons for the systematic biases between CBCT and histology. First, noise was present in the CBCT images as a close fine layer in the surface of titanium implants. Second, 3D CBCT results were calculated as an average value of different VOIs around the implant, while 2D histologic results came from the most central section plane of the bone samples. Third, the histologic sections in the study were $\sim 6 \mu\text{m}$ thick whereas the CBCT slice was $80 \mu\text{m}$ thick. Finally, the thresholding performed during image reconstruction and binarization resulted in a systematic impact on subsequent quantitative results. A 10% change in the threshold of micro-CT causes a 5% change in BV/TV.²⁵ Whether this

linear relationship exists between morphometric parameters and the thresholding during the image processing remains to be examined for various CBCT imagers.

The quality of CT images could be largely influenced by metal artifacts, which in general leads to a combination of beam hardening, scattering, nonlinear partial volume effect, and noise in CT images.²⁶ According to micro-CT findings, a blurred border of 60 μm was found around 3.5 mm-diameter screw-shaped titanium implants.²⁷ Although metal artifacts caused by titanium implant were present along the bone-implant direct interface in this study, specimen-specific threshold values were chosen manually based on the histogram of each image to minimize these artifacts. The intra-examiner reliability of CBCT measurements could be a further proof that the deviation derived from those manually adjustments is still desirable, suggested as another 3D bone structure analyses using CBCT.¹⁷ Moreover, it was shown that at the lower part of implant, the range and scale of the artifacts were significantly wider and larger than the upper and middle part.²⁸ To compensate for the heterogeneity of artifact distribution around implants, morphometric analyses in our study were applied at three levels of VOIs along the bone-implant interface. In addition, there was little difference in correlations and biases between the groups with and without implants in this study, suggesting that CBCT is qualified for the evaluation of trabecular bone structures, regardless of the presence or absence of implants.

It has also to be acknowledged that even a micro-CT scanning with low resolution (*e.g.*, large voxel size > 0.1 mm) relative to the size of the structure of interest may cause an underestimation of bone mineral density owing to partial-volume effects and overestimation of object thickness.²¹ On the other hand, it should also be considered that the fast development of CBCT techniques results in systems enabling to display bone details at a voxel size of 80 μm , being better than the thinnest trabecular thickness of mandibular bone, whether in dogs or humans.^{5,29} From a clinical point of view, this may provides the possibility for jaw bone structural analysis bases on CBCT.

A limitation of the present study is that the bone samples were scanned *ex vivo* by

CBCT. There was only one implant in each bone sample while CBCT scanning, which means the beam-hardening artifacts derived from multiple implants in the ROI (*i.e.*, number of implants and corresponding spatial distribution) are not considered. Additionally, the stationary situation of the samples might have enhanced the visibility of the trabecular structures because the scans did not subject to patient's movement. It could also be argued that there was no enough soft tissue surrounding the bone to mimic the real oral scanning situation. Despite this, a previous study already showed that CBCT yields similar morphometric parameters at the 3D level for all protocols with and without water as a mimic of soft-tissue while scanning.¹⁵

4.5 Conclusions

Considering the good accuracy and strong correlations between CBCT-based and histological bone characteristics, it might be considered feasible to use a high resolution 3D CBCT for clinically diagnosing and analyzing trabecular bone structure in general and more specifically around implants. Yet true clinical use can only follow after further studies focusing on the most accurate and reliable morphometric parameters, meanwhile identifying and dropping the biased ones. Such action may further enhance the diagnostic validity of CBCT-based analyses of peri-implant trabecular structures.

References

1. Jemt T, Lekholm U. Implant treatment in edentulous maxillae: a 5-year follow-up report on patients with different degrees of jaw resorption. *Int J Oral Maxillofac Implants* 1995; **10**: 303-311.
2. Herrmann I, Lekholm U, Holm S, Kultje C. Evaluation of patient and implant characteristics as potential prognostic factors for oral implant failures. *Int J Oral Maxillofac Implants* 2005; **20**: 220-230.
3. Griffith JF, Genant HK. Bone mass and architecture determination: state of the art. *Best Pract Res Clin Endocrinol Metab* 2008; **22**: 737-764.
4. Felsenberg D, Boonen S. The bone quality framework: determinants of bone strength and their interrelationships, and implications for osteoporosis management. *Clin Ther* 2005; **27**: 1-11.
5. Imoto H, Yamada A, Shimamura I, Matsunaga S, Ide Y. Influence of mechanical loading on resonance frequency analysis and trabecular structure of peri-implant bone. *Prosthodont Res Pract* 2007; **6**: 120-126.
6. Müller R, Van Campenhout H, Van Damme B, Van Der Perre G, Dequeker J, Hildebrand T, Ruegsegger P. Morphometric analysis of human bone biopsies: a quantitative structural comparison of histological sections and micro-computed tomography. *Bone* 1998; **23**: 59-66.
7. Majumdar S. Magnetic resonance imaging for osteoporosis. *Skeletal Radiology* 2008; **37**: 95-97.
8. Issever AS, Link TM, Kentenich M, Rogalla P, Burghardt AJ, Kazakia GJ, Majumdar S, Diederichs G. Assessment of trabecular bone structure using MDCT: comparison of 64-and 320-slice CT using HR-pQCT as the reference standard. *Eur Radiol* 2010; **20**: 458-468.
9. Mozzo P, Procacci C, Tacconi A, Martini PT, Andreis IA. A new volumetric CT machine for dental imaging based on the cone-beam technique: preliminary results. *Eur Radiol* 1998; **8**: 1558-1564.
10. Arai Y, Tammisalo E, Iwai K, Hashimoto K, Shinoda K. Development of a compact computed tomographic apparatus for dental use. *Dentomaxillofac Radiol* 1999; **28**: 245-248.
11. Liang X, Lambrichts I, Sun Y, Denis K, Hassan B, Li L, Pauwels R, Jacobs R. A comparative evaluation of Cone Beam Computed Tomography (CBCT) and Multi-Slice CT (MSCT). Part II: On 3D model accuracy. *Eur J Radiol* 2010; **75**: 270-274.
12. Hua Y, Nackaerts O, Duyck J, Maes F, Jacobs R. Bone quality assessment based on cone beam computed tomography imaging. *Clin Oral Implants Res* 2009; **20**: 767-771.

13. De Vos W, Casselman J, Swennen GR. Cone-beam computerized tomography (CBCT) imaging of the oral and maxillofacial region: a systematic review of the literature. *Int J Oral Maxillofac Surg* 2009; **38**: 609-625.
14. Corpas Ldos S, Jacobs R, Quirynen M, Huang Y, Naert I, Duyck J. Peri-implant bone tissue assessment by comparing the outcome of intra-oral radiograph and cone beam computed tomography analyses to the histological standard. *Clin Oral Implants Res* 2011; **22**: 492-499.
15. Van Dessel J, Huang Y, Depypere M, Rubira-Bullen I, Maes F, Jacobs R. A comparative evaluation of cone beam CT and micro-CT on trabecular bone structures in the human mandible. *Dentomaxillofac Radiol* 2013; **42**: 20130145.
16. Huang Y, Van Dessel J, Liang X, Depypere M, Zhong W, Ma G, Lambrichts I, Maes F, Jacobs R. Effects of Immediate and Delayed Loading on Peri-Implant Trabecular Structures: A Cone Beam CT Evaluation. *Clin Implant Dent Relat Res* 2013.
17. Ibrahim N, Parsa A, Hassan B, van der Stelt P, Aartman I, Wismeijer D. Accuracy of trabecular bone microstructural measurement at planned dental implant sites using cone-beam CT datasets. *Clin Oral Implants Res* 2013.
18. Klintström E, Smedby Ö, Moreno R, Brismar TB. Trabecular bone structure parameters from 3D image processing of clinical multi-slice and cone-beam computed tomography data. *Skeletal Radiol* 2014; **43**: 197-204.
19. Pauwels R, Beinsberger J, Collaert B, Theodorakou C, Rogers J, Walker A, Cockmartin L, Bosmans H, Jacobs R, Bogaerts R, Horner K, Consortium SP. Effective dose range for dental cone beam computed tomography scanners. *Eur J Radiol* 2012; **81**: 267-271.
20. Perilli E, Parkinson IH, Reynolds KJ. Micro-CT examination of human bone: from biopsies towards the entire organ. *Ann Ist Super Sanita* 2012; **48**: 75-82.
21. Bouxsein M, Boyd S, Christiansen B, Guldborg R, Jepsen K, Müller R. Guidelines for assessment of bone microstructure in rodents using micro-computed tomography. *J Bone Miner Res* 2010; **25**: 1468-1486.
22. Parfitt AM, Mathews CHE, Villanueva AR, Kleerekoper M, Frame B, Rao DS. Relationships between Surface, Volume, and Thickness of Iliac Trabecular Bone in Aging and in Osteoporosis - Implications for the Microanatomic and Cellular Mechanisms of Bone Loss. *J Clin Invest* 1983; **72**: 1396-1409.
23. Chappard D, Retailleau-Gaborit N, Legrand E, Basle MF, Audran M. Comparison insight bone measurements by histomorphometry and microCT. *J Bone Miner Res* 2005; **20**: 1177-1184.
24. Tjong W, Kazakia GJ, Burghardt AJ, Majumdar S. The effect of voxel size on high-resolution peripheral computed tomography measurements of trabecular and cortical bone microstructure. *Med Phys* 2012; **39**: 1893-1903.

25. Ruegsegger P, Koller B, Muller R. A microtomographic system for the nondestructive evaluation of bone architecture. *Calcif Tissue Int* 1996; **58**: 24-29.
26. De Man B. X-ray computed tomography In: Suetens Ps, ed. *Proceedings of the Fundamentals of Medical Imaging*. Cambridge: Cambridge University, 2009: 33-62.
27. Stoppie N, van der Waerden JP, Jansen JA, Duyck J, Wevers M, Naert IE. Validation of microfocus computed tomography in the evaluation of bone implant specimens. *Clin Implant Dent Relat Res* 2005; **7**: 87-94.
28. Volpon J, Shimano A. Methods in bone biology in animals: imaging In: Duque G, Watanabe Ks, eds. *Proceedings of the Osteoporosis Research*. Springer London, 2011: 29-36.
29. Giesen EB, van Eijden TM. The three-dimensional cancellous bone architecture of the human mandibular condyle. *J Dent Res* 2000; **79**: 957-963.

Chapter 5

A comparative evaluation of cone-beam CT and micro-CT on trabecular bone structures in the human mandible

This chapter is based on following manuscript:

*A comparative evaluation of cone-beam CT and micro-CT on
trabecular bone structures in the human mandible*

Jeroen Van Dessel, Yan Huang, Maarten Depypere, Izabel Rubira-Bullen,
Frederik Maes, Reinhilde Jacobs

Published in *Dentomaxillofacial Radiology*

2013;42(8):20130145

Abstract

Objectives: The main purpose of this study was to determine the accuracy of cone beam CT (CBCT) in measuring the trabecular bone microstructure, in comparison with micro-CT. The subobjective was to examine to what extent bone quality assessment is influenced by X-ray tube current and voltage settings as well as soft tissue surrounding the bone. **Methods:** Eight human mandibular bone samples were scanned using three different clinical exposure protocol within water (W1–3) and without water (NW1–3) by a high-resolution (80 μ m) CBCT machine (3D Accuitomo 170[®]; Morita, Kyoto, Japan). Subsequently, the samples underwent micro-CT scanning (SkyScan 1174[®]; SkyScan, Antwerp, Belgium). After image acquisition, similar volumes of interest of the trabecular structures captured with CBCT and micro-CT were aligned with each other. Segmentation was then performed, and the morphometric parameters were quantified within the volumes of interest by CTAn software (CTAnalyser[®]; SkyScan, Antwerp, Belgium). Descriptive statistical analyses and multiple comparisons between all protocols were applied in R software. **Results:** High positive Pearson's correlation coefficients were observed between CBCT and micro-CT protocols for all tested morphometric indices except for trabecular thickness. No significant differences were observed between all exposure protocols except for trabecular separation. When examining the soft-tissue effect on trabecular bone structures, no significant differences between NW (1–3) and W (1–3) protocols were observed for all variables. **Conclusions:** The present study demonstrated the potential of high-resolution CBCT imaging for *in vivo* applications of quantitative bone morphometry and bone quality assessment. However, the overestimation of morphometric parameters and acquisition settings in CBCT must be taken into account.

5.1 Introduction

Quantitative bone morphometry is the standard method to assess structural properties of trabeculae by means of morphometric indices.¹ In the past, microarchitectural characteristics of trabecular and cortical bone have been intensively investigated by examining two-dimensional (2D) sections of bone biopsies, combined with calculation of morphometric parameters using stereological methods.² Although such histological analysis offers a high spatial resolution and good image contrast, it remains a labor-intensive and thus time-consuming job. Moreover, it is a destructive technique that allows tissue quantification in only a limited number of 2D sections and therefore, prevents the specimens from being used for other comparative measures. The latter is highly desirable because of the anisotropic nature of cancellous bone. To overcome some of the limitations of 2D analyses, various three-dimensional (3D) imaging modalities of analysis techniques have been proposed. Recently, micro-CT (μ CT) has been validated as a highly reliable tool to determine trabecular bone parameters, while being considered as the new reference method for *ex vivo* bone studies.³ Nevertheless, μ CT has hardly any clinical value for structural bone analysis. This is where cone beam CT (CBCT) may come into play.

CBCT is a new emerging radiographic method possessing plenty of benefits regarding radiation dose, cost effectiveness, scanning time and 3D modalities in evaluating the trabecular bone structure in a clinically objective and quantitative way. Still, bone characterization using morphometry with CBCT has not yet been properly investigated. To establish CBCT as a method for 3D assessment and analysis of trabecular bone, the method needs proper validation by comparing the results to 3D μ CT, serving as the reference (gold standard). For a long time, CBCT's main drawback, when compared with μ CT, was its low spatial resolution (order of 200 - 300 μ m).⁴ During the last decade, various advancements within the CBCT imaging chain have led to clear improvements in resolution. However, spatial resolution is highly variable between CBCT devices, with voxel sizes between 76 μ m and 400 μ m and actual sharpness showing wide ranges on both a clinical level and a technical level. A previous study

has shown that images with voxel sizes higher than 300 μm would be unsuitable for imaging individual trabeculae.⁵ Given that various CBCT devices use voxel sizes well below that limit, it may be possible to use them to evaluate trabecular morphology. It remains to be investigated to what degree the resolution provided by CBCT scans allows correct computation of morphometric indices, considering that the smallest voxel sizes in CBCT are in the order of typical trabecular thicknesses. Additionally, X-ray tube settings and soft tissue surrounding samples could affect the morphological parameters and the associated clinical evaluation of bone architecture.

The main purpose of this study was to determine the accuracy of CBCT for measuring the trabecular bone microstructure in comparison with μCT . Secondly, the effect of X-ray tube current and voltage settings, as well as soft tissue surrounding the bone, on bone quality assessment was investigated.

5.2 Materials & methods

5.2.1 Image acquisition

Eight edentulous human bone samples of left and right mandible (1st premolar to 3rd molar) were scanned using a high resolution CBCT (80 μm), which has been calibrated for the radiographic study (3D Accuitomo 170® CBCT, Morita, Kyoto, Japan). Each sample was placed in a sponge block in order to prevent any movement during the scanning process. The mandibles were scanned using three different clinical exposure protocols within (W) and without water (NW). Scanning parameters were fixed at 360° rotation, 30.8 s exposure time, 80 μm voxel size, high resolution and a field of view (FOV) of 40x40 mm. Tube voltage and current were varied, using three combinations: (1) 90kVp, 5mA, 8.1 mGy CT dose index (CTDI_{vol}); (2) 90kVp, 2mA, 3.4mGy CTDI_{vol} and (3) 70kVp, 5mA, 4.8mGy CTDI_{vol} . All CTDI_{vol} values were predetermined by the manufacturer and served as dose estimation.

The bone samples were subsequently scanned with the SkyScan 1174® μCT system (SkyScan, Antwerp, Belgium). The μCT parameters were 26 μm voxel size, 50 kVp,

800 μ A, 1 mm aluminum filter, angular rotation step 0.8°, 360° scanning, 450 projections and an exposure time of 9s with a total scan duration of 2h 20min.

5.2.2 Image processing and analysis

To evaluate the microarchitecture of the trabecular bone, a volume of interest (VOI) comprising trabecular bone only was delineated in the μ CT image of each sample. To minimize errors generated by comparing different morphological structures, it is desirable to obtain a VOI comprising the exact same structures in the CBCT images of the respective samples. This was achieved by computing the rigid transformation that spatially aligns each CBCT scan of a sample with the μ CT image of the corresponding sample, using registration software based on mutual information.⁶ This transformation was applied to the VOI of the μ CT images, resulting in highly accurate delineation of the VOI in the coordinate system of the CBCT images. This approach does not alter the resolution of the μ CT or CBCT images, allowing a fair comparison without introducing errors by unmatched VOIs. An impression of how the same VOI is applied to different images is given in Figure 5.1.

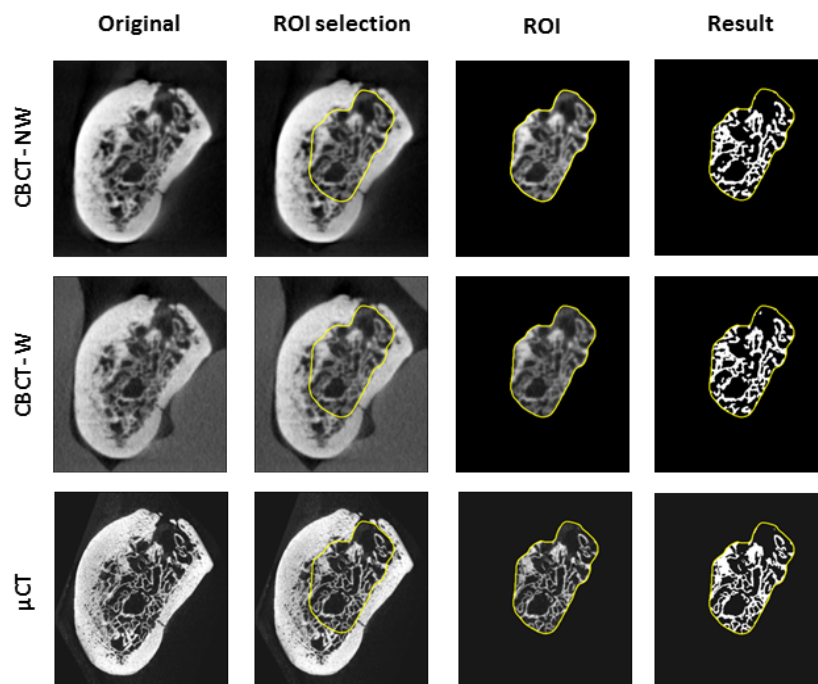


Figure 5.1: Registered cone beam CT (CBCT) and micro-CT (μ CT) images with the same volume

of interest (VOI) containing the trabecular bone. For display purposes, images are transformed to the coordinate system of the CBCT scan with water. In our method, only the VOI is transformed to prevent loss of resolution of the images during transformation

After precise registration, images were segmented to allow trabecular bone structure quantification with CTAn software (CTAnalyser[®], SkyScan, Antwerp, Belgium). Bone voxels were determined by using the adaptive thresholding algorithm, with a radius of four voxels for CBCT images and six voxels for μ CT images, and a visually determined background threshold. Voxel radius values were visually determined in CTAnalyser to give the best segmentation overlap with the original image. The adaptive threshold approach, chosen as adaptive or local thresholding algorithms, has been shown to perform better than global thresholding on low-resolution images.⁷ From the resulting binary images, the trabecular morphometric parameters were computed for each scan within the corresponding VOI (Figure 5.1). Selected CBCT and μ CT VOI were additionally visualized in 3D (MeVisLab[®]; MeVis Medical Solutions AG, Bremen, Germany) to facilitate the interpretation of the morphometric results (Figure 5.2).

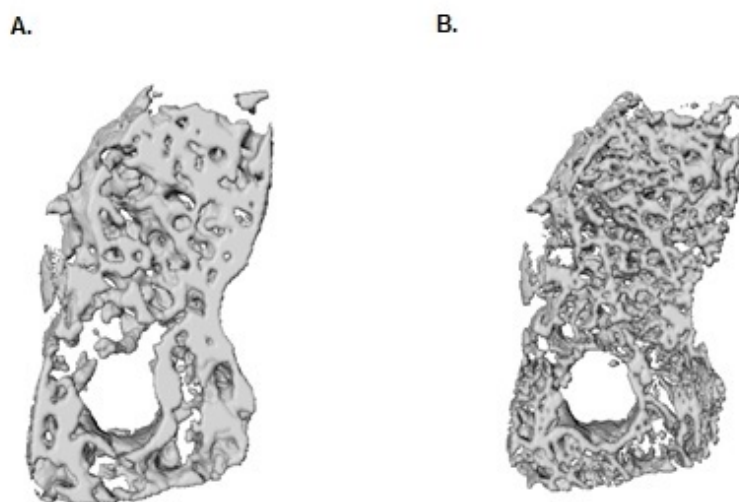


Figure 5.2: Visual three-dimensional representation from cone beam CT (CBCT) (a) and the micro-CT (μ CT) (b) bone sample. The difference in morphology shown by the three-dimensional models was reflected by various morphometric parameters.

In the present study, it was opted to follow the recommendations of American Society of Bone and Mineral Metabolism for calculation of 3D bone parameters and structural indices.⁸ All dimension units were given in millimeters, and parameters were named according to the Parfitt's system:¹ bone volume (BV), total volume of interest (TV), bone volume fraction (BV/TV), bone surface (BS), bone surface density (BS/TV), trabecular thickness (Tb.Th), trabecular separation (Tb.Sp), trabecular number (Tb.N), total porosity percentage [Po(tot)] and connectivity density (Conn.Dn).

To investigate the effect of X-ray tube current and voltage settings on bone quality assessment, image quality was quantified by the signal-to-noise ratio (SNR), which is defined as the ratio of the mean intensity over the standard deviation of the intensity in a homogenous region. Higher SNR values indicate less noise in the image. The SNR was measured in four VOIs containing only water in the images of jaw samples surrounded by water (Figure 5.3).

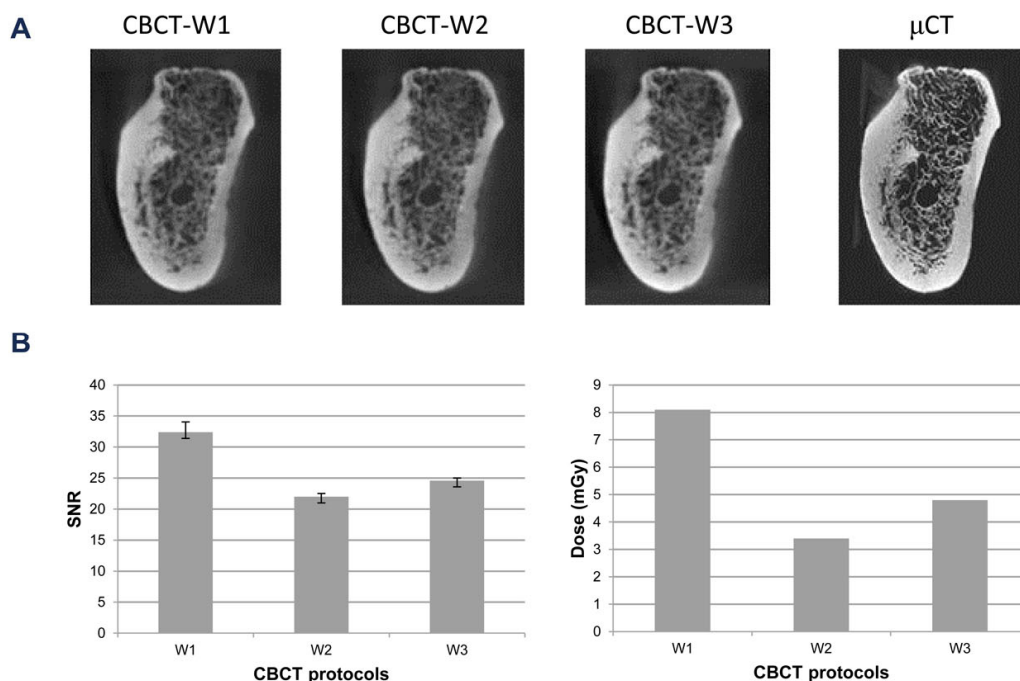


Figure 5.3: Visual and quantitative evaluation on image quality for three different cone beam CT (CBCT) acquisition protocols in water. (a) No obvious visual difference in image quality can be observed between different CBCT protocols; (b) higher signal-to-noise ratio values are obtained in higher dose protocols (W1).

5.2.3 Statistical analysis

Statistical analysis was performed in R 2.14.2 (<http://www.R-project.org>). Descriptive analysis expressed data as central tendency and dispersion measurements. The Fisher exact test was used to compare variance between the groups and the Tukey's honestly significant difference (HSD) test to compare variables. Non-parametric statistical methods were used when normality was not confirmed. Bivariate linear association between morphometric CBCT parameters was sought by calculating Pearson's or Spearman's coefficients. For all tests performed, the confidence level α was 5%.

5.3 Results

Descriptive comparison between different μ CT and CBCT scanning protocols are shown in Table 5.1. The Tukey's HSD test was used to compare mean values among groups. No significant differences between NW (1–3) and W (1–3) protocols were observed for all variables, indicating that all CBCT scan protocols result in similar morphometric indices. The influence of water and scan settings does not effect significant differences.

Statistically significant differences ($\alpha < 0.05$) were observed for the variable BV/TV, BS/TV, Po(tot), Tb.Th, Tb.N and Conn.Dn between CBCT and μ CT protocols. No significant differences were observed between all scanning protocols for the variable Tb.Sp, demonstrating that morphometric indices obtained by CBCT imaging differ from those obtained with μ CT. These structural differences can also be observed on the 3D reconstructions of the VOI from both CBCT and μ CT images (Figure 5.2).

Table 5.2 shows the direct relationship between all scanning protocols. High positive Pearson's correlation coefficients were observed between CBCT and μ CT protocols for all variables, except for Tb.Th.

CBCT acquisition Protocol 2 has a lower correlation with μ CT than Protocols 1 and 3, which is in accordance with low-obtained SNR values (Figure 5.3b). However, no

visual difference in image quality can be observed between all scanning protocols (Figure 5.3a).

5.4 Discussion

Although the accuracy of μ CT morphology measurements for the non-destructive assessment of trabecular bone quality has already been extensively studied in both animal^{7,9,10} and human^{3,11} specimens, these techniques are not used regularly in clinical routines. This study addresses the use of CBCT in evaluating the trabecular bone architecture by means of morphometric parameters, and the effect of X-ray tube current and voltage settings, as well as soft tissue surrounding the bone, on bone quality assessment was investigated. This has paved the way for clinical evaluation of bone healing (whether or not this is peri-implant) and for follow-up assessment studies.

In the present study, water was used to mimic the soft tissue surrounding the bone.¹² Table 5.1 shows that CBCT yields similar results at the 3D level for all W- and NW protocols. Therefore, it can be demonstrated that the soft tissue around the bone has limited influence on the CBCT and μ CT comparison, making it applicable for clinical settings.

After a more detailed comparison of both analysis techniques, it seemed that radiographic CBCT analysis tended to slightly over estimate BV/TV, Tb.Sp and Tb.Th compared with μ CT (Table 5.1 and Figure 5.2). The possible explanation for the over estimation of CBCT is its lower resolution. Waarsing *et al* showed using μ CT that decreasing the image resolution resulted in over estimation of these parameters.⁷ Trabeculae that were thin with respect to the image resolution were smeared out and appeared thicker. The high spatial resolution of μ CT has always been considered crucial for accurate assessment of individual trabecular characteristics using structural analysis. In particular, measurements such as Tb.Th are known to have a strong resolution dependency requiring very high resolutions for precise measurement,⁷ explaining the lower correlation between CBCT and μ CT for this particular parameter (Table 5.2). The actual spatial resolution of a 3D image is determined by various

factors, including the voxel size and the amount of noise. Early generation CBCT machines were characterized by small voxel sizes but a high degree of noise, limiting their spatial and contrast resolution. The present study used one of the best quality CBCT machines currently in the market (3D Accuitomo). When these over estimations persist, a correction factor can be calculated to reduce these inaccuracies. Despite the low number of bone samples, the present study demonstrates the potential of high-resolution CBCT imaging for *in vivo* applications of quantitative bone morphometry and bone quality assessment.

However, the present study was conducted *in vitro* and thus in the absence of motion artefacts. Patient movement may reduce CBCT spatial resolution substantially.¹³ Head-motion artefacts can be simulated by application of phantoms.¹⁴ However, in the present study, human jaw bones were used instead, as the primary focus was to simulate jaw bone structure as close to clinical reality as possible. Thus, it was opted to make the CBCT scans by applying clinical scanning protocols, soft-tissue simulation and evaluation of the human trabecular bone structures. Though, we realize that this choice hampered us to further include motion artefacts. In the future, an integrated phantom with a human trabecular bone might offer the possibility to include this variable as well.

There is a common belief that grey scale values in the reconstructed CBCT database do not allow for bone density assessment.^{15,16} However, bone density is only one factor representing bone quality. Bone structure also largely contributes to bone quality. It is note worthy to stress that CBCT images may enable bone structural analysis by thresholding CBCT images to a binary format, provided that high enough image resolution is attained.¹⁷ With further advancements in CBCT resolution, morphological analysis of bone structure is most promising for clinical implementation.

Table 5.1: Descriptive statistics of 3D morphometric parameters for different scanning protocols

Morphometric parameters	Mean (SD)							Min-Max						
	NW1	NW2	NW3	W1	W2	W3	μ CT	NW1	NW2	NW3	W1	W2	W3	μ CT
TV	994.5 (449.9)	994.5 (449.9)	1014.0 (464.1)	1030.0 (460.8)	1030.0 (460.8)	1030.0 (460.8)	989.9 (448.2)	355.0 - 1633.0	355.0-1633.0	371.0-1680.0	373.0-1685.0	373.0-1685.0	373.0-1685.0	353.5-1627.0
BV	520.2 (214.2)	523.9 (217.1)	519.5 (210.8)	530.9 (225.6)	553.2 (242.2)	502.8 (202.3)	323.9 (121.2)	201.5 - 844.5	198.8-849.7	206.7-848.9	215.0-894.7	222.8-936.5	214.1-840.5	137.6-489.8
BV/TV	53.74 (5.69)	53.98 (5.60)	52.96 (6.46)	52.77 (5.10)	54.57 (3.90)	50.63 (6.41)	34.39 (5.41)	45.36 - 60.66	45.64-60.63	44.93-61.14	45.24-58.86	49.33-59.72	43.09-58.80	28.90-42.99
BS	4302 (1877)	4474 (1964)	4327 (1869)	4615 (2108)	5341 (2498)	4587 (1986)	6104 (2044)	1579 - 7269	1598-7550	1603-7310	1750-8216	1999-9534	1826-8019	2769-8720
BS/TV	4.40 (0.46)	4.56 (0.51)	4.36 (0.51)	4.53 (0.40)	5.19 (0.31)	4.55 (0.47)	6.61 (1.32)	3.67 - 4.79	3.81-5.04	3.66-4.86	3.88-4.92	4.78-5.66	3.87-5.11	5.06-8.52
Tb.Th	0.42 (0.01)	0.41 (0.01)	0.42 (0.01)	0.40 (0.01)	0.38 (0.01)	0.39 (0.01)	0.19 (0.01)	0.40 - 0.43	0.40-0.41	0.40-0.42	0.39-0.41	0.37-0.39	0.38-0.40	0.17-0.20
Tb.Sp	0.64 (0.20)	0.61 (0.20)	0.66 (0.21)	0.68 (0.17)	0.55 (0.12)	0.72 (0.19)	0.54 (0.18)	0.44 - 0.94	0.41--0.92	0.44-0.95	0.47-0.91	0.42-0.69	0.47--0.92	0.28-0.77
Tb.N	1.29 (0.13)	1.32 (0.14)	1.27 (0.15)	1.31 (0.13)	1.44 (0.10)	1.29 (0.16)	1.85 (0.32)	1.09 - 1.45	1.11-1.48	1.07-1.46	1.11-1.46	1.29-1.56	1.08-1.50	1.51-2.33
Po(tot)	46.26 (5.69)	46.02 (5.60)	47.04 (6.46)	47.23 (5.10)	45.43 (3.90)	49.37 (6.41)	65.61 (5.41)	39.34 - 54.64	39.37-54.36	38.86-55.07	41.14-54.76	40.28-50.67	41.20-56.91	57.01-71.10
Conn.Dn	5.45 (1.99)	6.34 (2.35)	5.43 (2.05)	6.41 (1.53)	9.89 (1.70)	6.91 (1.17)	54.27 (30.51)	3.65 - 9.13	4.10-10.56	3.59-9.14	4.96-8.95	8.52-13.04	4.96-8.25	23.73-107.70

TV: Total volume of interest in mm³; BV: Bone volume in mm³; BV/TV: Bone volume fraction in %; BS: Bone surface in mm²/mm³; BS/TV: Bone surface density in mm²/mm³; Tb.Th: Trabecular thickness in mm; Tb.Sp: Trabecular separation in mm; Tb.N: Trabecular number in 1/mm; Po(tot): Total porosity percentage in %; Conn.Dn: connectivity density in %; NW1-3: CBCT scanning protocol 1-3 without water; W1-3: CBCT scanning protocol 1-3 in water; μ CT: micro-CT scanning protocol.

Table 5.2: Correlation of morphometric parameters between μ CT and CBCT protocols

Morphometric parameters	μ CT-NW1	μ CT-NW2	μ CT-NW3	μ CT-W1	μ CT-W2	μ CT-W3
BV/TV ^a	0.80	0.76	0.78	0.86	0.82	0.89
BS/TV ^a	0.75	0.69	0.74	0.73	0.68	0.73
Tb.Th	0.29	0.21	0.43	0.43	0.57	0.32
Tb.Sp ^a	0.82	0.80	0.84	0.62	0.61	0.63
Tb.N ^a	0.83	0.77	0.81	0.82	0.72	0.86
Po(tot) ^a	0.80	0.76	0.78	0.86	0.82	0.89
Conn.Dn	0.73	0.70	0.73	0.74	0.70	0.73

^aPearson and Spearman correlation coefficients have a $p < 0.05$.

BS/TV, bone surface density in mm^2 per mm^3 ; BV/TV, bone volume fraction in %; Conn.Dn, connectivity density in %; μ CT, micro-CT scanning protocol; NW1–3, CBCT scanning Protocols 1–3 without water; Po(tot), total porosity percentage in %; Tb.N, trabecular number in 1 per mm; Tb.Sp, trabecular separation in mm; Tb.Th, trabecular thickness in mm; W1–3: CBCT scanning Protocols 1–3 in water.

A morphometric analysis of mandibular trabecular bone reported that BV/TV obtained using CBCT images was highly correlated with CT values obtained using multi slice CT images, suggesting that trabecular bone morphometry can be used to evaluate the density of mandibular cancellous bone.¹⁸ The resolution of currently clinically used CBCT equipment also allows for detailed observation of the peri-implant bone,¹⁹ which is consistent with research evaluated in the zygomatic bone.²⁰ Furthermore, morphometric indices of the trabecular bone structure have been proven to have evident correlation with the physical property of the bone in many histology and μ CT studies.^{2,11,21} In the present study, the correlation among morphometric parameters has been proven between CBCT as well. The occurrence of positive significant correlations indicates that there are definitely strong relations among CBCT parameters for all the scanning protocols (Table 5.2).

Table 5.2 shows that CBCT acquisition Protocol 2 has a lower correlation with μ CT than Protocols 1 and 3 for all parameters. This indicates that image quality is hardly affected by altering the peak voltage between 90 kVp (Protocol 1) and 70 kVp (Protocol 3) compared with the effect of lowering the tube current from 5mA (Protocols 1 and 3) to 2mA (Protocol 2). The drop in correlation because of the lower tube current can be

explained by an inverse relationship between tube current and imagenoise.²² Consequently, lower tube currents yield noisier images (Figure 5.3b), hampering accurate segmentation.

5.5 Conclusions

The present study demonstrates the potential of high-resolution CBCT imaging for *in vivo* applications of quantitative bone morphometry and bone quality assessment. This is especially true for repetitive follow-up measurements, which cannot be performed using histological sections. Additionally, the method offers reliable easy access to the 3D structure of trabecular bone, which is mandatory for the analyses of the anisotropic mechanical behaviour of the cancellous bone. Therefore, the development of this technique seems promising for clinical use of low-dose CBCT and offers an ideal accurate alternative to multi-slice CT to determine the 3D trabecular bone structure during the pre-operative phase and also, if necessary, during the bone healing phase. However, one must still take into account the over estimation of CBCT while measuring BV/TV, Tb.Sp and Tb.Th and the used acquisition settings.

References

1. Parfitt AM, Drezner MK, Glorieux FH, Kanis JA, Malluche H, Meunier PJ, *et al.* Bone histomorphometry: standardization of nomenclature, symbols, and units. Report of the ASBMR Histomorphometry Nomenclature Committee. *J Bone Miner Res* 1997; **2**:595-610.
2. Parfitt AM, Mathews CH, Villanueva AR, Kleerekoper M, Frame B, Rao DS. Relationships between surface, volume, and thickness of iliac trabecular bone in aging and in osteoporosis. Implications for the micro anatomic and cellular mechanisms of bone loss. *J Clin Invest* 1983; **72**:1396-1409.
3. Müller R, Van Campenhout H, Van Damme B, Van Der Perre G, Dequeker J, Hildebrand T, *et al.* Morphometric analysis of human bone biopsies: a quantitative structural comparison of histological sections and micro-computed tomography. *Bone* 1998; **23**:59-66.
4. Kothari M, Keaveny TM, Lin JC, Newitt DC, Genant HK, Majumdar S. Impact of spatial resolution on the prediction of trabecular architecture parameters. *Bone* 1998; **22**:437-443.
5. Issever AS, Link TM, Kentenich M, Rogalla P, Burghardt AJ, Kazakia GJ, *et al.* Assessment of trabecular bone structure using MDCT: comparison of 64- and 320- slice CT using HR-pQCT as the reference standard. *Eur Radiol* 2010; **20**:458-468.
6. Maes F, Collignon A, Vandermeulen D, Marchal G, Suetens P. Multimodality image registration by maximization of mutual information. *IEEE Trans Med Imaging* 1997; **16**:187-198.
7. Waarsing JH, Day JS, Weinans H. An improved segmentation method for in vivo microCT imaging. *J Bone Miner Res* 2004; **19**:1640-1650.
8. Bouxsein ML, Boyd SK, Christiansen BA, Guldberg RE, Jepsen KJ, Müller R. Guidelines for assessment of bone microstructure in rodents using micro-computed tomography. *J Bone Miner Res* 2010; **25**:1468-1486.
9. Kapadia RD, Stroup GB, Badger AM, Koller B, Levin JM, Coatney RW, *et al.* Applications of micro-CT and MR microscopy to study pre-clinical models of osteoporosis and osteoarthritis. *Technol Health Care* 1998; **6**: 361-372.
10. Bonnet N, Laroch N, Vico L, Dolleans E, Courteix D, Benhamou CL. Assessment of trabecular bone microarchitecture by two different X-ray micro computed tomographs: a comparative study of the rat distal tibia using Skyscan and Scanco devices. *Med Phys* 2009; **36**:1286-1297.
11. Chappard D, Retailleau-Gaborit N, Legrand E, Baslé MF, Audran M. Comparison insight bone measurements by histomorphometry and microCT. *J Bone Miner Res* 2005; **20**:1177-1184.
12. Sandborg M, AlmCarlsson G, Persliden J, Dance DR. Comparison of different

- materials for test phantoms in diagnostic radiology. *Radiat Prot Dosimetry* 1993; **49**: 345-347.
13. Schulze R, Heil U, Gross D, Bruellmann DD, Dranischnikow E, Schwanecke U, *et al.* Artefacts in CBCT: a review. *Dentomaxillofac Radiol* 2011; **40**:265-273.
14. Ens S, Bruder R, Ulrici J, Hell E, Buzug TM. A validation framework for head-motion artifacts in dental cone-beam CT. In: World Congress on Medical Physics and Biomedical Engineering, 7–12 September 2009; Munich, Germany. Munich, Germany: *IFMBE Proceedings* Volume **25**; 2009.
15. Katsumata A, Hirukawa A, Noujeim M, Okumura S, Naitoh M, Fujishita M, *et al.* Image artifact in dental cone-beam CT. *Oral Surg Oral Med Oral Pathol Oral Radiol Endod* 2006; **101**:652–657.
16. Pauwels R, Stamatakis H, Manousaridis G, Walker A, Michielsen K, Bosmans H, *et al.* Development and applicability of a quality control phantom for dental cone-beam CT. *J Appl Clin Med Phys* 2011; **12**:3478.
17. Kothari M, Keaveny TM, Lin JC, Newitt DC, Genant HK, Majumdar S. Impact of spatial resolution on the prediction of trabecular architecture parameters. *Bone* 1998; **22**: 437–443.
18. Naitoh M, Aimiya H, Hirukawa A, Arijji E. Morphometric analysis of mandibular trabecular bone using cone beam computed tomography: an in vitro study. *Int J Oral Maxillofacial Implants* 2010; **25**:1093-1098.
19. Huang Y, Van Dessel J, Liang X, Depypere M, Zhong W, Ma G, *et al.* Effects of immediate and delayed loading on peri-implant trabecular structures: a cone beam CT evaluation. *Clin Implant Dent Relat Res* Apr 2013. Epub ahead of print. doi:10.1111/cid.12063
20. Liu SM, Zhang ZY, Li JP, Liu DG, Ma XC. A study of trabecular bone structure in the mandibular condyle of healthy young people by cone beam computed tomography. *Zhong Hua Kou Qiang Yi Xue Za Zhi* 2007; **42**:357-360.
21. de Oliveira RC, Leles CR, Lindh C, Ribeiro-Rotta RF. Bone tissue microarchitectural characteristics at dental implant sites. Part 1: identification of clinical-related parameters. *Clin Oral Implants Res* 2012; **23**:981-986.
22. Goldman LW. Principles of CT: radiation dose and image quality. *J Nucl Med Technol* 2007; **35**:213-225.

Chapter 6

Effects of immediate and delayed loadings on peri-implant trabecular structures: a cone-beam CT evaluation

This chapter is based on following manuscript:

Effects of immediate and delayed loadings on peri-implant trabecular structures: a cone-beam CT evaluation

Yan Huang, Jeroen van Dessel, Xin Liang, Maarten Depypere, Weijian Zhong, Guowu Ma, Ivo Lambrichts, Frederik Maes, Reinhilde Jacobs

Published in *Clinical Implant Dentistry and Related Research*

[Epub ahead of print]

Abstract

Purpose: To develop a method for characterizing trabecular bone micro architecture using cone beam computed tomography (CBCT) and to evaluate trabecular bone changes after rehabilitation using immediate versus delayed implant protocols.

Materials and Methods: Six mongrel dogs randomly received 27 titanium implants in the maxillary incisor or mandibular premolars are as following one of four protocols: (1) normal extraction socket healing; (2) immediate implant placement and immediate loading; (3) delayed implant placement and delayed loading; (4) delayed implant placement and immediate loading. The animals were euthanized at 8 weeks and block biopsies were scanned using high resolution CBCT. Standard bone structural variables were assessed in coronal, middle, and apical levels. **Results:** Coronal and middle regions had more compact, more plate-like, and thicker trabeculae. Protocols (2), (3) and (4) had significantly higher values ($p<0.01$) than the protocol (1) for specific bone surface and connectivity density, while significantly lower values ($p<0.001$) were found for trabecular separation and fractal dimension. However, protocols (2), (3) and (4) did not show significantly different bone remodeling. **Conclusions:** Compared with normal extraction healing, the implant protocols have an improved bone structural integration. Results do not suggest a different bone remodeling pattern when a delayed versus an immediate implant protocol is used.

6.1 Introduction

While traditional dental implant protocols incorporate a healing period prior to placing the implant (delayed implant placement), several attempts have been reported and specific treatment protocols introduced in order to reduce the total treatment time. The advent of new implant materials, surface coating, and adaptations to the mechanical design has opened up the path towards immediate implant placement, thus increasing patient comfort by shortening treatment periods, while preserving some of the bone volume.¹ Some clinical studies found similar implant survival rates and marginal bone loss in the short and medium term when comparing delayed and immediate implant placement protocols.^{2, 3} Moreover, several histological studies on humans and experimental animals suggested that immediate loading implants show a higher percentage of bone-to-implant contact (BIC) than either delayed loading implants or implants left unloaded.⁴⁻⁶ Nevertheless, the available literature has so far not been conclusively determined the superiority of immediate loading protocols, particularly with regard to 3D micro structure of peri-implant bone.

The survival rate of implants is significantly affected by the bone quality,⁷ which not only relates to the bone mineral density but also critically depends on the 3D micro structure of the peri-implant bone.⁸ Trabecular bone is more metabolically active than cortical bone⁸ and therefore is a more sensitive indicator of early physiopathologic changes. Consequently, objective quantitative assessment of trabeculae architecture around the implant may provide comprehensive structural information related to different implant placements for better determining the status of osseointegration.

For decades, the most common method used to evaluate peri-implant tissue has been histomorphometry, which allows two-dimensional measurements on thin histological sections. As this classical technique is invasive, time-consuming and prone to sampling errors, 3D imaging using micro computed tomography (μ CT) has been validated as a non-invasive and accurate method for assessment of bone geometry.⁹ Yet, although μ CT has been widely applied for 3D evaluation of trabeculae structures in bone biopsies and

small animal bones,^{9, 10} it is of limited use at present in the clinical routine. For imaging of trabecular bone *in vivo*, both high-resolution magnetic resonance imaging (HR-MRI) and multi-detector computed tomography (MDCT) have been investigated.^{11, 12} However, the potential of MRI is limited by the long scan times needed to obtain high-resolution imaging of trabecular bone and by metal artifacts because of magnetic susceptibility.¹³ MDCT on the other hand, requires substantial radiation exposure to achieve enough spatial resolution.¹⁴ Recently, low-dose dental cone beam CT (CBCT) has become widely available in clinical practice as a new technique for rapid non-invasive imaging at even higher image quality than MDCT.¹⁴ Whereas the accuracy of CBCT in the measurement of bone-related parameters (*e.g.*, bone thickness) has been investigated thoroughly,¹⁵ little is known about the potential of CBCT for analyzing peri-implant trabecular bone morphology.

Therefore, the purpose of the present study was to evaluate the 3D morphology of peri-implant trabecular bone in a dog model after 2 months of immediate and delayed implant protocols, by means of high-resolution CBCT.

6.2 Materials & methods

The experimental protocol was approved by the bioethics committee of Dalian Medical University, Hasselt University, and KU Leuven (P059-2012-TK). A split-mouth randomized design, using four treatment protocols on six tooth positions in six male mongrel dogs (Table 6.1), was employed. The dogs (weight 14.8-18.1 kg, age 20-24 months old) were without any oral or systemic diseases and were housed individually in indoor cages. The diet during the course of the experiment was whole grain flour, corn meal, soybean cake, fish bone meal and eggs according to the general feeding program at the Experimental Animal Center of Dalian Medical University, China. The whole surgical procedure performed by one and the same surgeon (W.Z.), with a decade of clinical experience in implant dentistry. The surgeon was blinded to the allocation process, but once tooth extraction had been carried out, he could no longer be blinded to the allocated implant placement.

Table 6.1: Random distribution of split-mouth design in six experimental dogs

Dog	I (R)	I (L)	P3 (R)	P3 (L)	P4 (R)	P4 (L)
1 #	Control	DIP+DL	DIP+DL	DIP+IL	Control	IIP+IL
2 #	DIP+DL	DIP+IL	DIP+IL	IIP+IL	DIP+DL	Control
3 #	DIP+IL	IIP+IL	IIP+IL	Control	DIP+IL	DIP+DL
4 #	IIP+IL	Control	Control	DIP+DL	IIP+IL	DIP+IL
5 #	Control	DIP+DL	DIP+DL	DIP+IL	Control	IIP+IL
6 #	DIP+DL	DIP+IL	DIP+IL	IIP+IL	DIP+DL	Control

In total, 36 samples were used in the study (Control = 9; IIP + IL = 8; DIP + DL = 10; DIP + IL = 9). The investigators ensured unpredictability of the allocation sequence by coin toss before surgeries. I, 3rd maxillary incisors; P3, 3rd mandibular premolars; P4, 4th mandibular premolars; R, right side; L, left side; DIP, delayed implant placement; IIP, immediate implant placement; DL, delayed loading; IL, immediate loading.

6.2.1 Surgical procedures

Tooth extraction. The dogs got 1 week of antibiotics prophylaxis (gentamicin in sulfate, 1600000U/day, Lingrui Pharmaceutical Co. Ltd., Zhengzhou, China) to prevent infection. In each dog, bilateral 3rd and 4th mandibular premolars (P3 and P4) as well as 3rd maxillary incisors (I) were chosen as the implant recipient sites (Figure 6.1A). During all surgical procedures, the dogs were anaesthetized with Sumianxin (0.1 ml/kg xylazine hydrochloride, Changchun Military Academy of Medical Sciences, China). Local anesthesia (2-4 ml lidocaine 2% with epinephrine 1:100000, Tianjin Pharmaceutical Co. Ltd., Tianjin, China) was used at the surgical site. After tooth extraction, these sites were sutured with 4-0 vicryl resorbable sutures.

Implant placement. Sample size calculation was based on a preliminary experiment. Given $\alpha = 0.05$ and $\beta = 0.10$, it was calculated that at least seven samples in each group were needed to reach significance level for connectivity density (Conn.Dn) when differences of 3.5 mm^{-3} and a standard deviation of 2 mm^{-3} were assumed. Twenty-seven custom-made threaded implants of grade 5 pure titanium (machined surface, $\text{Ø}=3.1\text{mm}$ for I and 4.1mm for P3 and P4, L=11mm, Figure 6.1B) were thoroughly examined first

to reject failed test pieces and were sterilized prior to surgery. Each implant recipient site was randomly assigned to one of four treatment protocols (Figure 6.2) and two-stage implant placement was applied accordingly: (1) control group (n=9); (2) immediate implant placement and immediate loading group (IIP+IL, n = 8); (3) delayed implant placement and delayed loading group (DIP+DL, n=10); (4) delayed implant placement and immediate loading group (DIP+IL, n=9).

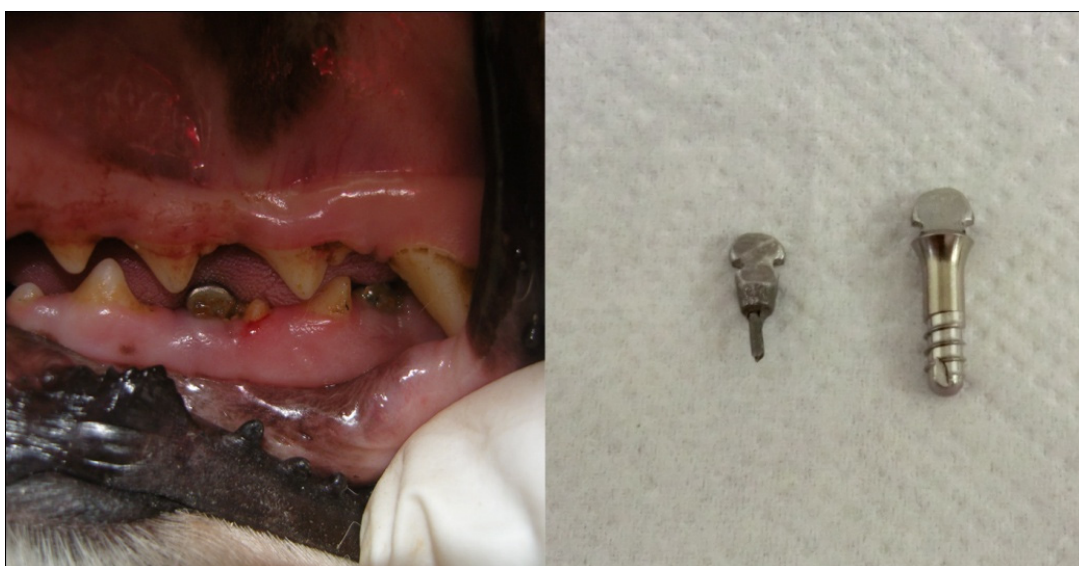


Figure 6.1: *Implant recipient sites and the custom-made implant, post, and crown used in the study. (A) Mesial part of P3 and distal part of P4 were extracted, while the distal part of P3 and mesial part of P4 were kept in the socket. (B) Custom-made titanium implant and NiTi-based post and crown.*

Before insertion, to ensure that the shoulder of the implant was placed at the level of the marginal bone, each site was drilled at low speeds (800 rpm) while being cooled with sterile saline at 4°C. Implants were placed under the same surgical conditions as the tooth extractions in terms of sterility, operation room, and anesthesia. The primary stability of implants was checked after implant insertion by percussion testing, which was carried out by a simple percussion with the handle of a dental instrument on the implant abutment while listening to the resulting sound to detect non-osseointegration. Then, customized posts with a crown made of NiTi alloy (College of Stomatology, Dalian Medical University, Figure 6.1B) were set using resin cement (RelyX, Unicem, RX, 3M ESPE, St. Paul, MN, USA). During the experimental period, the loading pressure on the implants was kept similar using 20- μ m articulating papers (Accufilm II,

RX, 3M ESPE). Combined with general anesthesia, plaque control was ensured three times per week using a 0.2% chlorhexidine gel on implant placement sites with a soft toothbrush.

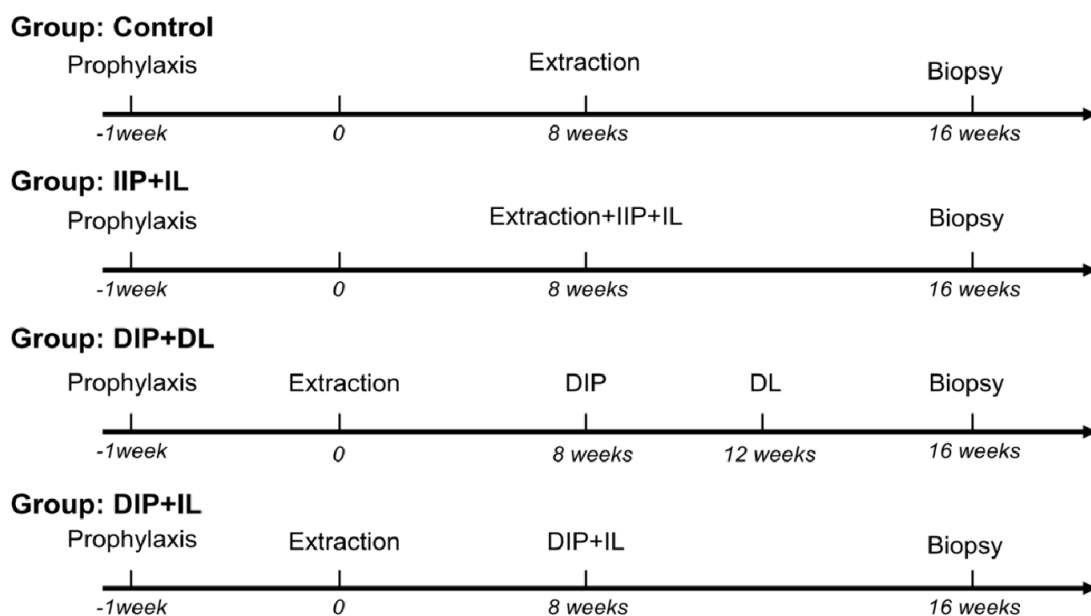


Figure 6.2: Time frame for different protocols. DIP = delayed implant placement; DL = delayed loading; IIP = immediate implant placement; IL = immediate loading.

Biopsies. At week 17 (Figure 6.2), all dogs were sacrificed by means of an intravenous injection of an overdose of Sumianxin and immediately perfused through the carotid arteries with a fixative solution of 4% paraformaldehyde and 0.0125% glutaraldehyde in 0.1M phosphate buffer, pH7.4. The jawbones were dissected and defleshed. Then, each implant was removed with a carefully preserved 3- to 5-mm piece of peri-implant bone as one piece of sample. The samples were placed into a sealable container with the fixative Unifix® (4% formaldehyde, Tianjin Chemical Reagent Company, China) for 3 weeks at 4°C.

6.2.2 Morphometric CBCT analysis

Thirty-six samples were scanned using a high-resolution had been calibrated before the radiographic study by the manufacturer at the time of installation and when updates

were performed. Each sample was placed vertically in a sponge block in order to prevent any movement during the scanning process, with the long axis of the implant perpendicular to the scanning beam. All samples were scanned using the following exposure conditions: 0.08 mm voxel size, 360° rotation, 90 kV tube voltage, 2 mA tube current, 30.8-second scanning time, and a field of view (FOV) of 40×40 mm. Four ring-shaped volumes of interest (VOIs) were defined around the surface of the implant at coronal (A), middle (B) and apical (C1 and C2) sections along the axis of the implant, as indicated in Figure 6.3. The VOIs comprised trabecular bone only, which was selected through intermediate cross sections by using a custom processing in the CTAn V1.11 (CTAnalyser, Skyscan, Antwerp, Belgium) (Figure 6.4). The irregular anatomic regions of interest (ROIs) were drawn in each section,¹⁶ either manually in case of control group or automatically in case of implant protocols group, such that cortical bone in the ring shaped ROIs were excluded and only trabecular structures were retained for assessment.

Standard 3D structural parameters of trabecular bone architecture (Table 6.2) were quantified from the CBCT images using CTAn on the VOIs, following the recommendations of the American Society of Bone and Mineral Metabolism¹⁶ and Parfitt's system.¹⁷ The group allocation was blinded to the examiner responsible for morphological analyses (JVD).

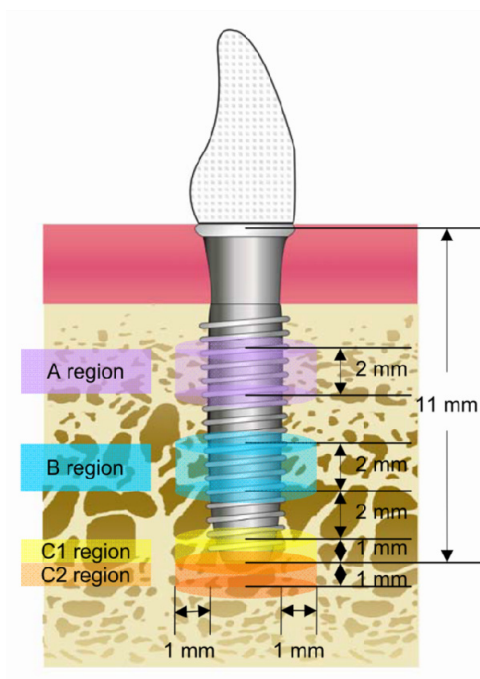


Figure 6.3: Schematic representation of the volumes of interest (VOIs) selected for regional morphometric analysis of peri-implant bone. Four different VOIs were defined in coronal (A), middle (B), and apical (C1 and C2) sections along the axis of the implant (width = 1 mm; height = 2 mm for A and B, 1 mm for C1 and C2).

6.2.3 Statistical analysis

Descriptive analysis expressed data as central tendency and dispersion measurements. The Fisher exact test was used to compare variance between groups, followed by post-hoc Tukey's HSD Test allowing multiple comparisons. Non-parametric statistical methods were used when normality was not confirmed. For all tests performed, the significance level α was 5%. Statistical analysis was performed in RV2.14.2 (R Development Core Team 2012)

Table 6.2: Parameters quantified from CBCT images for regional bone morphometric evaluation in selected volumes of interest (VOIs)

Abbreviation	Morphologic parameter	Standard unit	Description
TV	Total volume of interest	(mm ³)	Volume of the entire region of interest
BV	Bone volume	(mm ³)	Volume of the region segmented as bone
BV/TV	Bone volume fraction	(%)	Ratio of the segmented bone volume to the total volume of the region of interest
BS	Bone surface	(mm ²)	Surface of the region segmented as bone
BS/BV	Specific bone surface	(mm ² /mm ³)	Ratio of the segmented bone surface to the segmented bone volume
Tb.Th	Trabecular thickness	(mm)	Mean thickness of trabeculae, assessed using direct 3D methods
Tb.Sp	Trabecular separation	(mm)	Mean distance between trabeculae, assessed using 3D methods
Tb.N	Trabecular number	(1/mm)	Measure of the average number of trabeculae per unit of length
Tb.Pf	Bone pattern factor	(1/mm)	Index of connectivity of bone
SMI	Structural model index		An indicator for the structure of trabeculae
FD	Fractal dimension		Measure of surface complexity of a trabeculae
Po (tot)	Total porosity percentage	(%)	Ratio of the volume of all open plus closed pores to the total volume of interest
Conn.Dn	Connectivity density	(1/mm ³)	Measure of the degree of connectivity of trabeculae normalized by TV

6.3 Results

All animals recovered well after the surgery without any clinical signs of infection or inflammation, and all behaved normally throughout the experimental period. The surgical procedures and follow-up showed no complications regarding the procedural conditions and all implants were clinically stable until euthanization. Although trabeculae were clearly visible, they were not overall well defined. No artifacts were present in the CBCT images except that along the bone–implant direct interface, a thin blurred layer occurred due to titanium scatter, which was later reduced by custom-made CTAn software.

6.3.1 3D morphometric comparison of the anatomical regions

Morphometric parameters for the VOIs were summarized in Table 6.3. One sample Shapiro-Wilk test showed that most of the parameters were not normally distributed, except for BV/TV and Tb.Pf. In the A, B, C1 and C2 region, a same trend of central tendency and dispersion was visible.

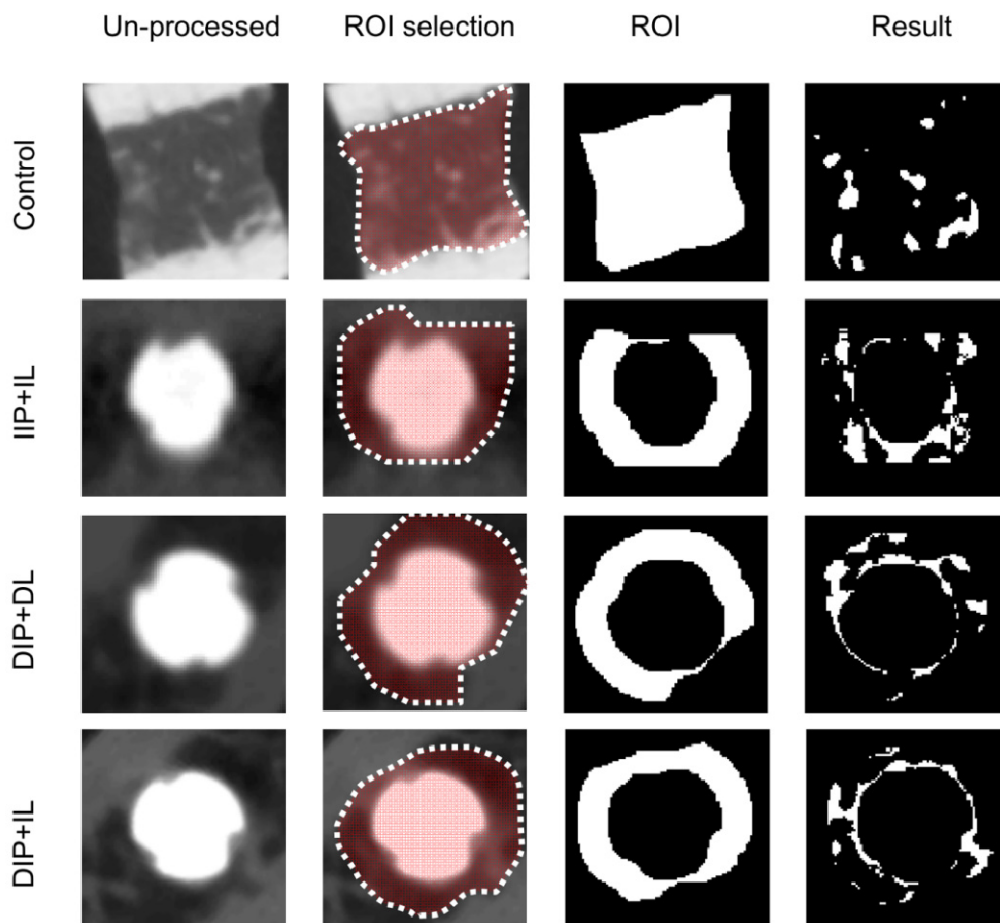


Figure 6.4: Quantification of regional bone morphometry from CBCT images for different implant protocols. From left to right: original CBCT image; manually rough selection of the region of interest (ROI) for the control (approximately 5×5 mm) and for the implant protocols; binary ROI automatically generated by a custom processing algorithm based on thresholding segmentation for the implant protocols, according to the specifications in Figure 6.3, excluding implant and cortical bone; binary segmentation of trabecular bone in this ROI, from which trabecular morphometric parameters were calculated. DIP = delayed implant placement; DL = delayed loading; IIP = immediate implant placement; IL = immediate loading.

Table 6.3: Descriptive statistics of 3D morphometric parameters for different anatomical regions

Morphometric Parameters (unit)	Mean (SD)				Min-Max				Median			
	A	B	C1	C2	A	B	C1	C2	A	B	C1	C2
TV (mm ³)	33.34 (23.19)	39.98 (27.94)	21.48 (25.11)	21.21 (19.02)	12.11 - 114.90	12.70 - 93.21	5.98 - 113.47	9.42 - 66.14	23.98	24.91	10.15	10.80
BV (mm ³)	15.12 (10.63)	16.21 (10.57)	5.78 (5.92)	5.17 (5.50)	2.19 - 44.14	3.77 - 40.15	0.64 - 21.89	0.52 - 19.50	10.43	12.28	5.92	3.35
BV/TV (%)	44.59 (11.47)	43.88 (10.11)	28.73 (11.45)	24.49 (13.35)	15.37 - 71.63	24.67 - 62.32	8.14 - 52.58	4.77 - 46.05	43.65	44.49	31.00	24.11
BS (mm ²)	143.08 (72.76)	155.53 (79.31)	68.47 (59.68)	55.27 (54.46)	34.58 - 345.29	53.89 - 357.94	12.89 - 257.31	7.88 - 193.62	113.33	128.32	46.24	39.83
BS/BV (mm ² /mm ³)	10.75 (2.33)	10.55 (2.00)	14.27 (4.02)	11.77 (2.42)	5.01 - 15.76	5.50 - 14.63	9.31 - 26.51	8.14 - 17.01	10.74	10.38	13.32	11.17
Tb.Th (mm)	0.45 (0.06)	0.45 (0.05)	0.37 (0.07)	0.39 (0.08)	0.36 - 0.69	0.36 - 0.67	0.18 - 0.48	0.23 - 0.52	0.45	0.45	0.39	0.42
Tb.Sp (mm)	0.57 (0.15)	0.63 (0.21)	0.62 (0.15)	0.80 (0.19)	0.40 - 1.08	0.40 - 1.15	0.43 - 0.95	0.51 - 1.05	0.53	0.55	0.57	0.82
Tb.N (1/mm)	0.97 (0.19)	0.97 (0.19)	0.77 (0.25)	0.62 (0.30)	0.43 - 1.32	0.62 - 1.28	0.33 - 1.36	0.19 - 1.02	0.98	0.99	0.80	0.63
Tb.Pf (1/mm)	0.42 (1.65)	0.53 (1.17)	3.69 (1.86)	3.39 (2.16)	-3.44 - 3.77	-2.16 - 2.67	-0.33 - 8.01	-0.93 - 7.52	0.63	0.61	3.77	3.53
SMI	1.29 (0.60)	1.38 (0.41)	1.97 (0.39)	1.89 (0.47)	-0.34 - 2.14	0.36 - 2.03	1.21 - 2.69	0.66 - 2.98	1.48	1.41	2.00	1.94
FD	2.20 (0.14)	2.21 (0.11)	1.97 (0.19)	2.01 (0.22)	1.83 - 2.46	1.97 - 2.46	1.54 - 2.28	1.52 - 2.23	2.18	2.21	2.01	2.06
Po (tot) (%)	55.41 (11.47)	56.12 (10.11)	71.27 (11.45)	75.51 (13.35)	28.37 - 84.63	37.68 - 75.33	47.42 - 91.86	53.95 - 95.23	56.35	55.51	69.00	75.89
Conn.Dn (1/mm ³)	6.12 (2.63)	6.16 (3.02)	5.79 (3.58)	2.40 (2.04)	1.96 - 12.28	1.43 - 12.80	0.30 - 15.00	0.18 - 7.40	6.24	6.49	5.53	1.81

The coronal and middle regions had higher BV/TV, BS/BV and Conn.Dn values than the apical regions. Lower values of Tb.Th and Tb.N were found in the most apical region. However, the differences in these values between the coronal and apical trabeculae were not as large as for BV/TV, BS/BV and Conn.Dn. The apical trabecular bone exhibited much larger Tb.Pf and Po (tot) compared to the coronal bone. The highest values of SMI were found in the apical trabecular bone which is characterized by rods (ideal rods: SMI=3) and the lowest values were identified in the coronal and middle region showing more plate-like structures (ideal plates: SMI=0).

6.3.2 3D morphometric comparison of the implant protocols

Data from different anatomical regions were combined together and were then compared according to different implant protocols. Statistical analyses revealed significant differences ($p < 0.05$) in bone characteristics for control vs. IIP+IL, DIP+IL and DIP+DL, for BS/BV, FD, Tb.Sp and Conn.Dn (Table 6.4).

All implant protocols had significantly higher values than the control for BS/BV and Conn.Dn, while significantly lower values were found for Tb.Sp and FD. However, no significant difference was observed between any two of the treatment groups. The highest values of BV/TV, Tb.N and Conn.Dn, as well as the lowest values of Tb.Sp and Po (tot), were found in the IIP+IL group.

6.4 Discussion

To our knowledge, this is the first study that uses CBCT imaging to quantitatively examine the effects of different implant protocols on the 3D microstructure of peri-implant bone during a 2-month follow-up, laying the groundwork for clinical application of CBCT imaging for the diagnosis and prognosis of osseointegration. The potential advantages of using CBCT images are the ability to image non-invasively, to visualize all serial slices for unbiased comparison and to repeat follow-up measurements, which is almost impossible with histology, where only a limited number of 2D thin

slices can be inspected. While it is generally acknowledged that grayscale values in the reconstructed CBCT images do not allow direct assessment of bone mineral density,^{18, 19} it is feasible to quantify bone structural variables from CBCT images, provided that the spatial resolution is higher than the thinnest trabecular structures.²⁰ The CBCT imager used in this study can display bone details at a minimum voxel size of 80 μm , which is still finer than the thinnest trabecular thickness of mandibular bone, in both humans and dogs, as revealed by μCT .^{21, 22} A morphometric analysis of mandibular trabeculae reported that BV/TV obtained using CBCT images was highly correlated with CT values obtained using multi slice CT images, suggesting that trabecular morphometry can even be used to evaluate the density of mandibular cancellous bone.²³ In addition to the application reported in human condyle bone,²⁴ the high-resolution CBCT imager in our study further showed the ability of 3D visualizing and analyzing peri-implant bone structures.

Table 6.4: Comparison of 3D CBCT morphometric parameters for different implant protocols

Morphometric parameters	Unit	All regions			
		Control (n=9)	DIP+DL (n=10)	DIP+IL (n=9)	IIP+IL (n=8)
BV/TV	(%)	36.67±13.46	35.28±14.26	37.83±14.62	39.16±15.12
BS/BV	(mm^2/mm^3)	9.52±1.70	13.41±4.13*	12.29±2.82§	12.02±2.27†
Tb.Th	(mm)	0.46±0.07	0.39±0.08*	0.42±0.07	0.41±0.07
Tb.Sp	(mm)	0.79±0.19	0.58±0.12*	0.59±0.15§	0.57±0.17†
Tb.N	(1/mm)	0.80±0.24	0.87±0.24	0.88±0.28	0.92±0.29
Tb.Pf	(1/mm)	1.24±2.17	2.35±2.13	1.45±2.21	1.93±2.48
SMI		1.48±0.74	1.70±0.39	1.54±0.49	1.60±0.55
FD		2.23±0.18	2.04±0.19*	2.10±0.15§	2.08±0.20†
Po (tot)	(%)	63.33±13.46	64.72±14.26	62.17±14.62	60.84±15.13
Conn.Dn	($1/\text{mm}^3$)	2.47±1.05	6.45±2.79*	6.55±2.41§	6.73±3.66†

Values are shown as mean \pm SD; *Significant difference ($p < 0.05$) between control and DIP+DL group; §Significant difference ($p < 0.05$) between control and DIP+IL group; †Significant difference ($p < 0.05$) between control and IIP+IL group.

The present study revealed structural variation of trabecular bone between different anatomical regions, suggesting that coronal and middle bone sections had an optimal trabecular structure around the implant to initiate better modeling or osteogenic responses, while the apical bone section required more bone healing. The coronal and middle regions had higher BV/TV values, indicating a more compact trabecular structure, which corresponds with a lower porosity percentage of bone matrices in this area. This can also be explained by observed thicker trabeculae (higher Tb.Th) with less complexity (lower BS/BV) and more plate-like trabecular bone (lower SMI) in the coronal and middle region. On the contrary, the apical region showed lower FD and Conn.Dn which implies less trabecular bone connectedness exists in this region. Furthermore, the apical trabecular bone had a loose structure (lower Tb.N), which also reflected in an increased spacing between trabeculae (higher Tb.Sp). The finding is in full accordance with previous studies performed with μ CT^{25,26} and thus provides the first evidence for CBCT as a reliable modality to analyse trabecular bone.

In view of the paucity of randomized controlled trials applied to compare effects of different implant protocols, we compared all the main available options for implant protocols in both jaws of dogs, ranging from IIP+IL to DIP+DL, including DIP+IL as well as a natural healing group. The results confirmed significant differences in microstructure parameters between implant protocols and control group, but failed to support the clear superiority of one treatment over the others to achieve remodeling and adaptation of micro architecture over a 2-month follow-up period. It seems that the mastication, whether biting or chewing forces, received from these implant protocols, had some level of significance with controls, but was not sensitive enough to have a measurable effect in the micro structures between implant protocols. Moreover, the relatively short observation period of the present examination might be a restriction to a generalization of our findings to humans. It is still unclear to what extent the mastication as a separate loading factor can influence the bone micro architecture and whether it is dominant in initiating the bone remodeling. However, given that the loading protocols may have other confounding factors, such as the strain magnitude, frequency, orientation

and duration of loading,²⁷⁻²⁹ the present results probably can be used to establish a lower bound on the achievable accuracy of prediction of morphometric measures by CBCT.

Our results are consistent with those found in other histomorphometric studies on 2D histological slices. Romanos *et al.* (2003) reported that in a circle of 500 μ m around the implant, no difference existed for BV/TV between DIP+IL and IIP+IL protocols.³⁴ Later, other researchers indicated that within 2 mm of the implants, loading time does not seem to significantly affect the degree of osseointegration or of BIC or the composition of newly formed bone around dental implants.³⁰ However, it has also been described in other studies that BV/TV, Tb.Th and the plate-like structure increased according to loadings, mechanical stimulations or masticatory forces.^{26, 31, 32} Interestingly, though the differences for the parameters between these two protocols were not statistically significant, there was a trend that IIP+IL group, compared with DIP+DL group, had more plate-shape trabeculae (lower SMI and Tb.Pf), denser bone (higher BV/TV), more trabeculae (higher Tb.N), thicker trabeculae (higher Tb.Th), higher trabecular connectivity (lower Po (tot)) and structure strength (higher Conn.Dn).

However, it should be pointed out that the ROIs were set as far as 1mm away from the surface of the implant. Generally, the ROIs in the histological analysis of peri-implant bone reactions range from 100 to 300 μ m.³³ The adaptive remodeling occurred more frequently nearer to the implant surface in comparison to the areas that are 500 μ m away from the implant.³⁴ Nevertheless, it has also been suggested that the bone remodeling area could extend beyond 500 μ m from the implant socket margin.³⁵ According to a histomorphometric comparison in four species including humans, the remodeling is greatest in the bone adjacent to the interface (*i.e.* within 1 mm of the implant,) and decreases dramatically with increasing distance from the implant.³⁶ Moreover, a recent study stated that the loading effect seems to decrease along with the distance from the implant although significant loading effects were found in a distance range of 0-1mm.³⁷ Of the young generated bone and old degenerated bone around implants, the one that lies further from the implant (mature bone) has a more denser trabecular bone structure

while the one closer to the implant (younger bone) is more loosely structured after 2 months of healing.³⁸ Therefore, over or under estimations of morphometric parameters may occur depending on how much mature bone is included in the ROIs.

In our study, the voxel size of 80 μm combined with certain exposure situations from the CBCT imager, especially when an initial optimized reconstruction was applied, displayed high level of bone structural details at the peri-implant level. Yet, titanium scatter during CBCT imaging cannot be completely avoided, even when reconstruction algorithms on the imaging data largely compensated for it. This, theoretically, may lead to a deviation between the morphometric parameters obtained from CBCT and histomorphometry, especially at ROIs which are immediately close to the implant. According to μCT findings, a blurred border of 60 μm was found around 3.5 mm-diameter screw-shaped titanium implants.³⁹ Therefore, a custom-made CTAn protocol was performed in order to automatically exclude implants and threshold values were chosen manually based on the histogram of each image to correct for metal artifacts. By using this method and adjusting the binary pixels with the histogram, the exact contour of the trabeculae in each image was determined. A drawback of this method is that adjustments are defined visually, resulting in a relative variability of intra- and inter-observer measurements. More research is needed to fully standardize imaging processing, minimize artifacts and optimize reconstruction algorithm and exposure factors, such as selecting the appropriate FOV or mAs, for potential clinical applications of CBCT on bone structural analyses.

6.5 Conclusions

Despite the limitations, the immediate implant placement and loading protocol may have an improved bone structural integration compared to that obtained by normal extraction healing. The present findings do not seem to suggest a different bone remodeling pattern when using a delayed vs. an immediate implant placement and loading protocol. Additionally, CBCT combined with image processing is a potential feasible tool in evaluating the complex micro architecture of peri-implant trabecular bone, opening

gates for clinical follow-up analysis of bone healing, whether or not this is peri-implant, and for clinical quality assessment studies.

References

1. Esposito M, Grusovin MG, Polyzos IP, Felice P, Worthington HV. Interventions for replacing missing teeth: dental implants in fresh extraction sockets (immediate, immediate-delayed and delayed implants). *Cochrane Database Syst Rev* 2010; CD005968.
2. Schropp L, Isidor F. Timing of implant placement relative to tooth extraction. *J Oral Rehabil* 2008; **35 Suppl 1**: 33-43.
3. Kacer CM, Dyer JD, Kraut RA. Immediate loading of dental implants in the anterior and posterior mandible: a retrospective study of 120 cases. *J Oral Maxillofac Surg* 2010; **68**: 2861-2867.
4. Romanos GE, Testori T, Degidi M, Piattelli A. Histologic and histomorphometric findings from retrieved, immediately occlusally loaded implants in humans. *J Periodontol* 2005; **76**: 1823-1832.
5. Schincaglia GP, Marzola R, Giovanni GF, Chiara CS, Scotti R. Replacement of mandibular molars with single-unit restorations supported by wide-body implants: immediate versus delayed loading. A randomized controlled study. *Int J Oral Maxillofac Implants* 2008; **23**: 474-480.
6. Romanos G, Froum S, Hery C, Cho SC, Tarnow D. Survival rate of immediately vs delayed loaded implants: analysis of the current literature. *J Oral Implantol* 2010; **36**: 315-324.
7. Herrmann I, Lekholm U, Holm S, Kultje C. Evaluation of patient and implant characteristics as potential prognostic factors for oral implant failures. *Int J Oral Maxillofac Implants* 2005; **20**: 220-230.
8. Griffith JF, Genant HK. Bone mass and architecture determination: state of the art. *Best Pract Res Clin Endocrinol Metab* 2008; **22**: 737-764.
9. Müller R, Van Campenhout H, Van Damme B, Van Der Perre G, Dequeker J, Hildebrand T, Ruegsegger P. Morphometric analysis of human bone biopsies: a quantitative structural comparison of histological sections and micro-computed tomography. *Bone* 1998; **23**: 59-66.
10. Gomes de Oliveira RC, Leles CR, Lindh C, Ribeiro-Rotta RF. Bone tissue microarchitectural characteristics at dental implant sites. Part 1: Identification of clinical-related parameters. *Clin Oral Implants Res* 2011.
11. Ladinsky GA, Vasilic B, Popescu AM, Wald M, Zemel BS, Snyder PJ, Loh L, Song HK, Saha PK, Wright AC, Wehrli FW. Trabecular structure quantified with the MRI-based virtual bone biopsy in postmenopausal women contributes to vertebral deformity burden independent of areal vertebral BMD. *J Bone Miner Res* 2008; **23**: 64-74.
12. Issever AS, Link TM, Kentenich M, Rogalla P, Burghardt AJ, Kazakia GJ,

- Majumdar S, Diederichs G. Assessment of trabecular bone structure using MDCT: comparison of 64- and 320-slice CT using HR-pQCT as the reference standard. *Eur Radiol* 2010; **20**: 458-468.
13. Majumdar S. Magnetic resonance imaging for osteoporosis. *Skeletal Radiol* 2008; **37**: 95-97.
14. Burghardt AJ, Link TM, Majumdar S. High-resolution computed tomography for clinical imaging of bone microarchitecture. *Clin Orthop Relat Res* 2011; **469**: 2179-2193.
15. Vandenberghe B, Jacobs R, Bosmans H. Modern dental imaging: a review of the current technology and clinical applications in dental practice. *Eur Radiol* 2010; **20**: 2637-2655.
16. Bouxsein ML, Boyd SK, Christiansen BA, Guldberg RE, Jepsen KJ, Müller R. Guidelines for assessment of bone microstructure in rodents using micro-computed tomography. *J Bone Miner Res* 2010; **25**: 1468-1486.
17. Parfitt AM, Drezner MK, Glorieux FH, Kanis JA, Malluche H, Meunier PJ, Ott SM, Recker RR. Bone histomorphometry: standardization of nomenclature, symbols, and units. Report of the ASBMR Histomorphometry Nomenclature Committee. *J Bone Miner Res* 1987; **2**: 595-610.
18. Katsumata A, Hirukawa A, Noujeim M, Okumura S, Naitoh M, Fujishita M, Arijji E, Langlais RP. Image artifact in dental cone-beam CT. *Oral Surg Oral Med Oral Pathol Oral Radiol Endod* 2006; **101**: 652-657.
19. Pauwels R, Stamatakis H, Manousaridis G, Walker A, Michielsen K, Bosmans H, Bogaerts R, Jacobs R, Horner K, Tsiklakis K. Development and applicability of a quality control phantom for dental cone-beam CT. *J Appl Clin Med Phys* 2011; **12**: 245-260.
20. Kothari M, Keaveny TM, Lin JC, Newitt DC, Genant HK, Majumdar S. Impact of spatial resolution on the prediction of trabecular architecture parameters. *Bone* 1998; **22**: 437-443.
21. Giesen EB, van Eijden TM. The three-dimensional cancellous bone architecture of the human mandibular condyle. *J Dent Res* 2000; **79**: 957-963.
22. Hiroyuki Imoto AY, Ichiro Shimamura, Satoru Matsunaga, Yoshinobu Ide. Influence of mechanical loading on resonance frequency analysis and trabecular structure of peri-implant bone. *Prosthodontic Research & Practice* 2007; **6**: 120-126.
23. Naitoh M, Aimiya H, Hirukawa A, Arijji E. Morphometric analysis of mandibular trabecular bone using cone beam computed tomography: an in vitro study. *Int J Oral Maxillofac Implants* 2010; **25**: 1093-1098.
24. Liu SM, Zhang ZY, Li JP, Liu DG, Ma XC. [A study of trabecular bone structure in the mandibular condyle of healthy young people by cone beam computed tomography]. *Zhonghua Kou Qiang Yi Xue Za Zhi* 2007; **42**: 357-360.

25. van Ruijven LJ, Giesen EB, Mulder L, Farella M, van Eijden TM. The effect of bone loss on rod-like and plate-like trabeculae in the cancellous bone of the mandibular condyle. *Bone* 2005; **36**: 1078-1085.
26. Moon HS, Won YY, Kim KD, Ruprecht A, Kim HJ, Kook HK, Chung MK. The three-dimensional microstructure of the trabecular bone in the mandible. *Surg Radiol Anat* 2004; **26**: 466-473.
27. Grunheid T, Langenbach GE, Brugman P, Everts V, Zentner A. The masticatory system under varying functional load. Part 2: Effect of reduced masticatory load on the degree and distribution of mineralization in the rabbit mandible. *Eur J Orthod* 2011; **33**: 365-371.
28. Zhang X, Vandamme K, Torcasio A, Ogawa T, van Lenthe GH, Naert I, Duyck J. In vivo assessment of the effect of controlled high- and low-frequency mechanical loading on peri-implant bone healing. *J R Soc Interface* 2012; **9**: 1697-1704.
29. Barak MM, Lieberman DE, Hublin JJ. A Wolff in sheep's clothing: trabecular bone adaptation in response to changes in joint loading orientation. *Bone* 2011; **49**: 1141-1151.
30. Ghanavati F, Shayegh SS, Rahimi H, Sharifi D, Khalessheh N, Eslami B. The effects of loading time on osseointegration and new bone formation around dental implants: a histologic and histomorphometric study in dogs. *J Periodontol* 2006; **77**: 1701-1707.
31. Borah B, Dufresne TE, Cockman MD, Gross GJ, Sod EW, Myers WR, Combs KS, Higgins RE, Pierce SA, Stevens ML. Evaluation of changes in trabecular bone architecture and mechanical properties of minipig vertebrae by three-dimensional magnetic resonance microimaging and finite element modeling. *J Bone Miner Res* 2000; **15**: 1786-1797.
32. Rubin C, Turner AS, Müller R, Mitra E, McLeod K, Lin W, Qin YX. Quantity and quality of trabecular bone in the femur are enhanced by a strongly anabolic, noninvasive mechanical intervention. *J Bone Miner Res* 2002; **17**: 349-357.
33. Corpas Ldos S, Jacobs R, Quirynen M, Huang Y, Naert I, Duyck J. Peri-implant bone tissue assessment by comparing the outcome of intra-oral radiograph and cone beam computed tomography analyses to the histological standard. *Clin Oral Implants Res* 2011; **22**: 492-499.
34. Romanos GE, Toh CG, Siar CH, Wicht H, Yacoob H, Nentwig GH. Bone-implant interface around titanium implants under different loading conditions: a histomorphometrical analysis in the *Macaca fascicularis* monkey. *J Periodontol* 2003; **74**: 1483-1490.
35. Futami T, Fujii N, Ohnishi H, Taguchi N, Kusakari H, Ohshima H, Maeda T. Tissue response to titanium implants in the rat maxilla: ultrastructural and histochemical observations of the bone-titanium interface. *J Periodontol* 2000; **71**: 287-298.
36. Garetto LP, Chen J, Parr JA, Roberts WE. Remodeling dynamics of bone supporting

rigidly fixed titanium implants: a histomorphometric comparison in four species including humans. *Implant Dent* 1995; **4**: 235-243.

37. Ogawa T, Zhang X, Naert I, Vermaelen P, Deroose CM, Sasaki K, Duyck J. The effect of whole-body vibration on peri-implant bone healing in rats. *Clin Oral Implants Res* 2011; **22**: 302-307.

38. Cochran DL. The evidence for immediate loading of implants. *J Evid Based Dent Pract* 2006; **6**: 155-163.

39. Stoppie N, van der Waerden JP, Jansen JA, Duyck J, Wevers M, Naert IE. Validation of microfocus computed tomography in the evaluation of bone implant specimens. *Clin Implant Dent Relat Res* 2005; **7**: 87-94.

7.1 Discussion

During the last decades, the understanding and improvement of recovery of peri-implant tissues after dental implant treatment has attracted a lot of attention in oral implantology. This doctoral thesis was in an endeavor to elaborate the effects of delayed and immediate implant placement and loading protocols on the healing of peri-implant nerve fibres and bone structures. To achieve such aims in a clinical trial would not only be very hard in identifying homogenous samples, yet ethical issues might also be involved when it would come to peri-implant histology. Therefore, it was opted to work with a split mouth dog model in 2 chapters (**Chapters 3 & 6**) of this thesis.

In this general discussion, an extensive summary was given to each chapter in this thesis. The various hypotheses proposed in the Introduction part (**Chapter 1**) were then discussed. Next, the impact of the current results on tissues healing followed by various implant protocols was described. Finally, the validation of the radiographic measurements, including their primary limitation, was elaborated.

In **Chapter 2**, the available literature on the influence of dental implant placement and loading protocols on peri-implant innervation were systematically reviewed and assessed for their study characteristics. Furthermore, histological evidence from peri-implant tissues, histomorphological characteristics of peri-implant nerve fibres, loading parameters were discussed with a focus on the question of prognosis: “Is there peri-implant innervation and if so, what is the effect of the time between tooth extraction and implant placement or implant loading on neural fibre content in the peri-implant hard and soft tissues?” For ease of understanding, we further formulated the aforementioned research question into a population, exposure and outcome (PEO) question.¹ Since the most included studies were observational, we try to use a combined approach of PRISMA and MOOSE instead of only PRISMA, which would markedly improve our evaluation.

All papers included in the review reported sensory innervation around osseointegrated

implants, either in the bone-implant interface or peri-implant epithelium, which expressed a particular distinct innervation pattern. Compared to unloaded implants or extraction sites without implantation, a significant higher density of nerve fibres around loaded dental implants was confirmed. These results suggested that external loading may lead to more reinnervation around dental implants. However, the included studies did not permit to report obvious differences on the innervation of peri-implant tissues between immediate and delayed groups. In addition, it is worth mentioning that the number and density of free nerve endings are two of the most reported estimates for reinnervation. Variations of other morphologic parameters which could be closely related to nerve regeneration, such as myelinated/unmyelinated fibre diameter, axon diameter, myelin thickness and conduction velocity, are still far from clear. Although this review was mainly focused on histological proofs on innervation around dental implants, it is worth reminding that most psychophysical and neurophysiological assessments evaluated occlusal tactile thresholds not only in peri-implant bone, but also in the neighboring mucosa, which indicated that these studies did not exclude sensory information originating from soft tissues. It has been reported that the responses to vibrational loading of implants was less strong than that to the loading of the natural tooth.^{2,3} A recent human study using functional MRI indicated that punctate mechanical stimulation of oral implants is able to activate both primary and secondary cortical somatosensory areas representing an underlying hot field at the cortex level for osseoperception.⁴

The study in **Chapter 3** illustrated the recovery pattern and the morphological characteristics of myelinated nerve fibres around dental implants followed by immediate vs. delayed implant placement and loading protocols in dogs. The quantitative observation by Light Microscopy and Transmission Electron Microscopy on peri-implant myelinated nerve fibres was addressed and characterized histomorphologically in this study. Immunohistochemistry was further performed in each group to confirm the presence of myelinated nerve structures.

This study adds to our understanding of the basic mechanisms of osseoperception. Previous histological evidence revealed the presence of specialized Ruffini mechanoreceptive terminals in the peri-implant area^{5,6} and increased free nerve endings with implant loading.⁷ For the first time, the comparisons between various clinical related implant protocols were included in this randomized controlled animal study by a split-mouth design, which is one of popular designs in oral health research.⁸ The main reason of using this design was that it could help removing vast amounts of inter-individual variability from the estimates of the treatment effect. More specifically, to assist the comparison under standardized healing and test conditions, the application of split-mouth design with randomized implant recipient site selection and isolated loading conditions of individual implants, can minimize the potential bias and variations (*e.g.*, dynamic loading forces in the mouth of different dogs) between experimental animals and thus exclude potential carry-over effects.

The most important findings were the higher nerve density with optimized morphometric indices for implants immediately placed and loaded, which actually supported the hypothesis that early loading produces more favorable peri-implant innervation recovery. Although it should be noted that the specific physiological function of these regenerated nerve fibres is still unclear, it can be assumed that immediate implant placement after extraction leaves the nerves in place with activation of periphery regrowth signal preventing degeneration. The implant loading might result in activation of peri-implant nerve signals and further promote peri-implant nerve regeneration. What we also found was that gingival and apical regions are more densely innervated than other peri-implant areas. Another result in this study was that nerve density around mandible implants is higher compared to those around maxilla implants, especially in the peri-implant gingiva of the three implant groups (DIP+DL, IIP+IL and DIP+IL). Therefore, it is reasonable to assume that the distribution of reinnervation not only relies on the external loading protocol, but also on the location and distribution of loadings. Although the evaluation of the functional role of the identified nerve fibres were not covered in this study due to the limitation of animal study, the psychophysical

and neurophysiological evidence from peri-implant tissues has already been addressed, as discussed in **Chapter 2**.

The study described in **Chapter 4** was designed to evaluate and validate the use of CBCT for 3D peri-implant trabecular bone structure analyses by comparing the 3D morphometric CBCT parameters with 2D histomorphometry.

As a gold standard, histology has been used to investigate the bone morphometry in 2D due to its high spatial resolution and image contrast.⁹ It was, nevertheless, limited by the destructive nature of the procedure, preventing specimens from being used for subsequent static or dynamic analyses. Since the introduction of the application of CBCT in bone structure analyses,¹⁰ there has been an increasing demand for determining the accuracy of CBCT in trabecular bone structure measurements. The specific objective of this chapter was to examine the accuracy and potential limitations in respect to 3D structural properties of cancellous bone, especially in the peri-implant area. To avoid the potential effects by the observed outliers or extreme values,¹¹ the Pearson's correlation coefficient and Bland-Altman analyses were applied in the evaluation of the agreement between CBCT and conventional histology techniques.

Moderate to high correlation ($r= 0.65-0.85$) were found for both measurements on the peri-implant trabecular bone structures. The Bland-Altman plots further showed strong agreement for Tb.Th, Tb.Sp, Tb.N and BV/TV, regardless of the presence of implants in the samples. Similarly, strong correlation and agreements were observed when comparing the trabecular bone microstructure measurements with μ CT on human jawbones.¹² However, we also need to be aware of significant higher Tb.Th and Tb.Sp values and lower BV/TV and Tb.N values which were found on CBCT images ($P < 0.001$). The latter could be explained by discrepancy of the voxel size between CBCT (80 μm) and histology images (6 μm), resulting in smaller trabecular boundaries less well defined by CBCT than the histologic images. As suggested by other studies, small trabeculae are normally poorly depicted by low-resolution systems when comparing HR-pQCT (82 μm) with CT (18 μm)¹³ and MSCT (247 μm) with CT (16 μm).¹⁴ For the

overestimation of CBCT while comparing with histomorphometry, one possible reason was the algorithm difference between 3D and 2D measurements, which has been reported in the similar comparison between μ CT and histomorphometry.^{9, 11} Therefore, it is necessary to take into account these limitations while applying and extrapolating those morphometric indices.

The aim of **Chapter 5** was to validate the scanning protocol of CBCT enabling accurate quantification of the trabecular bone microstructure by comparing the scanning results with those from μ CT. The effect of X-ray tube current, voltage settings and the soft tissue surrounding the bone on the various bone morphometric parameters were investigated in human jaw bones.

This accuracy analysis is essential while introducing a novel imaging modality.^{15, 16} Although the effect of CBCT scanning indices on image quality, bone density and linear measurements were extensively studied in the literature,¹⁷⁻²⁰ the degree to which trabecular bone microstructure measurements differs between the available settings on the CBCT has not been well documented. Generally, smallest voxel size in the small FOVs of CBCT machines could typically produce a better image quality and consequently improve the measurement accuracy.^{17, 21, 22} More recently, Ibrahim *et al.* reported that the reconstruction algorithm (standard or high) and rotation steps (180° or 360°) does not influence the trabecular bone microstructure measurements by using the same CBCT model as we did (3D Accuitomo 170).¹² Thus, the objective of this chapter was to exclusively assess potential influence of the tube voltage and current and surrounding soft-tissue on trabecular bone microstructure measurements.

The results of this study confirmed that there is no significant difference ($\alpha > 0.05$) in the trabecular microstructure analyses obtained with the investigated tube voltage and current, though radiographic CBCT analysis tended to slightly overestimate BV/TV, Tb.Sp and Tb.Th compared to μ CT. The possible reason for this overestimation, as discussed before, was that CBCT has lower image resolution than μ CT. This drawback might be overcome with the optimization of image reconstruction algorithm or the

calculation of a correction factor. The soft-tissue effect was not observed for all variables, which again showed the potential value of high-resolution CBCT imaging for *in vivo* applications of quantitative bone morphometry and bone quality assessment. Our outcome is helpful to determine a scanning protocol to reduce exposure dose, tube voltage and current, which could also result in better image quality.

Chapter 6 comprised a study on the characterization of trabecular bone changes after immediate and delayed implant protocols using the novel method of high-resolution CBCT, which was validated in previous two chapters. This experiment shared the same study design of the animal experiment in **Chapter 3**.

The reasons why we focused on the peri-implant trabecular bone structure were that it severely affects the dental implant's primary stability and survival rate,^{23,24} and is more metabolically active to indicate early physiopathologic changes than cortical bone.²⁵ While the bone-implant contact area (BIC), an important index of interfacial strength, has been confirmed to directly influence this primary stability among the structural parameters of trabecular bones, BIC is still a 2D parameter.²⁶ Thus, it is crucial to objectively quantify the 3D trabecular bone structures of the jawbone before and after inserting a dental implant for to enable improved assessment of osseointegration.

Nowadays, μ CT is widely applied for 3D evaluation of trabeculae structures of bone biopsies and small animal bones,^{9,27} though it is limited for clinical application because of its scanning range restrictions. On the other hand, CBCT is becoming more suitable and promising for applying bone structure analysis thanks to the improvement of CBCT's resolution, which is now achieving spatial resolutions similar to those produced by high resolution-peripheral quantitative CT and higher than the thinnest trabecular structures.^{28,29} Nevertheless, dental CBCT was once adopted to assess bone mineral density using a single gray scale value, simply considering the trabecular bone as a non-porous homogeneous structure.³⁰ Now it is also acknowledged that grayscale values in the reconstructed CBCT images do not allow direct assessment of bone mineral density.^{31,32} Until recently, CBCT at a resolution of 125 μ m with image processing was

successfully applied for bone structure assessments in the area of the human mandibular condyle.¹⁰ Naturally, this brings up the question whether CBCT could be applied for bone structure analyses around dental implants. For these reasons, CBCT imaging has been applied in this chapter to quantify the effects of different implant protocols on the 3D microstructure of peri-implant bone, which was also the first attempt to analyze peri-implant bone structures of alveolar bones in the history of using dental CBCT. These morphologic findings were consistent with a previous observation conducted by μ CT on the human mandible.³³

The main limitation of the CBCT technique, as in conventional CT, is associated with metal artifacts, which occur particularly when the X-rays pass through metal objects (*e.g.*, titanium implants). It is known that dense objects absorb a considerably higher amount of X-rays than less dense objects.³⁴ As a result, the artifacts such as edge gradients, halo effects and beam-hardening could generate.³⁵ In theory, these artifacts could cause interference in discriminating the bone from non-bone tissue, especially at the interface immediately close to the implant surface. For this reason, special attention was paid to metal artifact reduction in this study. The exact contour of the trabeculae in each ROI was determined and the metal artifact was controlled at the lowest level by using a custom-made image analysis protocol and adjusting the binary pixels manually with the histogram. This adaptive thresholding was also proved significantly better in segmenting the bone structure out of CBCT images in a recent study.³⁶ However, the inevitable question of this method was that the adjustments were defined visually, resulting in a relative variability of intra- and inter-observer measurements. Interestingly, 3D bone structure quantification conducted with CBCT have attracted much interest due to their possible and promising clinical application, either being applied on human mandible or comparing with μ CT and MSCT.^{12, 37,38}

The present results confirmed significant differences in microstructure parameters between implant protocols and control group, but failed to support a different bone remodeling pattern when using a delayed vs. an immediate implant placement and

loading protocol in an observation time of 8 weeks. These were consistent with other similar 2D histomorphometric studies between DIP+IL (delayed implant placement and immediate loading) group and IIP+IL (immediate implant placement and immediate loading) group within a perimeter of 0.5 mm around the implant.^{39, 40}

7.2 Conclusions

From the studies mentioned in the previous chapters, the following conclusions can be drawn:

-In **Chapter 2**, the available literature described peri-implant innervation with a distinct pattern in hard and soft tissues. It seems that implant loading could increase the density of nerve fibres in peri-implant tissues. Nevertheless, due to the variability in loading protocols and the high risk of bias in the studies included, there is still little confirmed information about the effects of different loading protocols and time-dependent changes in osseoperception following various implant placement and loading protocols. On the other hand, it further reveals the need for more uniformity in performing randomized controlled trials, longer observation periods and standardization of protocols.

-Within a range of 300 µm around implants, immunocytochemistry and transmission electron microscopy confirmed the presence of neural structures and revealed their ultrastructural characteristics in **Chapter 3**. Myelinated nerve fibres densely populated peri-implant crestal gingival and apical regions. In comparison with the normal extraction healing, all implant groups showed higher innervation, smaller fibre diameter and g-ratio. Furthermore, IIP+IL group had improved peri-implant innervations pattern in both jaws than in DIP+DL and DIP+IL, albeit with a tendency towards significance. The immediate placed and loaded implants may promote optimized peri-implant reinnervation. However, further functional measures on the peri-implant nerve fibres are still required.

-**Chapter 4** supported the assumption that high-resolution CBCT allows the 3D

peri-implant bone morphometry quantification at the micro structural level, after comparing 3D morphometric bone parameters to the 2D indices assessed from conventional histomorphometry. CBCT measurement showed higher Tb.Th and Tb.Sp, lower BV/TV and Tb.N. Both measurements on the peri-implant trabecular bone structure revealed moderate to high correlation. Strongest agreement for Tb.Th followed by Tb.Sp, Tb.N and BV/TV were found in this study, regardless of the presence of implants. In addition, high-resolution CBCT (80 μm) combined with image processing in our study showed its potential ability in evaluating the complex microarchitecture of peri-implant trabecular bone. This supplements and provides justifications to **Chapter 6**, which indicates a potential clinical diagnostic value of CBCT-based peri-implant bone morphometric characterization.

-Furthermore, **Chapter 5** confirmed that there was no significant difference in the trabecular micro structure analyses except for Tb.Sp obtained with the investigated CBCT and μCT exposure protocols. Both measurements on the peri-implant trabecular bone structure revealed high positive correlation except for Tb.Th. However, radiographic CBCT analyses tended to slightly overestimate BV/TV, Tb.Sp and Tb.Th comparing with μCT . The soft-tissue effect on the bone morphometry analyses was not observed, which again showed the potential value of high-resolution CBCT imaging for *in vivo* applications of quantitative bone morphometry and bone quality assessment. Our outcome is helpful to determine a scanning protocol to reduce the exposure dose, tube voltage and current, which could also provides a precise morphometric measurements. The clinical use of low-dose CBCT as an accurate and low-dose alternative to MSCT in determining the 3D trabecular bone structure during the pre-operative phase and even during the whole bone healing phase seems promising.

-Finally, the recovery of peri-implant bone structures was primarily established in **Chapter 6** within the early weeks of regeneration. Coronal and middle regions had more compact, plate-like and thicker trabeculae. The immediate placed and loaded implants might have an improved bone structural integration than normal extraction healing.

Nevertheless, this study did not support the hypothesis of a different bone remodeling pattern when using a delayed vs. an immediate implant protocol. This study could also lay the groundwork for clinical applications of CBCT imaging for diagnosis and prognosis of differential bone healing and osseointegration.

7.3 Future prospects

This thesis reported the nerve fibres and bone structures healing following immediate and delayed implant placement and loading protocols in a split-mouth designed animal model, followed by the validation of radiographic way. Apart from serving as a comprehensive understanding of the recovery of peri-implant tissues, the main objectives were to provide randomized controlled evidence for the development of peri-implant nerve fibres and bone structures in the jaw bones, and to develop a radiographic way which could enable standardized evaluation of peri-implant bone structures.

The findings in this thesis provide solid evidence at a microscopic level for understanding mechanisms of tissue recovery under various implant placement and loading protocols, along with some limitations in the implementation of the experiment. Specific interesting and valuable prospects for future researches which could be addressed are:

- Well-designed RCTs and animal experiments with enhanced control on biological, psychological, or methodological factors, including additional neurophysiological testing to standardize the frequency and direction of loading, are needed to predict and generalize the impact of timing of implant placement and loading protocols on the recovery of sensory perception in peri-implant tissues. Further observation should be planned over a longer follow-up period.
- Despite the neurophysiological and psychophysical evidence from (pre) clinical trials, it would be of interest to determine whether those differences we found in morphometric

parameters resulted in the actual sensory activation with clinical significance. It might be possible to further explore osseoperception in a clinical level by collecting data or samples from patients who can offer retrieved implants.

- The morphological findings in this doctoral thesis promote related studies on peripheral mechanism and new hypotheses, such as local grafting of Schwann cells or calcitonin gene-related peptide-alpha to improve peripheral nerve fibers regeneration after dental implant surgery. It is interesting to know whether osseoperception could be improved and accelerated by an external growth factor. There is also reason to believe that the potential morphophysiological relationship would become a hot topic for osseoperception in future studies.

- To validate the CBCT technique as a clinical imaging modality in measuring trabecular microstructure at oral implant sites, more research is required to fully standardize imaging processing, optimize reconstruction algorithm and exposure factors (*e.g.*, FOV, contrast to noise ratio) and minimize metal artefacts during CBCT scanning on the visibility of the trabecular microstructure (*e.g.*, a comparison between CBCT and μ CT with respect to the streak pattern differences caused by beam hardening; the effects of number of implants and corresponding spatial distribution on the image artifacts; motion artifacts due to patient movement).

- Given rapid progress in CBCT, it might be helpful to initiate further *in vitro* investigations dealing with the influence of using varying types of CBCT systems, different scanning parameters in comparison to MSCT and μ CT systems, before applying our observation as an accurate clinical reference.

- As mentioned above, this doctoral thesis may contribute to mastering the relativity of bone micro architecture and nerve reinnervation. We expect these findings to improve our understanding on the influence of morphological and ultrastructural factors in osseoperception. This improved understanding may, eventually, lead to more clinical approaches in the promotion of the success of implant treatment.

References

1. Holly C, Salmond SW, Sabbatini M. Comprehensive systematic review for advanced nursing practice. New York: Springer Publishing Company, 2011.
2. Hsieh WW, Luke A, Alster J, Weiner S. Sensory discrimination of teeth and implant-supported restorations. *Int J Oral Maxillofac Implants* 2010; **25**: 146-152.
3. Weiner S, Sirois D, Ehrenberg D, Lehrmann N, Simon B, Zohn H. Sensory responses from loading of implants: a pilot study. *Int J Oral Maxillofac Implants* 2004; **19**: 44-51.
4. Habre-Hallage P, Dricot L, Jacobs R, van Steenberghe D, Reyckler H, Grandin CB. Brain plasticity and cortical correlates of osseoperception revealed by punctate mechanical stimulation of osseointegrated oral implants during fMRI. *Eur J Oral Implantol* 2012; **5**: 175-190.
5. Suzuki Y, Matsuzaka K, Ishizaki K, Tazaki M, Sato T, Inoue T. Characterization of the peri-implant epithelium in hamster palatine mucosa: behavior of Merkel cells and nerve endings. *Biomed Res* 2005; **26**: 257-269.
6. Yamaza T, Kido MA, Wang B, Danjo A, Shimohira D, Murata N, Yoshinari M, Tanaka T. Distribution of substance P and neurokinin-1 receptors in the peri-implant epithelium around titanium dental implants in rats. *Cell Tissue Res* 2009; **335**: 407-415.
7. Wada S, Kojo T, Wang YH, Ando H, Nakanishi E, Zhang M, Fukuyama H, Uchida Y. Effect of loading on the development of nerve fibers around oral implants in the dog mandible. *Clin Oral Implants Res* 2001; **12**: 219-224.
8. Lesaffre E, Philstrom B, Needleman I, Worthington H. The design and analysis of split-mouth studies: what statisticians and clinicians should know. *Stat Med* 2009; **28**: 3470-3482.
9. Müller R, Van Campenhout H, Van Damme B, Van Der Perre G, Dequeker J, Hildebrand T, Rueggsegger P. Morphometric analysis of human bone biopsies: a quantitative structural comparison of histological sections and micro-computed tomography. *Bone* 1998; **23**: 59-66.
10. Liu SM, Zhang ZY, Li JP, Liu DG, Ma XC. [A study of trabecular bone structure in the mandibular condyle of healthy young people by cone beam computed tomography]. *Zhonghua Kou Qiang Yi Xue Za Zhi* 2007; **42**: 357-360.
11. Chappard D, Retailleau-Gaborit N, Legrand E, Basle MF, Audran M. Comparison insight bone measurements by histomorphometry and microCT. *J Bone Miner Res* 2005; **20**: 1177-1184.
12. Ibrahim N, Parsa A, Hassan B, van der Stelt P, Aartman IHA, Wismeijer D. The effect of scan parameters on cone beam CT trabecular bone microstructural measurements of the human mandible. *Dentomaxillofac Radiol* 2013; **42**.
13. Tjong W, Kazakia GJ, Burghardt AJ, Majumdar S. The effect of voxel size on

high-resolution peripheral computed tomography measurements of trabecular and cortical bone microstructure. *Med Phys* 2012; **39**: 1893-1903.

14. Issever AS, Link TM, Kentenich M, Rogalla P, Burghardt AJ, Kazakia GJ, Majumdar S, Diederichs G. Assessment of trabecular bone structure using MDCT: comparison of 64- and 320-slice CT using HR-pQCT as the reference standard. *Eur Radiol* 2010; **20**: 458-468.

15. Bland JM, Altman DG. Measuring agreement in method comparison studies. *Stat Methods Med Res* 1999; **8**: 135-160.

16. Bland JM, Altman DG. Statistical Methods for Assessing Agreement between Two Methods of Clinical Measurement. *Lancet* 1986; **1**: 307-310.

17. Hassan B, Couto Souza P, Jacobs R, de Azambuja Berti S, van der Stelt P. Influence of scanning and reconstruction parameters on quality of three-dimensional surface models of the dental arches from cone beam computed tomography. *Clin Oral Investig* 2010; **14**: 303-310.

18. Parsa A, Ibrahim N, Hassan B, Motroni A, van der Stelt P, Wismeijer D. Influence of cone beam CT scanning parameters on grey value measurements at an implant site. *Dentomaxillofac Radiol* 2013; **42**.

19. Vandenberghe B, Jacobs R, Bosmans H. Modern dental imaging: a review of the current technology and clinical applications in dental practice. *Eur Radiol* 2010; **20**: 2637-2655.

20. Sennerby L, Andersson P, Pagliani L, Giani C, Moretti G, Molinari M, Motroni A. Evaluation of a Novel Cone Beam Computed Tomography Scanner for Bone Density Examinations in Preoperative 3D Reconstructions and Correlation with Primary Implant Stability. *Clin Implant Dent Relat Res* 2013.

21. Maret D, Telmon N, Peters OA, Lepage B, Treil J, Inglese JM, Peyre A, Kahn JL, Sixou M. Effect of voxel size on the accuracy of 3D reconstructions with cone beam CT. *Dentomaxillofac Radiol* 2012; **41**: 649-655.

22. Bauman R, Scarfe W, Clark S, Morelli J, Scheetz J, Farman A. Ex vivo detection of mesiobuccal canals in maxillary molars using CBCT at four different isotropic voxel dimensions. *International Endodontic Journal* 2011; **44**: 752-758.

23. Huang HL, Tu MG, Fuh LJ, Chen YC, Wu CL, Chen SI, Hsu JT. Effects of Elasticity and Structure of Trabecular Bone on the Primary Stability of Dental Implants. *J Med Biol Eng* 2010; **30**: 85-89.

24. Hsu JT, Fuh LJ, Tu MG, Li YF, Chen KT, Huang HL. The Effects of Cortical Bone Thickness and Trabecular Bone Strength on Noninvasive Measures of the Implant Primary Stability Using Synthetic Bone Models. *Clin Implant Dent Relat Res* 2013; **15**: 251-261.

25. Griffith JF, Genant HK. Bone mass and architecture determination: state of the art.

Best Pract Res Clin Endocrinol Metab 2008; **22**: 737-764.

26. Hsu JT, Huang HL, Tsai MT, Wu AY, Tu MG, Fuh LJ. Effects of the 3D bone-to-implant contact and bone stiffness on the initial stability of a dental implant: micro-CT and resonance frequency analyses. *Int J Oral Maxillofac Surg* 2013; **42**: 276-280.
27. de Oliveira RCG, Leles CR, Lindh C, Ribeiro-Rotta RF. Bone tissue microarchitectural characteristics at dental implant sites. Part 1: Identification of clinical-related parameters. *Clin Oral Implants Res* 2012; **23**: 981-986.
28. Kothari M, Keaveny TM, Lin JC, Newitt DC, Genant HK, Majumdar S. Impact of spatial resolution on the prediction of trabecular architecture parameters. *Bone* 1998; **22**: 437-443.
29. Giesen EB, van Eijden TM. The three-dimensional cancellous bone architecture of the human mandibular condyle. *J Dent Res* 2000; **79**: 957-963.
30. Ho JT, Wu J, Huang HL, Chen MYC, Fuh LJ, Hsu JT. Trabecular bone structural parameters evaluated using dental cone-beam computed tomography: cellular synthetic bones. *Biomed Eng Online* 2013; **12**.
31. Katsumata A, Hirukawa A, Noujeim M, Okumura S, Naitoh M, Fujishita M, Ariji E, Langlais RP. Image artifact in dental cone-beam CT. *Oral Surg Oral Med Oral Pathol Oral Radiol Endod* 2006; **101**: 652-657.
32. Pauwels R, Stamatakis H, Manousaridis G, Walker A, Michielsen K, Bosmans H, Bogaerts R, Jacobs R, Horner K, Tsiklakis K, Consortium SP. Development and applicability of a quality control phantom for dental cone-beam CT. *J Appl Clin Med Phys* 2011; **12**: 3478.
33. Moon HS, Won YY, Kim KD, Ruprecht A, Kim HJ, Kook HK, Chung MK. The three-dimensional microstructure of the trabecular bone in the mandible. *Surg Radiol Anat* 2004; **26**: 466-473.
34. Bernhardt R, Scharnweber D, Muller B, Thurner P, Schliephake H, Wyss P, Beckmann F, Goebbels J, Worch H. Comparison of microfocus- and synchrotron X-ray tomography for the analysis of osteointegration around Ti6Al4V implants. *Eur Cell Mater* 2004; **7**: 42-51.
35. Schulze RK, Berndt D, d'Hoedt B. On cone-beam computed tomography artifacts induced by titanium implants. *Clin Oral Implants Res* 2010; **21**: 100-107.
36. Nackaerts O, Depypere M, Zhang G, Vandenberghe B, Maes F, Jacobs R, Consortium S. Segmentation of Trabecular Jaw Bone on Cone Beam CT Datasets. *Clin Implant Dent Relat Res* 2014.
37. Parsa A, Ibrahim N, Hassan B, van der Stelt P, Wismeijer D. Bone quality evaluation at dental implant site using multislice CT, micro-CT, and cone beam CT. *Clin Oral Implants Res* 2013.

38. Klintström E, Smedby Ö, Moreno R, Brismar TB. Trabecular bone structure parameters from 3D image processing of clinical multi-slice and cone-beam computed tomography data. *Skeletal Radiol* 2014; **43**: 197-204.
39. Romanos GE, Toh CG, Siar CH, Wicht H, Yacoob H, Nentwig GH. Bone-implant interface around titanium implants under different loading conditions: a histomorphometrical analysis in the *Macaca fascicularis* monkey. *J Periodontol* 2003; **74**: 1483-1490.
40. Ghanavati F, Shayegh SS, Rahimi H, Sharifi D, Ghanavati F, Khalessah N, Eslami B. The effects of loading time on osseointegration and new bone formation around dental implants: a histologic and histomorphometric study in dogs. *J Periodontol* 2006; **77**: 1701-1707.

For the past few years, osseoperception has received more and more attention since the introduction of osseointegrated implants. However, the histomorphometric evidence on the mechanoreceptors around dental implants is still insufficient and the fundamental mechanism of osseoperception remains unclear. Therefore, the primary goal of this doctoral thesis was to explore the innervation of peri-implant tissues in a split-mouth designed animal study, with a special focus on the impacts of various implant placement and loading protocols. Subsequently, the accuracy and applicability of CBCT for the assessment of trabecular microstructures were analyzed by comparing to histomorphology and μ CT, respectively. Finally, an attempt was made to evaluate the changes of trabecular bone structures around dental implants which received immediate and delayed loadings by using the validated CBCT imaging technique.

The thesis started with a general description of the morphometric characterization of nerve fibres in periodontal ligament and peri-implant area, the history of osseoperception, as well as the application of current imaging modalities in bone morphometric quantification in **Chapter 1**. Next, the overall aims and hypotheses of the whole thesis were presented.

In **Chapter 2**, we summarized and discussed the available literature concerning the influence of dental implant placement and loading protocols on peri-implant innervation by systematic review methods. Implant loading increases the density of nerve fibres in peri-implant tissues than those implants without loading or extraction sites without implantation. However, there was insufficient evidence to distinguish between the innervation patterns following immediate and delayed implant placement and loading protocols. The results revealed the need for more uniformity reporting, randomized controlled trials, longer observation periods and standardization of protocols.

In **Chapter 3**, a split-mouth designed animal study was performed to provide comprehensive histomorphometric evidence of osseoperception at the site of implant placements subjected to different implant placement and loading protocols, as well as the information of origin and distribution of peri-implant innervation. Myelinated nerve

fibres were mostly found in peri-implant crestal gingival and apical regions. The results also suggested that immediate implant placement and immediate loading was preferred to allow optimized peri-implant reinnervation. This exploration based on the histomorphology of peri-implant neuroreceptors could contribute to understand the osseoperception and, as a result, improve the success rate of osseointegration.

In the following **Chapter 4**, we turned to determine the accuracy of the new imaging modality, named CBCT, in peri-implant bone structure analyses in comparison with histomorphometry. Both measurements on the trabecular bone structure showed moderate to high correlation and strong agreements regardless of the presence of implants. However, CBCT showed tendency to overestimate Tb.Th and Tb.Sp; on the other hand, BV.TV and Tb.N were lower than those assessed from histomorphometry. The current findings indicated a potential clinical application of CBCT on bone morphometric quantification.

The further evaluation in **Chapter 5** was to validate the scanning protocol of CBCT for measuring trabecular bone microstructure by comparing to μ CT. Under different setting of tube voltage and current, we did not find any significant difference between two kinds of measurements except for Tb.Sp. And those measurements showed high positive correlation except for Tb.Th. Nevertheless, CBCT analyses tended to slightly overestimate BV/TV, Tb.Sp and Tb.Th comparing with μ CT. The soft-tissue effect on the bone structure analyses was not observed. In addition to the previous chapter, this study showed the potential value of high-resolution CBCT imaging, as an accurate and low-dose alternative to MSCT, for *in vivo* bone morphometry assessment.

Based on the former two chapters, we evaluated 3D morphology of peri-implant trabecular bone in a dog model under immediate and delayed implant protocols by means of high-resolution CBCT in **Chapter 6**. Coronal and middle regions around implants showed more compact, plate-like and thicker trabeculae. Immediate placed and loaded implants might have an improved bone structural integration than normal extraction healing. Nevertheless, a different bone remodeling pattern was not observed

when using a delayed vs. an immediate implant protocol.

Finally, the general discussion and conclusions of the above-mentioned studies and recommendations for future researches were presented in **Chapter 7**. To further uncover osseoperception phenomenon, this doctoral thesis was in an endeavor to elaborate the effects of delayed and immediate implant placement and loading protocols on the healing of nerve fibres and bone structures around dental implants. Eventually, the current results would raise a new range of pertinent questions and studies in fundamental physiology and clinical rehabilitation.

Sinds de introductie van osseointegratie, nu ruim 50 jaar geleden is heel wat histologisch, klinisch, biomechanisch en psychofysisch onderzoek verricht naar dit mechanisme. Ondanks het grote aantal onderzoeken, is de studie van de peri-implantaire harde weefselzone en de mogelijke bezenuwing daarvan amper onderzocht. Bovendien werden (histo)morfometrische karakterisatietechnieken weinig gebruikt. Het primaire doel van deze thesis bestaat erin om na te kijken of er peri-implantaire gevoelsbezenuwing is, en indien dat zo is, of dat mogelijks ook afhankelijk is van de aard van de plaatsing en belasting van de implantaten. Daartoe werd een gerandomiseerde hondenstudie uitgevoerd op basis van een split-mouth design met verschillende protocols voor plaatsing en belasting van implantaten. Daarnaast werd ook de nauwkeurigheid van de morfometrische karakterisatie van de peri-implantaire botzone verder onderzocht, met het oog op een validatie in de klinische praktijk door gebruik te maken van CBCT in plaats van histologische of microCT analyses. Er werd ook gepoogd om deze CBCT karakterisatie verder te gebruiken om verschillen in remodeling te bestuderen, gerelateerd aan de verschillende protocols voor plaatsing en belasting van implantaten.

De thesis start met een algemene beschrijving van morfometrische karakteristieken van parodontale en peri-implantaire karakteristieken van zenuwvezels. Daarnaast wordt ook de (histo)morfometrische karakterisatie beschreven in **hoofdstuk 1**. Daarna worden de algemene doelstellingen en hypothesen voorgesteld.

In **hoofdstuk 2** wordt de literatuur onderzocht, waarbij werd besloten dat belasting van implantaten leidt tot een stijging van de peri-implantaire zenuwvezeldensiteit. Jammer genoeg blijken er onvoldoende kennis en gegevens om een onderscheid te maken tussen meer specifieke behandelprotocollen. Gestandaardiseerd onderzoek met grotere onderzoeksgroepen, meer implantaten en opgevolgd over een langere tijd lijkt een onontbeerlijke stap voor verder onderzoek.

In **hoofdstuk 3** wordt een gerandomiseerde hondenstudie uitgevoerd op basis van een split-mouth design met verschillende protocollen voor plaatsing en belasting van implantaten. Hierdoor kon men nagaan of er peri-implantaire gevoelsbezenuwing is, en

indien dat zo is, of dat mogelijks ook afhankelijk is van de aard van de plaatsing en belasting van de implantaten. Gemyeliniseerde zenuwvezels wijzen op gevoelszenuwen en werden in de huidige studie zowel apicaal als crestaal (gingiva niveau) geïdentificeerd. De resultaten in de huidige studie wijzen in de richting van een betere bezenuwing bij onmiddellijke plaatsing en belasting van implantaten. Deze bevinding betekent een belangrijke stap in de richting van een verklaring voor het osseoperceptiefenomeen.

In het volgende **hoofdstuk 4**, wordt de karakterisatie van het bot via histomorfometrie vergeleken met CBCT analyses gebaseerd op microCT software met meerdere variabelen. De studie liet toe om het gebruik van klinische cone beam CT in het kader van osseointegratie te valideren. Er was een goede en sterke correlatie in het onderzoek tussen de verschillende variabelen gemeten met CBCT in vergelijking met andere of aanvullende onderzoeken. Het huidige hoofdstuk valideert het gebruik van CBCT in een klinische setting om zo botkarakterisatie na te gaan en veranderingen in de tijd op te volgen.

De meer diepgaande evaluatie in **hoofdstuk 5** laat toe om de verschillende CBCT scanprotocollen te vergelijken met betrekking tot de microstructuur van het trabeculair bot en dat ten opzichte van een referentie microCT van hetzelfde bot. Correlaties tussen CBCT en microCT zijn goed. Er werd geen verandering in botkarakterisatie waargenomen na wijziging van de CBCT opnameparameters. In de huidige studie werd deze techniek voor verdere botkarakterisatie gevalideerd, waarbij deze ook werd aangeduid als een lage dosis alternatief voor medische CT en microCT, zonder histologische invasiviteit.

Gebaseerd op de resultaten beschreven in hoofdstukken 4 en 5, wordt in de huidige studie 3D morfologie van het peri-implantaire trabeculaire bot beschreven in een hondenstudie (**Hoofdstuk 6**). Coronale en middenste implantaatzones tonen meer compact bot met meer plaatvormige en dikkere trabeculae. Onmiddellijke belasting van onmiddellijk geplaatste implantaten blijken daarbij gunstiger, doch dit kon statistisch

niet worden bevestigd.

Tot slot worden de discussie en conclusies van bovenstaande onderzoeken besproken in **hoofdstuk 7** met advies voor verder onderzoek en klinische perspectieven. De huidige thesis levert een belangrijke bijdrage tot de verdere verklaring van het osseoperceptiemechanisme. Meer specifiek geeft de thesis ons meer informatie over de invloed van onmiddellijke belasting en plaatsing van implantaten op de peri-implantaire bezenuwing en botappositie. Uiteindelijk zullen de huidige bevindingen leiden tot verdere vragen, waarbij meer diepgaand fysiologisch, neurofysiologisch (fMRI) en klinisch onderzoek een noodzaak blijkt.

Curriculum Vitae

Name: Yan HUANG
 Date of birth: 6th Oct. 1981
 Place of birth: Hefei, China
 Street address: Oral Imaging Center,
 Oral and Maxillo-facial Surgery - Imaging and Pathology,
 Kapucijnenvoer 7 blok a - box 7001,
 3000 Leuven, Belgium
 Email: yan.huang@med.kuleuven.be
yanhuangcn@gmail.com

Education

2009-2014	PhD candidate in Biomedicine, K.U Leuven & University Hasselt, Belgium
2008-2009	Postgraduate Study in Advanced Medical Imaging, K.U Leuven, Belgium
2005-2008	Postgraduate Study in Clinical Stomatology, West China College of Stomatology, Sichuan University, P.R. China
2000-2005	Bachelor Study in Medicine, College of Stomatology, Anhui Medical University, P.R. China

Publications in Peer-Reviewed Journals

Huang, Y., Van Dessel, J., Depypere, M., Ezeldeen, M., Iliescu, A., Santos, E., Lambrichts, I., Liang, X., Jacobs, R. (2014) Validating cone-beam computed tomography for peri-implant bone morphometric analysis. *Bone Research (Conditional Acceptance)*

Huang, Y., Van Dessel, J., Martens, W., Lambrichts, I., Liang, X., Andre Iliescu, A., Zhong, W., Ma, G., Jacobs, R. (2014) Sensory innervation around immediately vs. delayed loaded implants. *International Journal of Oral Science. (Conditional Acceptance) (IF:2.7)*

Huang, Y., Jacobs, R., Van Dessel, J., Bornstein, M., Lambrichts, I., Politis, C. (2014) A systematic review on the innervation of peri-implant tissues with special emphasis on the influence of implant placement and loading protocols. *Clinical Oral Implants Research. (IF:3.4)*

Van Dessel, J., **Huang, Y.**, Depypere, M., Rubira-Bullen, I., Maes, F., Jacobs, R. (2013). A comparative evaluation of cone beam CT and micro-CT on trabecular bone structures in the human mandible. *Dentomaxillofacial Radiology*, 42(8). 20130145. **(IF:1.1)**

Huang, Y., Van Dessel, J., Liang, X., Depypere, M., Zhong, W., Ma, G., Lambrichts, I., Maes, F., Jacobs, R. (2013). Effects of immediate and delayed loadings on peri-implant trabecular structures: a cone-beam CT evaluation. *Clinical Implant Dentistry and Related Research*. **(IF:3.8)**

Pittayapat, P., Galiti, D., **Huang, Y.**, Dreesen, K., Schreurs, M., Couto Souza, P., Rubira-Bullen, I., Westphalen, F., Pauwels, R., Kalema, G., Willems, G., Jacobs, R. (2013). An in vitro comparison of subjective image quality of panoramic views acquired via 2D or 3D imaging. *Clinical Oral Investigations*, 17(1):293-300. **(IF:2.2)**

Huang, Y., Corpas, L., Martens, W., Jacobs, R., Lambrichts, I. (2011). Histomorphological study of myelinated nerve fibres in the periodontal ligament of human canine. *Acta Odontologica Scandinavica*, 69(5), 279-86. **(IF:1.4)**

Dos Santos Corpas, L., Jacobs, R., Quirynen, M., **Huang, Y.**, Naert, I., Duyck, J. (2011). Peri-implant bone tissue assessment by comparing the outcome of intra-oral radiograph and cone beam computed tomography analyses to the histological standard. *Clinical Oral Implants Research*, 22(5), 492-499. **(IF:3.4)**

Huang, Y., Xian, S., Wang, S., Wang, T., Liao Y. (2007). Preparation and Biological Evaluation of A Novel Diphase Ca-P Scaffold Material. *Rare Metal Materials and Engineering*, 36(s2):75-78. **(IF:0.2)**

Huang, Y., Xian S. (2007). Effects of Design of Dental Implant on Immediate Implant and Immediate Loading. *International Journal of Stomatology*, 34(2): 131-133.

Zhou, M., Li, Y., **Huang, Y.**, Xian, S. (2007). Effects of the Number of Firing on the Porcelain Color. *Chinese Journal of Prosthodontics*, 8(4):248-250.

Wang, T., Xian, S., Tian, K., **Huang, Y.**, Liao, Y. (2007). Preparation of Toughness Alumina-Zirconia Nano-composite Infiltrated Ceramic. *Chinese Journal of Synthetic Chemistry*, 15(3):284-287.

Huang, Y., Wang, B., Yuan, L., Wang, L.(Ed) 1st Biomedical Innovation Forum of Leuven-Book of Abstracts [Leuven,2013] Organized by Education Section, Embassy of the People's Republic of China in the Kingdom of Belgium, Chinese Students and Scholars in Leuven(CSAL) and International Office, KU Leuven.

Presentations in International & National Meetings

Huang, Y., Van Dessel, J., Depypere, M., EzEldeen, M., Iliescu, A., Santos, E., Lambrichts, I., Liang, X., Jacobs, R. Agreement between dental cone-beamed computed tomography and histomorphometry in analyzing peri-implant bone architecture. European Congress of Dento-maxillo facial Radiology. Cluj, Romania, 25-28 June 2014.

Van Dessel, J., **Huang, Y.**, Nicolielo, L., Slagmolen, P., Jacobs, R. (2014). Accuracy of different cone-beam CT devices for trabecular bone structure analysis: an in vitro study. European Congress of Dento-maxillofacial Radiology. Cluj, Romania, 25-28 June 2014.

Van Dessel, J., **Huang, Y.**, Nicolielo, L., Slagmolen, P., Jacobs, R. (2014). Accuracy of cone-beam CT devices for trabecular bone structure analysis. European Congress of Dento-Maxillo Facial Radiology Junior Meeting. Umea, Sweden, 9-12 February 2014.

Huang, Y., Van Dessel, J., Lambrechts, I., Liang, X., Iliescu, A., Zhong, W., Ma, G., Santos, E., Jacobs, R. (2013). Innervation in peri-implant hard and soft tissues following immediate and delayed implant loading. European Association for Osseointegration. Dublin, Ireland, 17-20 Oct 2013. **(Finalists of Basic Research Competition)**

Van Dessel, J., **Huang, Y.**, Rubira-Bullen, I., Depypere, M., Maes, F., Jacobs, R. (2013). A comparative evaluation of cone-beam computed tomography (CBCT) and micro-CT on trabecular bone structures in human mandible. International Congress Of Dento-Maxillo-Facial Radiology. Bergen, Norway, 22-27 June 2013. **(Finalists of Research Awards)**

Van Dessel, J., **Huang, Y.**, Rubira-Bullen, I., Depypere, M., Nicolielo, L., Maes, F., Duarte, M., Jacobs, R. (2013). Evaluation of CBCT and μ CT on bone structure analysis. Congresso Odontológico de Bauru. Bauru, Brazil, 16-18 May 2013. **(1st Prize for Best Oral Presentation)**

Huang, Y., Van Dessel, J., Liang, X., Depypere, M., Ma, G., Zhong, W., Lambrechts, I., Maes, F., Jacobs, R. (2013). Different loadings on peri-implant trabecular structures using CBCT. Biomedical Innovation Forum of Leuven. Leuven, Belgium, 11 May 2013.

Huang, Y., Van Dessel, J., Liang, X., Depypere, M., Ma, G., Zhong, W., Lambrechts, I., Maes, F., Jacobs, R. (2012). Effects of immediate and delayed implant loadings on trabecular structures: a cone-beam CT evaluation. European Association for Osseointegration. Copenhagen, Denmark, 10-13 October 2012. **(Finalists of Basic Research Competition)**

Liang, X., **Huang, Y.**, Van Dessel, J., Zhong, W., Depypere, M., Gu, J., Vandenberghe, B., Maes, F., Lambrechts, I., Zhang, Z., Ma, G., Jacobs, R., Ma, X. (2012). CBCT instead of micro CT for studying the trabecular bone: a feasible option? Asian Congress of Oral and Maxillofacial Radiology. Xi'an, China, 14-16 September 2012.

Huang, Y., Van Dessel, J., Zhong, W., Depypere, M., Kou, N., Ma, G., Liang, X., Lambrechts, I., Maes, F., Jacobs, R. (2012). Radiographic analysis on peri-implant bone subjected to various implant protocols. European congress of dentomaxillofacial radiology - EADMFR 2012. Leipzig, Germany, 13-16 June 2012. **(2nd Prize for Research Awards)**

Pittayapat, P., Galati, D., **Huang, Y.**, Dreesen, K., Schreurs, M., Couto Souza, P., Rubira, I., Westphalen, F., Jacobs, R. (2011). An in vitro comparison of panoramic views acquired via 2D or 3D imaging to aid diagnosis of oral health. JBR-BTR Book of Proceedings ESHNR Annual Meeting September 2011. ESHNR. Brugge, Belgium, 8-10

September 2011.

Huang, Y., Corpas, L., Zhang, G., Maes, F., Lambrichts, I., Jacobs, R. (2011). 3D reconstruction of Malassez epithelial rests using light microscopic imaging. International Congress of Dentomaxillofacial Radiology. Hiroshima, Japan, 25-29 May 2011. (**Travel Grants**)

Corpas, L., **Huang, Y.**, Zhang, G., Maes, F., Lambrichts, I., Jacobs, R. (2010). Three dimensional reconstruction of human periodontal ligament structures using light microscopic imaging. European congress of dento-maxillo facial radiology- ECDMFR. Istanbul, Turkey, 2-5 June 2010.

Corpas, L., **Huang, Y.**, Collaert, B., Zhang, G., Struys, T., Lambrichts, I., Jacobs, R. (2010). Presence of myelinated nerve fibers in the periodontal ligament, peri-implant bone and bone substitute materials. ITI World Symposium. Geneva, Switzerland, 14-17 April 2010.

Huang, Y., Xian, S., Wang, S., Wang, T., Liao, Y. (2006). Preparation and Biological Evaluation of A Novel Diphasic Ca-P Scaffold Material. National Conference on High Technology Ceramics. Luoyang, China, 10-13 Oct 2006.